Modeling and Numerical Approximations of Optical Activity in the Chemical Oxygen-Iodine Laser

R. Chris Camphouse

Dissertation submitted to the Faculty of the
Virginia Polytechnic Institute and State University
in partial fulfillment of the requirements for the degree of

Doctor of Philosophy
in
Mathematics

John A. Burns, Chair
Eugene M. Cliff, Co-Chair
Jeff Borggaard
George Hagedorn
Belinda King
Robert Rogers

Date: July 10, 2001
Blacksburg, Virginia

Keywords: Finite Difference Method, Paraxial Wave Equation, Semigroup,
Partial Differential Equations, Hermite-Gaussian Beam Mode,
Chemical Oxygen-Iodine Laser, COIL

Modeling and Numerical Approximations of Optical Activity in the Chemical Oxygen-Iodine Laser

R. Chris Camphouse

(ABSTRACT)

The chemical oxygen-iodine laser (COIL) has several important military and industrial applications. The concern of this work is do develop a partial differential equation model describing optical behavior in the COIL. Optical behavior of the COIL has traditionally been investigated via a ray tracing method. Photons are represented as discrete particles, and their behavior is described by the geometry of the system. We develop an optical model wherein photons have a wave description. In order to construct the mathematical model, we utilize the theory of paraxial wave optics and Gaussian beams. Doing so allows us to incorporate physical effects such as diffusion/diffraction and refraction into the model. After describing the optical model, we present numerical methods for obtaining approximate solutions to the model in the cases of one and two transverse directions. Results are presented illustrating the efficacy of the numerical methods.

To My Wife Robbie,
Thank You For Your Constant Encouragement, Support, and Love

Acknowledgments

I would like to take this opportunity to express my appreciation to all of those involved in the completion of this work. I would like to thank my research advisor Dr. John Burns for his encouragement, leadership, and support during my stay at ICAM. I would especially like to thank Dr. Gene Cliff for his direction and motivation with regards to this dissertation. Dr. Cliff was always available to answer questions I had about various aspects of my research topic. Many times, Dr. Cliff and I met on a daily basis to discuss different aspects of the COIL model and corresponding numerical methods. I have truly gained a friend in Dr. Cliff, and look forward to working with him in the future.

Thanks are in order for everyone in the math department and at ICAM for their encouragement and support. Many people from ICAM and the math department have contributed to various aspects of this dissertation. In particular, Dr. Jeff Borggaard and Dr. George Hagedorn have always made themselves readily available to answer my never-ending questions. Dr. Borggaard has always been available to talk, even if the topic of discussion is the latest music, movies, or games. Dr. Borggaard was the first person I met from Virginia Tech, and has been a good friend ever since. Dr. Hagedorn was always willing to meet with me to discuss the physics involved in the problem and how I might incorporate the physics into the model. I would also like to thank Dr. Robert Rogers and Dr. Belinda King for their input and support while I worked on this dissertation.

Finally, I would like to thank my family and friends for their encouragement and support. I have gained many friends while at Virginia Tech, and all of them deserve a note of thanks. In particular, I would like to thank my wife Robbie for her unending belief in me and for her patience while I worked on this thesis.

Contents

List of Figures

List of Tables

Chapter 1

Introduction

The chemical oxygen-iodine laser (COIL) was invented in 1977 at the Air Force Weapons Laboratory at Kirtland Air Force Base, New Mexico. Since its inception, many new and exciting applications of COIL have been investigated. One avenue of research involves developing COIL as a tactical weapon for use by the Army, Air Force, and Navy. More recent applications being investigated include the decommissioning and dismantling of old nuclear facilities as well as industrial applications such as shipbuilding, automotive manufacturing, and machinery manufacturing.

Unlike most lasers, COIL can be scaled to very high power levels. Another remarkable feature of COIL is its short wavelength. COIL emits a wavelength of 1.315 micrometers. Correspondingly, COIL is the world's shortest wavelength, high-power chemical laser. As a result of its high power capabilities, COIL can rapidly cut through many materials, including concrete, stainless steel, and iron.

1.1 COIL Description

As its name implies, the chemical oxygen-iodine laser is a result of several chemical reactions. In particular, COIL is the result of a chemically reacting fluid flow. The desired effect of the chemical reactions in the flow is to create a population inversion. A population inversion yields more atoms at higher quantum levels than at lower quantum levels.

The necessary population inversion in the COIL results in a surplus of iodine atoms at higher quantum levels. If the high energy iodine atom interacts with a photon, the atom is stimulated to transform a high level to a low level. Stimulated radiation in the form of an additional photon is emitted.

The process of pumping an atom to an excited state in order to obtain lasing is referred to as stimulated emission. There are several important characteristics of the stimulated

emission process. The additional photon resulting from lasing is at the same frequency, at the same phase, in same sense of polarization, and propagates in the same direction as the photon that induced the atom to undergo the lasing transition [37]. As a result, stimulated emission produces very coherent light. The process of stimulated emission is the driving mechanism in a laser.

In the COIL apparatus, the iodine population inversion is created by converging and then expanding a chemically reacting flow. Several different versions of the COIL device are currently in development. The Research Assessment Device Improvement Chemical Laser (RADICL) is the device utilized for research and development. A schematic depicting the RADICL apparatus is given in Figure 1.1.

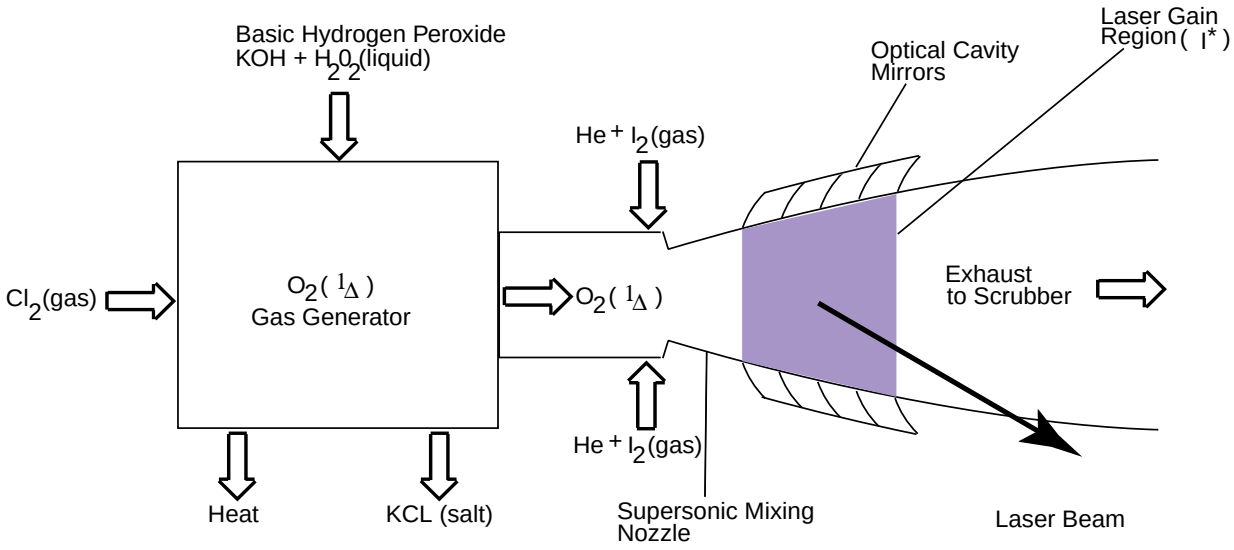

Figure 1.1: RADICL Configuration

The energy necessary to stimulate lasing in the COIL is a result of a chemical reaction between chlorine (Cl_2) gas and liquid hydrogen peroxide ($KOH + H_2O_2$). In an oxygen generator, Cl_2 gas is bubbled through a pool of basic hydrogen peroxide. The gaseous Cl_2 and hydrogen peroxide react to form gaseous molecular oxygen (O_2). The chemical reaction between the Cl_2 and hydrogen peroxide is exceptionally specific. All of the oxygen produced is in the electronically excited $^1\Delta$ quantum state [36].

Upstream of a mixing nozzle, a helium (He) flow transports the electronically excited $O_2(^1\Delta)$ from the gas generator. At this stage, the fluid flow is subsonic and consists of He and the products from the $O_2(^1\Delta)$ generator. Some of the products of the $O_2(^1\Delta)$ gas generator include $O_2(^1\Delta), O_2(^3\Sigma), H_20$, and Cl_2.

As the flow approaches the mixing nozzle, a mixture of iodine (I_2) and helium is injected normal to the flow. The injection results in a mixing/chemically reacting fluid flow.

Upon reaching the mixing nozzle, the mixing/chemically reacting flow is choked and rapidly expanded. As a result of the rapid expansion, the flow becomes supersonic with a Mach number of 2.5, a static pressure of 4 torr, and a temperature of 150K. Flow expansion is approximately three degrees, and is designed to match boundary layer growth as well as maintain constant pressure in the flow [21]. The region of constant pressure is referred to as the optical cavity. The optical cavity is the shaded region in Figure 1.1. The necessary population inversion begins upstream and continues inside the optical cavity.

In the optical cavity, the importance of the $O_2(^1\Delta)$ molecule is twofold. The electronically excited oxygen dissociates an injected I_2 molecule into two iodine atoms. The iodine atoms are then stimulated to the electronically excited $^2P_{\frac{1}{2}}$ quantum state by the $O_2(^1\Delta)$ molecule. The excited $I(^2P_{\frac{1}{2}})$ atom lases at a wavelength of 1.315 microns when it interacts with a photon [20].

The surplus of excited iodine atoms in the optical cavity creates a region of atomic gain. As photons pass through the atomic gain region, their intensity is amplified. Partially

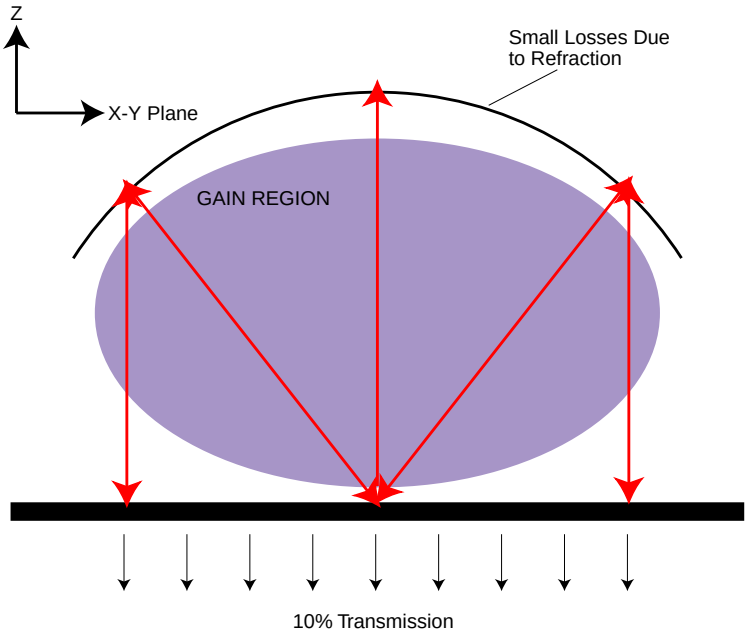

Figure 1.2: Ray Tracing Approach

reflective mirrors are placed around the optical cavity with the purpose of reflecting photons back and forth through the gain region. In order to ensure that photons do not travel outside of the gain region, the outer reflective mirror is spherical. The inner mirror is vertical. To minimize losses, the spherical mirror is made as completely reflective as possible. In one of the test configurations, the vertical mirror reflects approximately ninety percent of the electromagnetic radiation incident on it. Ten percent of the radiation is transmitted through the vertical mirror. It is via the vertical mirror that photons are extracted from the flow.

Downstream from the optical cavity, the pressure is recovered, and the flow is exhausted.

1.2 Optical Cavity

The goal of this work is to investigate optical aspects of the COIL. In particular, we are interested in the influence of atomic gain on laser intensity. Laser intensity sensitivity to various parameters inside the optical cavity is also of interest. As a result, we investigate the behavior of photons as they travel through the optical cavity.

Laser modeling has traditionally represented photons as particles. The path of a photon as it travels through the optical cavity is described by a process called ray tracing. In the ray tracing description, the direction a photon travels through the optical cavity is given by the geometry involved. Photons are treated as moving particles, and surface reflection is simply described. An excellent presentation of the ray tracing methodology is given in [37].

While it is convenient, a particle photon description does not completely suit our needs. Ray tracing provides useful information as to the path of a photon through the optical cavity. However, physical effects such as diffusion can not be incorporated into a ray tracing model because photons are treated as discrete points. A discrete description also disallows the application of the continuous sensitivity equation method, a powerful mathematical tool providing design sensitivity information. For these reasons, we abandon the particle photon description.

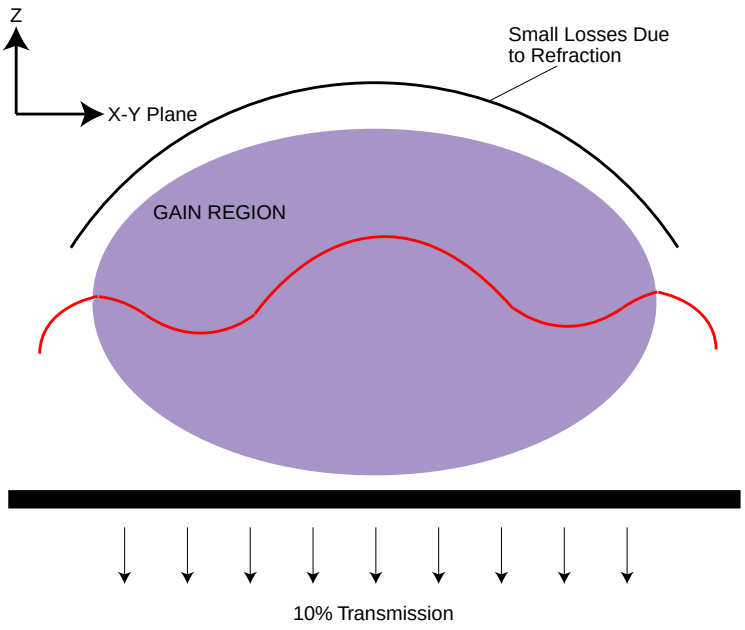

Figure 1.3: Propagating Wave Approach

In the work presented here, we model photons as waves moving toward increasing or decreasing values of z. There are several advantages of a wave model over a particle model. First, a wave model does not represent a photon as a discrete point. Thus, physical behavior such as diffusion can be incorporated into a wave model. Second, a wave has amplitude. Therefore, a wave model can provide information as to the influence of atomic gain on

laser intensity throughout the optical cavity. Finally, a wave description allows for the development of a partial differential equation model describing laser intensity inside the optical cavity. We can then apply the continuous sensitivity equation method to the partial differential equation model.

There are drawbacks to utilizing a wave photon model, however. In a particle description, reflection is easily described. However, wave reflection from a curved surface is not as obvious. Additionally, the geometry of the optical cavity leads to complications in the numerical methods used to approximate solutions of the partial differential equation model. However, there is so much more to be gained by a wave model that we accept these drawbacks for the sake of a better understanding of the optics in the COIL.

1.3 Dissertation Outline

In Chapter 2, the optical theory needed to develop a partial differential equation model describing COIL optics is presented. Beginning with the Maxwell equations, a general partial differential equation describing wave propagation in an atomic medium is derived. The z dependence of the wave amplitude is assumed to be small compared to the dependence in the x and y directions. This assumption is referred to as the paraxial approximation. Applying the paraxial approximation to the general partial differential equation describing wave propagation in an atomic medium results in the paraxial wave equation. Information regarding net atomic gain/loss is incorporated into the paraxial wave equation.

The geometry of the optical cavity leads to difficulties in determining the correct model for wave reflection. As a result, much of Chapter 2 is concerned with the topic of Gaussian beams and their properties. Reflection of Gaussian beams is fairly well understood. By utilizing the properties of Gaussian beams, the influence of the spherical mirror on the propagating wave can be determined.

A partial differential equation model describing optical behavior in the COIL is presented in Chapter 3. As the propagating wave travels toward increasing and decreasing radial values, the model is composed of two parts. The first part models propagation toward increasing values of z. The second part models propagation toward decreasing values of z. Upon arriving at the spherical mirror, the propagating wave is transformed utilizing aspects of Gaussian beam theory presented in Chapter 2.

Numerical schemes applied to a three dimensional optical cavity are significantly more complex than those applied to a two dimensional optical cavity. For this reason, a numerical scheme is developed in Chapter 4 which approximates the initial boundary value problem of Chapter 3 in the case of a two dimensional optical cavity. The numerical approximation presented is a Crank-Nicholson finite difference scheme. The numerical implementation of the wave transformation due to reflection is discussed. Results from the Crank-Nicholson scheme coupled with the mirror transformation are presented.

A numerical scheme is presented in Chapter 5 for the case of a three dimensional optical cavity. A Crank-Nicholson finite difference scheme is derived, and the numerical implementation of the wave transformation due to reflection is discussed. Numerical results are presented.

Finally, conclusions resulting from the work presented in this thesis are made in Chapter 6. Moreover, many avenues of future research are presented. One immediate avenue of future research involves applying the continuous sensitivity equation method to the optics model presented in Chapter 3.

Chapter 2

Paraxial Wave Optics and Gaussian Beams

One of the primary goals of this work is to develop a partial differential equation model describing laser intensity in the optical cavity. As we are interested in a system wherein behavior is a result of atomic interaction, an equation describing wave propagation in an atomic medium is needed.

In this chapter, we derive a general equation describing wave propagation in an atomic medium. An approximation is made which simplifies the resulting wave equation. The simplification yields an equation commonly referred to as the paraxial wave equation. Information about atomic gain and phase behavior are incorporated into the paraxial wave equation. The result is an equation describing the behavior of the electric field $\boldsymbol{E}$ inside the optical cavity. Laser intensity $\boldsymbol{I}$ is related to the electric field by

$$\boldsymbol{I} = |\boldsymbol{E}|^2. \tag{2.1}$$

The influence of mirror curvature on a solution of the paraxial wave equation also needs to be determined. As a result, a significant portion of this chapter is concerned with the topic of Gaussian beams. By utilizing the properties of Gaussian beams, the influence of a spherical mirror on a solution to the paraxial wave equation can be determined.

2.1 Wave Propagation in an Atomic Medium

In this section, the equation describing wave propagation in an atomic medium is derived. The resulting equation is the fundamental starting point in all that follows. The wave equation derived in this section yields the paraxial wave equation when a specific assumption is applied. As an atomic medium is the driving mechanism of the COIL, the equations needed to begin the derivation are the Maxwell equations.

In the work presented here, two of the Maxwell equations are used to derive the general wave equation for atomic media. The first Maxwell equation provides a relationship between the electric field $\boldsymbol{E}$ and the induced magnetic field $\boldsymbol{B}$. The second Maxwell equation describes the relationship between the magnetic field $\boldsymbol{H}$, the conduction current density $\boldsymbol{J}$, and the displacement field $\boldsymbol{D}$. In both of the Maxwell equations, ω is the frequency of the electric field.

The Maxwell equations we employ are of the form

$$\nabla \times \boldsymbol{E} = -j\omega \boldsymbol{B}, \text{ and} \tag{2.2}$$

$$\nabla \times \boldsymbol{H} = \boldsymbol{J} + j\omega \boldsymbol{D}. \tag{2.3}$$

Before proceeding further, four physical quantities need to be defined. The magnetic permeability of the host medium is given by μ. The quantity σ is defined to be the conductivity. The optical-frequency dielectric permeability of the host medium is given by ϵ. Finally, the resonant susceptibility associated with the transition in any laser atoms that may be present is given by $\chi_{at}(\omega)$.

There are three constitutive relations interrelating (2.2) and (2.3) involving the four physical quantities described above. They are of the form

$$\boldsymbol{B} = \mu \boldsymbol{H}, \tag{2.4}$$

$$\boldsymbol{J} = \sigma \boldsymbol{E}, \text{ and} \tag{2.5}$$

$$\boldsymbol{D} = \epsilon[1 + \chi_{at}]\boldsymbol{E}. \tag{2.6}$$

We now have everything that is needed to derive the partial differential equation describing wave propagation through an atomic media. We begin by examining $\nabla \times \nabla \times \boldsymbol{E}$. Utilizing a Cartesian product identity, we have

$$\nabla \times \nabla \times \boldsymbol{E} = \nabla(\nabla \cdot \boldsymbol{E}) - \nabla^2 \boldsymbol{E}. \tag{2.7}$$

It is assumed that the properties of the medium are spatially uniform. This assumption implies that

$$\nabla \cdot \boldsymbol{E} = 0. \tag{2.8}$$

As a result, we can write (2.8) as

$$\nabla^2 \boldsymbol{E} = -\nabla \times (\nabla \times \boldsymbol{E}). \tag{2.9}$$

The first Maxwell equation provides a relationship between $\nabla \times \boldsymbol{E}$ and $\boldsymbol{B}$. Substituting (2.2) into (2.9) yields

$$\nabla^2 \boldsymbol{E} = j\omega(\nabla \times \boldsymbol{B}). \tag{2.10}$$

Utilizing what is given by constitutive relation (2.4), we can write (2.10) as

$$\nabla^2 \boldsymbol{E} = j\omega\mu(\nabla \times \boldsymbol{H}). \tag{2.11}$$

Substituting the second Maxwell equation (2.3) into (2.11) yields an equation of the form

$$\nabla^2 \boldsymbol{E} = j\omega\mu(\boldsymbol{J} + j\omega\boldsymbol{D}). \tag{2.12}$$

We are now able to incorporate laser transition information into (2.12). Constitutive relation (2.5) provides a relationship between the conduction current density $\boldsymbol{J}$ and the electric field $\boldsymbol{E}$. Similarly, constitutive relation (2.6) expresses the displacement field $\boldsymbol{D}$ in terms of the electric field. As a result, (2.5) and (2.6) allow us to write (2.12) as

$$\nabla^2 \boldsymbol{E} = j\omega\mu(\sigma\boldsymbol{E} + j\omega\epsilon[1 + \chi_{at}]\boldsymbol{E}) \tag{2.13}$$

$$= \omega\mu[j\sigma - \omega\epsilon[1 + \chi_{at}])\boldsymbol{E} \tag{2.14}$$

$$= \omega^2\mu\epsilon\left[\frac{j\sigma}{\omega\epsilon} - 1 - \chi_{at}\right]\boldsymbol{E}. \tag{2.15}$$

The basic wave propagation constant k for the host medium is given by

$$k = \omega\sqrt{\mu\epsilon}. \tag{2.16}$$

Substituting (2.16) into (2.15) results in the partial differential equation describing wave propagation in an atomic medium. The result is an equation of the form

$$\left(\nabla^2 + k^2\left[1 + \chi_{at} - \frac{j\sigma}{\omega\epsilon}\right]\right)E(x, y, z) = 0, \tag{2.17}$$

where E is the complex amplitude of any one of the components of $\boldsymbol{E}$.

2.2 Paraxial Wave Equation Derivation

The wave equation given by (2.17) is used to yield a simpler equation describing the propagation of a wave front in primarily one direction. In the work done here, waves are assumed to propagate primarily in the z direction. In the COIL, wave fronts move towards increasing z as well as decreasing z. As a wave front moves towards the curved mirror of the optical cavity, it is moving towards increasing z. However, after reflecting from the spherical mirror around the optical cavity, the wave front moves toward decreasing z. As a result, it seems logical that two partial differential equations are needed to accurately model this behavior. One equation will have solutions that propagate toward increasing z, while the other has solutions that propagate toward decreasing z.

First, we concentrate on the case of propagation toward increasing z. Write any given vector component of the complex $\boldsymbol{E}$ vector as

$$E(x,y,z) \equiv u(x,y,z)e^{-jkz}. \tag{2.18}$$

Equation (2.18) describes the electric field as essentially a traveling wave of the form e^{-jkz} propagating toward increasing z. The expression given by (2.18) is substituted into the wave equation (2.17).

The wave equation (2.17) requires the evaluation of $\nabla^2 E(x,y,z)$. Second order derivatives in the transverse directions are obvious. The second order derivative in the z direction is more complicated. Applying the product rule for derivatives, we see that

$$\frac{\partial}{\partial z}E(x,y,z) = \frac{\partial}{\partial z}(u(x,y,z)e^{-jkz}) \tag{2.19}$$

$$= \frac{\partial u}{\partial z}e^{-jkz} - jkue^{-jkz}. \tag{2.20}$$

Taking another derivative of (2.20) in the z direction yields

$$\frac{\partial^2}{\partial z^2}E(x,y,z) = \frac{\partial}{\partial z}\left(\frac{\partial u}{\partial z}e^{-jkz} - jkue^{-jkz}\right) \tag{2.21}$$

$$= \left[\frac{\partial^2 u}{\partial z^2} - 2jk\frac{\partial u}{\partial z} - k^2 u\right]e^{-jkz}. \tag{2.22}$$

As a result,

$$\nabla^2 E(x,y,z) = \left[\frac{\partial^2 u}{\partial x^2} + \frac{\partial^2 u}{\partial y^2} + \frac{\partial^2 u}{\partial z^2} - 2jk\frac{\partial u}{\partial z} - k^2 u\right]e^{-jkz}. \tag{2.23}$$

At this stage, the *paraxial approximation* is made. For beams of interest in lasers, it has been shown [29] that

$$\left|\frac{\partial^2 u}{\partial z^2}\right| \ll \left|\frac{\partial^2 u}{\partial x^2}\right| \text{ and } \left|\frac{\partial^2 u}{\partial z^2}\right| \ll \left|\frac{\partial^2 u}{\partial y^2}\right|. \tag{2.24}$$

As a result, the second order derivative of u in the z direction is discarded from (2.23). In other words, for lasers of practical interest, the approximation is made that

$$\nabla^2 E(x,y,z) = \left[\frac{\partial^2 u}{\partial x^2} + \frac{\partial^2 u}{\partial y^2} - 2jk\frac{\partial u}{\partial z} - k^2 u\right] e^{-jkz}. \tag{2.25}$$

Substituting (2.25) into the wave equation (2.17) yields

$$\left[\left(\frac{\partial^2 u}{\partial x^2} + \frac{\partial^2 u}{\partial y^2}\right) - 2jk\frac{\partial u}{\partial z} + k^2\left(\chi_{at} - \frac{j\sigma}{\omega\epsilon}\right) u\right] e^{-jkz} = 0. \tag{2.26}$$

As a result, we have

$$\left(\frac{\partial^2 u}{\partial x^2} + \frac{\partial^2 u}{\partial y^2}\right) - 2jk\frac{\partial u}{\partial z} + k^2\left(\chi_{at} - \frac{j\sigma}{\omega\epsilon}\right) u = 0. \tag{2.27}$$

Equation (2.27) is the upward paraxial wave equation. Solutions of (2.27) propagate toward increasing z.

In the case of propagation toward decreasing z, any given vector component of the complex $\boldsymbol{E}$ vector is written as

$$E(x,y,z) \equiv g(x,y,z)e^{jkz}. \tag{2.28}$$

Thus, reversing the sign of k in (2.27) yields the equation describing propagation toward decreasing values of z. The result is an equation of the form

$$\left(\frac{\partial^2 g}{\partial x^2} + \frac{\partial^2 g}{\partial y^2}\right) + 2jk\frac{\partial g}{\partial z} + k^2\left(\chi_{at} - \frac{j\sigma}{\omega\epsilon}\right) g = 0. \tag{2.29}$$

2.2.1 Net Atomic Gain

In the work presented here, it is desirable to incorporate net atomic gain information into the paraxial equations. Several physical quantities are related to the real and complex components of $\chi_{at}(\omega)$. As a result, χ_{at} is written as the sum of its real and complex components as

$$\chi_{at} = \chi' + j\chi''. \tag{2.30}$$

The atomic gain (or loss) coefficient $\alpha_m(\omega)$ due to atomic transitions is related to the complex component of χ_{at} by

$$\alpha_m = \frac{k}{2}\chi''. \tag{2.31}$$

The coefficient α_0 describing background losses due to the medium itself is given by

$$\alpha_0 = \frac{k\sigma}{2\omega\epsilon}. \tag{2.32}$$

Finally, there is an added phase-shift factor $\triangle\phi(z,\omega) \equiv \triangle k(\omega)z$ due to atomic transition, where the quantity $\triangle k(\omega)$ is given by

$$\triangle k = \frac{k}{2}\chi'(\omega). \tag{2.33}$$

The physical quantities given by (2.30) - (2.33) are now used to incorporate net atomic gain (or loss) information into the paraxial wave equations. The paraxial equation (2.27) can be rewritten in the form

$$\frac{\partial u}{\partial z} = -\frac{j}{2k}\left(\frac{\partial^2 u}{\partial x^2} + \frac{\partial^2 u}{\partial y^2}\right) - \frac{jk}{2}\left[\chi_{at} - \frac{j\sigma}{\omega\epsilon}\right]u. \tag{2.34}$$

Utilizing the quantities given by (2.30) - (2.33), we can incorporate net atomic gain information by recognizing that

$$\frac{\partial u}{\partial z} = -\frac{j}{2k}\left(\frac{\partial^2 u}{\partial x^2} + \frac{\partial^2 u}{\partial y^2}\right) - \frac{jk}{2}\left[\chi_{at} - \frac{j\sigma}{\omega\epsilon}\right]u \tag{2.35}$$

$$= -\frac{j}{2k}\left(\frac{\partial^2 u}{\partial x^2} + \frac{\partial^2 u}{\partial y^2}\right) - \frac{jk}{2}\left[\chi' + j\chi'' - \frac{j\sigma}{\omega\epsilon}\right]u \tag{2.36}$$

$$= -\frac{j}{2k}\left(\frac{\partial^2 u}{\partial x^2} + \frac{\partial^2 u}{\partial y^2}\right) + \left[-j\triangle k + \alpha_m - \alpha_0\right]u \tag{2.37}$$

$$= -\frac{j}{2k}\left(\frac{\partial^2 u}{\partial x^2} + \frac{\partial^2 u}{\partial y^2}\right) + [\alpha - j\triangle k]u. \tag{2.38}$$

The quantity α in (2.38) is the net atomic gain given by

$$\alpha = \alpha_m - \alpha_0. \tag{2.39}$$

Thus, the paraxial wave equation describing propagation towards increasing z can be written as

$$\frac{\partial u}{\partial z} = -\frac{j}{2k}\left(\frac{\partial^2 u}{\partial x^2} + \frac{\partial^2 u}{\partial y^2}\right) + [\alpha - j\triangle k]u. \tag{2.40}$$

Reversing the sign of k in (3.2) yields the paraxial wave equation describing propagation toward decreasing values of z. This equation has the form

$$\frac{\partial g}{\partial z} = \frac{j}{2k}\left(\frac{\partial^2 g}{\partial x^2} + \frac{\partial^2 g}{\partial y^2}\right) + [\alpha + j\triangle k]g. \tag{2.41}$$

A more convenient form of (2.40) and (2.41) involves the index of refraction n. The index of refraction is the ratio of the speed of light in a vacuum, c, to the speed of light in a medium, c_{med}. In other words,

$$n = \frac{c}{c_{med}}. \tag{2.42}$$

The partial differential equations given by (2.40) and (2.41) are written in terms of the index of refraction as [12]

$$\frac{\partial u}{\partial z} = -\frac{j}{2k}\left(\frac{\partial^2 u}{\partial x^2} + \frac{\partial^2 u}{\partial y^2}\right) + [\alpha - jk(n-1)]u, \text{ and} \tag{2.43}$$

$$\frac{\partial g}{\partial z} = \frac{j}{2k}\left(\frac{\partial^2 g}{\partial x^2} + \frac{\partial^2 g}{\partial y^2}\right) + [\alpha + jk(n-1)]g. \tag{2.44}$$

2.3 Gaussian Beams

The equations given by (2.43) and (2.44) provide a convenient means of determining the electric field inside the optical cavity. There is a complication introduced by the geometry of the problem, however. The spherical mirror outside of the optical cavity leads to nontrivial wave reflection. That is, the curvature of the spherical mirror tends to focus the propagating wave. It is inherently difficult to specify a proper boundary condition at the curved mirror which correctly describes wave reflection for an arbitrary propagating wave. However, the most widely encountered optical beam in quantum electronics is one in which the electric field has a Gaussian distribution in the transverse directions [39]. Reflection of Gaussian beams by spherical mirrors is well understood for free space propagation.

2.3.1 Fundamental Gaussian-Beam Solution

There are an infinite number of equally valid solutions to the paraxial wave equation. The family of Gaussian-beam solutions arise by assuming particular characteristics with respect to the distribution of the electric field. The fundamental Gaussian-beam solution is a result of the assumption that the field variation depends only on the axial distance z and the square of the distance, $x^2 + y^2$, from the propagation axis.

To formulate the fundamental Gaussian-beam solution, the upward paraxial wave equation in free space in written as

$$-2kj\frac{\partial u}{\partial z} + \frac{\partial^2 u}{\partial x^2} + \frac{\partial^2 u}{\partial y^2} = 0. \tag{2.45}$$

A trial solution of (2.45) is specified of the form

$$\phi(x, y, z) = \exp\left[-j\left(S(z) + \frac{k(x^2 + y^2)}{2q(z)}\right)\right], \tag{2.46}$$

where $S(z)$ is a phase shift factor, and $q(z)$ is called the complex beam parameter.

Taking the first derivative of $\phi(x, y, z)$ in the z direction yields

$$\frac{\partial \phi}{\partial z} = -j\left[S'(z) - \frac{kq'(z)(x^2 + y^2)}{2q(z)^2}\right]\phi. \tag{2.47}$$

Second order derivatives of $\phi(x, y, z)$ in the x and y directions are of the form

$$\frac{\partial^2 \phi}{\partial x^2} = \left(-\frac{jk}{q(z)} - \frac{k^2 x^2}{q(z)^2}\right)\phi, \text{ and} \tag{2.48}$$

$$\frac{\partial^2 \phi}{\partial y^2} = \left(-\frac{jk}{q(z)} - \frac{k^2 y^2}{q(z)^2}\right)\phi. \tag{2.49}$$

Substituting (2.47) - (2.49) into the paraxial wave equation (2.45) yields

$$-2k\left(S'(z)+\frac{j}{q(z)}\right)-\left(\frac{k^2}{q(z)^2}-\frac{k^2}{q(z)^2}q'(z)\right)(x^2+y^2)=0. \tag{2.50}$$

Equation (2.50) holds for all (x, y, z). As a result, it must be the case that

$$S'(z)=\frac{-j}{q(z)}, \text{ and} \tag{2.51}$$

$$q'(z)=1. \tag{2.52}$$

The ordinary differential equation given by (2.52) is one of the simplest equations to solve. Integrating (2.52), we see that

$$q(z)=z+q_0 \tag{2.53}$$

where q_0 is a constant of integration.

We are now in a position to solve for the phase shift factor $S(z)$. Substituting the expression for $q(z)$ given by (2.53) into (2.51), we see that

$$S'(z)=-\frac{j}{z+q_0}. \tag{2.54}$$

The ordinary differential equation given by (2.54) is also solved simply by integrating. The resulting expression for $S(z)$ is of the form

$$S(z)=-j\ln(z+q_0)+(\theta+j\ln(q_0)) \tag{2.55}$$

where the constant of integration has been written as $\theta+j\ln(q_0)$.

Rearranging the expression given by (2.55) for $S(z)$, we see that

$$S(z)=-j\ln\left(1+\frac{z}{q_0}\right)+\theta. \tag{2.56}$$

As can be seen by (2.56), θ is a constant phase shift factor. As a result, we arbitrarily set $\theta=0$.

We now have everything that is needed to specify the trial solution $\phi(x, y, z)$. Substituting the expressions for $S(z)$ and $q(z)$ into (2.46), we see that

$$\phi(x,y,z)=\exp\left[-j\left(-j\ln\left(1+\frac{z}{q_0}\right)+\frac{k(x^2+y^2)}{2(z+q_0)}\right)\right]. \tag{2.57}$$

The constant of integration q_0 is now specified to be purely imaginary. The choice of complex q_0 leads to physically meaningful waves whose energy is confined near the z-axis [39]. In particular, q_0 is expressed in terms of a new constant w_0 by

$$q_0 = \frac{j\pi w_0^2}{\lambda} \tag{2.58}$$

where λ is the light wavelength. The wavelength λ is related to the wave number k by

$$k = \frac{2\pi}{\lambda}. \tag{2.59}$$

At this point, it is insightful to examine the terms comprising $\phi(x, y, z)$ in (2.57). Substituting the expression for q_0 given by (2.58) into (2.57), we see that

$$\exp\left[-j\left(-j\ln\left(1+\frac{z}{q_0}\right)\right)\right] = \exp\left[-\ln\left(1-\frac{j\lambda z}{\pi w_0^2}\right)\right]. \tag{2.60}$$

Utilizing a logarithm identity of the form

$$\ln(a+jb) = \ln\sqrt{a^2+b^2} + j\tan^{-1}\left(\frac{b}{a}\right) \tag{2.61}$$

we can rewrite (2.60) to get

$$\exp\left[-\ln\left(1-\frac{j\lambda z}{\pi w_0^2}\right)\right] = \exp\left[-\ln\sqrt{1+\frac{\lambda^2 z^2}{\pi^2 w_0^4}}\right]\exp\left[j\tan^{-1}\left(\frac{\lambda z}{\pi w_0^2}\right)\right] \tag{2.62}$$

$$= \frac{1}{\sqrt{1+\frac{\lambda^2 z^2}{\pi^2 w_0^4}}}\exp\left[j\tan^{-1}\left(\frac{\lambda z}{\pi w_0^2}\right)\right]. \tag{2.63}$$

Substituting the expression for q_0 into the second term comprising $\phi(x, y, z)$, rearranging terms, and using the relation given by (2.59) yields

$$\exp\left[-j\frac{k(x^2+y^2)}{2(z+q_0)}\right] = \exp\left[-\frac{x^2+y^2}{w_0^2\left(1+\left(\frac{\lambda z}{\pi w_0^2}\right)^2\right)} - \frac{jk(x^2+y^2)}{2z\left(1+\left(\frac{\lambda z}{\pi w_0^2}\right)^2\right)}\right] \tag{2.64}$$

We now specify several physically significant and mathematically convenient parameters. Define the quantities z_R, $w(z)$, $R(z)$, and $\eta(z)$ by

$$z_R = \frac{\pi w_0^2}{\lambda}, \tag{2.65}$$

$$w(z) = w_0\sqrt{1+\left(\frac{z}{z_R}\right)^2}, \tag{2.66}$$

$$R(z) = z + \frac{z_R^2}{z}, \text{ and} \tag{2.67}$$

$$\eta(z) = \tan^{-1}\left(\frac{z}{z_R}\right). \tag{2.68}$$

The expression for $\phi(x,y,z)$ given by (2.57) is written in terms of (2.65) - (2.68). The result is an equation of the form

$$\phi(x,y,z) = \frac{w_0}{w(z)}\exp\left[j\eta(z) - (x^2+y^2)\left(\frac{1}{w^2(z)} + \frac{jk}{2R(z)}\right)\right]. \tag{2.69}$$

We summarize the results of this section in the following theorem

THEOREM 2.3.1
The expression for $\phi(x,y,z)$ given by (2.69) is a solution to the upward paraxial wave equation in free space.

Recall that the electric field $E(x,y,z)$ is assumed to be of the form

$$E(x,y,z) = u(x,y,z)e^{-jkz},$$

where $u(x,y,z)$ is a solution of the upward paraxial wave equation. Thus, the electric field $E(x,y,z)$ resulting from (2.69) is of the form

$$E(x,y,z) = E_0\phi(x,y,z)e^{-jkz}. \tag{2.70}$$

where E_0 is an arbitrary constant. Equation (2.70) is the fundamental Gaussian-beam solution in free space. As the electric field variation is assumed to depend only on the axial distance z and the square of the distance, x^2+y^2, from the propagation axis, (2.70) is referred to as the lowest order Gaussian-beam mode. More complicated solutions with azimuthal variations have been excluded.

The physical significance of the parameters given by (2.65) - (2.68) can now be appreciated. From (2.69), it is clear that the entire Gaussian beam is completely characterized by the single parameter w_0 and the wavelength λ. The parameter $w(z)$, which varies according

to (2.66), is the distance from the propagation axis at which the electric field is down by a factor $\frac{1}{e}$ compared to its value on the axis. The quantity $w(z)$ is commonly referred to as the beam spot size. The quantity w_0 is the minimum spot size. It is the spot size at the plane $z = 0$.

The quantity $R(z)$ is the radius of curvature of the phase front at z. As can be seen by the expression given by (2.67), the wavefront has infinite radius of curvature at $z = 0$. As a result, the wavefront is planar at the location of the minimum spot size. As z increases, the radius of curvature decreases rapidly and has a value of $2z_R$ at $z = z_R$. As z increases further, the radius of curvature begins to increase and gets increasingly large for larger values of z.

The constant z_R is called the Rayleigh range. It is the distance which the beam travels from the plane $z = 0$ before the beam diameter increases by $\sqrt{2}$. The minimum radius of curvature $R(z)$ occurs for the wavefront at a distance z_R from the plane $z = 0$.

The quantity $\eta(z)$ is an axially varying phase shift. The net effect of this added phase shift for the fundamental Gaussian beam solution is to give an additional cumulative phase shift of $\pm\frac{\pi}{2}$ on either side of the plane $z = 0$. In other words, there is a total added phase shift of π in passing through the plane $z = 0$. Most of this additional phase shift occurs within one or two Rayleigh ranges on either side of $z = 0$ [29].

2.3.2 Higher Order Gaussian-Beam Modes

In the previous section, the lowest order Gaussian-beam mode was derived for free space propagation. The solution given by (2.69) is a result of a specific assumption with respect to the electric field $E(x, y, z)$. More general solutions of the paraxial wave equation exist, however. The solutions presented in this section allow for more general behavior of the electric field. Moreover, the Gaussian-beam modes presented in this section have convenient orthonormality properties. It is by way of the mode solutions derived in this section that wave reflection from the curved mirror surrounding the optical cavity can be accurately described.

In rectangular coordinates, the elementary solution to the paraxial wave equation can be separated into products of identical solutions in the x and y directions [30]. In other words

$$\phi_{nm}(x, y, z) = \phi_n(x, z)\phi_m(y, z) \tag{2.71}$$

where $\phi_n(x, z)$ and $\phi_m(y, z)$ have the same mathematical form. As a result, only solutions to the paraxial wave equation in one transverse coordinate are required. Solutions in the remaining transverse coordinate can be described by analogy.

Recall that the free space paraxial wave equation in one transverse direction is of the form

$$-2kj\frac{\partial u_n}{\partial z} + \frac{\partial^2 u_n}{\partial x^2} = 0, \tag{2.72}$$

where the dependence on n represents a family of solutions.

As in the derivation of the lowest order Gaussian-beam mode, a trial solution of (2.72) is supposed. However, in order to allow for more general types of solutions, we now consider a trial solution of the form

$$\phi_n(x,z) = A(q(z))h_n\left(\frac{x}{p(z)}\right)\exp\left[\frac{-jkx^2}{2q(z)}\right]. \tag{2.73}$$

In (2.73), the quantity $q(z)$ is the same complex beam parameter as was described in the derivation of the lowest order Gaussian-beam mode. However, to allow for a more general solution, h_n and A are unknown functions. The quantity $p(z)$ is a distance dependent scaling factor.

As before, the trial solution given by (2.73) is substituted into the paraxial wave equation (2.72). Thus, it is necessary to calculate the derivatives of ϕ_n in the x and z directions.

The first order derivative of ϕ_n in the z direction is of the form

$$\frac{\partial\phi_n}{\partial z} = A\left[\left(\frac{1}{A}\frac{\partial A}{\partial q}+\frac{jkx^2}{2q^2}\right)h_n - \frac{P'x}{p^2}h_n'\right]\exp\left(\frac{-jkx^2}{2q}\right). \tag{2.74}$$

The second order derivative of ϕ_n in the x direction is of the form

$$\frac{\partial^2\phi_n}{\partial x^2} = A\left[\frac{1}{p^2}h_n'' - \frac{2jkx}{qp}h_n' - \left(\frac{jk}{q}+\frac{k^2x^2}{q^2}\right)h_n\right]\exp\left(\frac{-jkx^2}{2q}\right). \tag{2.75}$$

Substituting (2.74) and (2.75) into the paraxial wave equation (2.72) results in an ordinary differential equation for the unknown function h_n. The resulting equation is of the form

$$h_n'' - 2jk\left(\frac{p}{q}-p'\right)xh_n' - \frac{jkp^2}{q}\left(1+\frac{2q}{A}\frac{\partial A}{\partial q}\right)h_n = 0. \tag{2.76}$$

The equation given by (2.76) is very similar to the differential equation for the Hermite polynomial of order n. The standard ordinary differential equation for the Hermite polynomial $H_n\left(\frac{x}{p}\right)$ is of the form

$$H_n'' - 2\left(\frac{x}{p}\right)H_n' + 2nH_n = 0. \tag{2.77}$$

Thus, equations (2.76) and (2.77) will be identical if $p(z)$ and $A(q(z))$ can be specified in such a way that

$$\frac{\partial p}{\partial z} = \frac{p}{q}+\frac{j}{kp} \text{ and} \tag{2.78}$$

$$\frac{2q}{A}\frac{\partial A}{\partial q} = \frac{2jnq}{kp^2} - 1. \tag{2.79}$$

There are several ways that (2.78) and (2.79) can be solved simultaneously. Each solution method leads to a different family of higher order Gaussian-beam modes. As all solutions yield modes involving the Hermite polynomials, the resulting modes are often referred to as Hermite-Gaussian modes.

The most widely used Hermite-Gaussian modes arise from the assumption that the scale factor $p(z)$ is purely real, and is related to the spot size $w(z)$ by

$$\frac{1}{p(z)} = \frac{\sqrt{2}}{w(z)}. \tag{2.80}$$

Using the fact that the spot size $w(z)$ is related to the complex beam parameter $q(z)$ by

$$\frac{1}{q(z)} = \frac{1}{R(z)} - j\frac{\lambda}{\pi w(z)^2} \tag{2.81}$$

it can be shown [29] that the expression for $p(z)$ given by (2.80) satisfies the differential equation (2.78).

The corresponding solution for $A(q(z))$ can be written in the form

$$A(q) = A_0 \left(\frac{q_0}{q(z)}\right)^{\frac{1}{2}} \left(\frac{q_0 q(z)^*}{q_0^* q(z)}\right)^{\frac{n}{2}}. \tag{2.82}$$

Substituting the expressions for $A(q)$ and $p(z)$ given by (2.80) and (2.82) into the trial solution $\phi_n(x,z)$ results in a Hermite-Gaussian mode of the form

$$\phi_n(x,z) = \left(\frac{2}{\pi}\right)^{\frac{1}{4}} \left(\frac{1}{2^n n! w_0}\right)^{\frac{1}{2}} \left(\frac{q_0}{q(z)}\right)^{\frac{1}{2}} \left[\frac{q_0 q^*(z)}{q_0^* q(z)}\right]^{\frac{n}{2}} H_n\left(\frac{\sqrt{2}x}{w(z)}\right) \exp\left[-j\frac{kx^2}{2q(z)}\right], \tag{2.83}$$

where H_n is the Hermite polynomial of order n. The quantities $q(z)$ and $w(z)$ are the same as for the fundamental Gaussian-beam solution. Note that in (2.83), the solution $\phi_n(x,z)$ has been normalized so that

$$\int_{-\infty}^{\infty} \phi_n^*(x,z)\phi_n(x,z)dx = 1. \tag{2.84}$$

In the case of two transverse directions, the higher order Hermite-Gaussian mode is specified, according to (2.71), as

$$\phi_{nm}(x,y,z) = \phi_n(x,z)\phi_m(y,z), \tag{2.85}$$

where $\phi_n(x,z)$ and $\phi_m(y,z)$ are given by (2.83).

We summarize the results of this section in the following theorem.

THEOREM 2.3.2
The expression for $\phi_n(x,z)$ given by (2.83) is a solution to the upward paraxial wave equation in free space for $n \in \{0,1,2,3,...\}$.

At first glance, it appears that the Hermite-Gaussian mode $\phi_n(x,z)$ given by (2.83) is quite complicated. In particular, specifying ϕ_n requires the specification of the Hermite polynomial H_n. The Hermite polynomial $H_n(x)$ is given by

$$H_n(x) = (-1)^n e^{\frac{x^2}{2}} \left(\frac{\partial^n}{\partial x^n} e^{\frac{-x^2}{2}} \right). \tag{2.86}$$

The Hermite polynomials can be found recursively, however. The Hermite polynomials for $n = 0$ and $n = 1$ are given by

$$H_0(x) = 1 \text{ and} \tag{2.87}$$

$$H_1(x) = 2x. \tag{2.88}$$

The remaining H_n can be found from the recursion formula

$$H_{n+1}(x) = 2xH_n(x) - 2nH_{n-1}x. \tag{2.89}$$

Representative intensity patterns for several of the Hermite-Gaussian modes $\phi_n(x,z)$ are illustrated in Figure 2.1. Intensity patterns of the higher dimensional Hermite-Gaussian modes $\phi_{nm}(x,y,z)$ are illustrated in Figure 2.2 for several values of n and m.

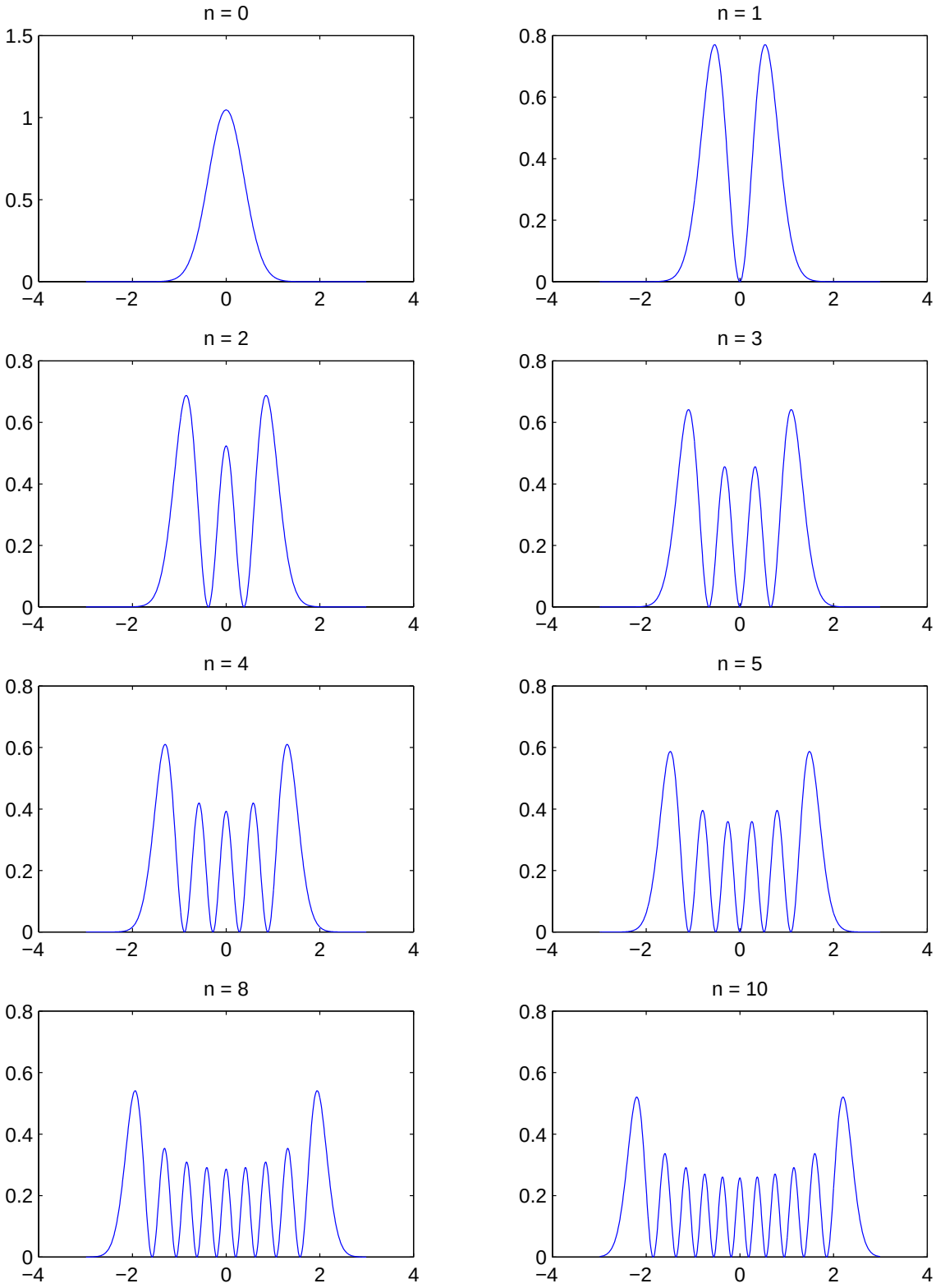

Figure 2.1: Intensity patterns of ϕ_n for various values of n.

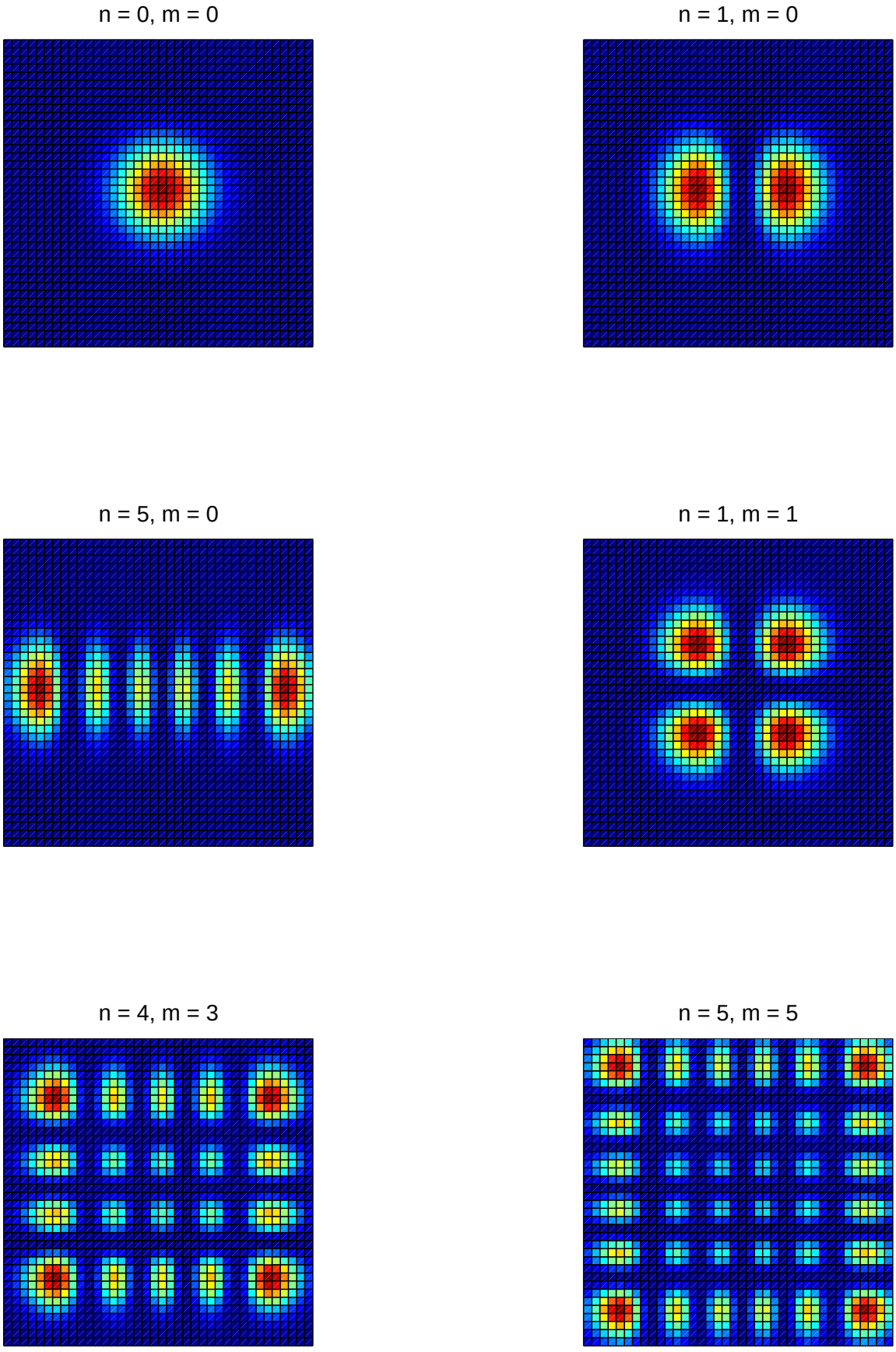

Figure 2.2: Intensity patterns of ϕ_{nm} for various values of n and m.

2.3.3 Hermite-Gaussian Mode Expansions

The Hermite-Gaussian modes $\phi_n(x,z)$ presented in the previous section obey the orthonormality relation

$$\int_{-\infty}^{\infty} \phi_n^*(x,z)\phi_m(x,z)dx = \delta_{nm}, \tag{2.90}$$

where δ_{nm} is the Kronecker delta. Moreover, the Hermite-Gaussian modes provide a complete set of basis functions characterized by the single complex parameter w_0 [30]. As a result, they can be used as a basis set to expand a solution $u(x,y,z)$ of the free space paraxial wave equation as

$$u(x,y,z) = \sum_n \sum_m c_{nm}(z)\phi_n(x,z)\phi_m(y,z). \tag{2.91}$$

Multiplying both sides of (2.91) by $\phi_n^*(x,z)\phi_m^*(y,z)$ and integrating over the transverse plane yields

$$c_{nm}(z) = \int_{-\infty}^{\infty}\int_{-\infty}^{\infty} u(x,y,z)\phi_n^*(x,z)\phi_m^*(y,z)dxdy. \tag{2.92}$$

Thus, a solution $u(x,y,z)$ of the paraxial wave equation, characterized by w_0, can be expanded as in (2.91) where the coefficients used in the expansion are given by (2.92).

2.3.4 Transformation of $q(z)$ by a Spherical Mirror

We are now in a position to specify the influence of the spherical mirror surrounding the optical cavity on a solution of the paraxial wave equation. In lens theory, the radius of curvature, R, of a purely spherical wave is transformed [37] by a thin lens according to the lens law

$$\frac{1}{R_2} = \frac{1}{R_1} - \frac{1}{f}. \tag{2.93}$$

In equation (2.93), R_1 is the radius of curvature of the incoming wave, and R_2 is the radius of curvature of the outgoing wave. The quantity f is the focal length of the thin lens. The radius of curvature of a Gaussian beam passing through a thin lens is changed in the same way, whereas the spot size w remains unchanged [29].

Recall that the radius of curvature $R(z)$ of a Gaussian beam is related to the complex beam parameter $q(z)$ by

$$\frac{1}{q(z)} = \frac{1}{R(z)} - j\frac{\lambda}{\pi w^2(z)}. \tag{2.94}$$

As a result, the transformation law for a Gaussian beam is analogous to the transformation law for a purely spherical wave. In other words, a thin lens transforms the complex beam parameter $q(z)$ according to

$$\frac{1}{q_2} = \frac{1}{q_1} - \frac{1}{f}. \tag{2.95}$$

In equation (2.95), q_2 is the value of the complex beam parameter immediately after the thin lens. The quantity q_1 is the value of $q(z)$ immediately before the thin lens.

As the focal length of a spherical mirror is one-half the mirror radius, the transformation law for a spherical mirror is given by

$$\frac{1}{q_2} = \frac{1}{q_1} - \frac{2}{r}, \tag{2.96}$$

where r is mirror radius.

As can be seen from (2.96), the spherical mirror transforms the complex beam parameter $q(z)$ used in the construction of the Hermite-Gaussian modes. Thus, the influence of the spherical mirror can be obtained by expanding a solution of the paraxial wave equation in terms of the Hermite-Gaussian modes at the curved mirror, transforming the modes, and then reconstructing the wave consisting of the transformed modes. In the following chapter, we utilize the properties of Gaussian beams to formulate a partial differential equation model describing the electric field inside the optical cavity of the COIL.

Chapter 3

Optical Cavity Model

In this chapter, we present a partial differential equation model describing the evolution of the electric field inside the optical cavity of the COIL. The physical system we are considering is illustrated in Figure 3.1.

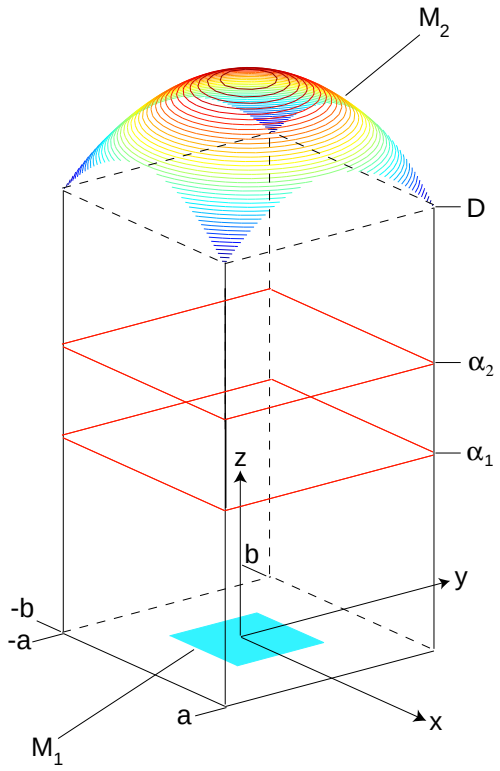

Figure 3.1: Optical Cavity Geometry

The schematic shown in Figure 3.1 depicts two mirrors separated by a distance D. The lower mirror is perfectly horizontal while the upper mirror is spherical. For notational con-

venience, we denote the flat out-coupling mirror as M_1. Similarly, M_2 denotes the spherical mirror.

Figure 3.1 also illustrates the region in which atomic gain takes place. In the work presented here, we specify a real-valued atomic gain function $\alpha(x, y, z)$ as

$$\alpha(x, y, z) = \begin{cases} f(x, y) & \text{if } z \in [\alpha 1, \alpha 2]; \\ 0, & \text{otherwise.} \end{cases} \tag{3.1}$$

The colored rectangle in Figure 3.1 is the region in which atomic gain influences the propagating wave.

In this work, we are interested in wave behavior after one round-trip through the optical cavity. Thus, we specify an initial condition at the horizontal mirror ($z = 0$). We then propagate through increasing z until the wave reaches the spherical mirror. At the spherical mirror, the propagating wave is reflected. After reflection, the wave propagates towards decreasing values of z until it arrives at the horizontal mirror again. Upon arriving at the outcoupling mirror, a portion of the wave energy is extracted due to energy transmission through the mirror. In the RADICL device, approximately ten percent of the wave energy is transmitted through the outcoupling mirror. Roughly ninety percent of the energy is reflected back into the optical cavity.

We are now in a position to describe the partial differential equation model describing the electric field inside the optical cavity. As we start with an initial condition at $z = 0$ and propagate the solution toward the spherical mirror, the first part of our model describes wave propagation toward increasing values of z.

3.1 Propagation Toward Increasing z

The first part of our model describes wave propagation from M_1 to M_2. Propagation is toward increasing values of z. As a result, wave behavior is modeled by

$$\frac{\partial u}{\partial z} = -\frac{j}{2k}\left(\frac{\partial^2 u}{\partial x^2} + \frac{\partial^2 u}{\partial y^2}\right) + [\alpha(x, y, z) - jk(n-1)]u, \ (k > 0) \tag{3.2}$$

An initial condition is specified at the horizontal mirror. Some care needs to be taken regarding the initial condition. Our aim is to utilize the properties of Gaussian-beam reflection at the spherical mirror. Recall that the Hermite-Gaussian basis functions presented in the previous chapter depend on the beam spot size $w(z)$. In this work, we specify that the minimum spot size w_0 is located at the outcoupling mirror initially. We use what is known as the 99% rule to initially specify w_0 at the flat mirror M_1. In optical resonator design literature, the 99 % rule is often discussed. This rule is used as a design criterion in determining proper aperture size. An aperture of half-length a_r will pass just over 99% of

the energy of a Gaussian beam if a_r satisfies

$$a_r = \frac{\pi}{2} w, \tag{3.3}$$

where w is the spot size at the aperture.

The relationship given in (3.3) is the 99% rule. We utilize (3.3) by specifying the half-length of the outcoupling mirror M_1, and then determine w_0 according to

$$w_0 = \frac{2M_r}{\pi}, \tag{3.4}$$

where M_r is the half-length of the flat mirror. We then specify an initial condition of the form

$$u(x, y, 0) = u_0(x, y, w_0), \tag{3.5}$$

where w_0 is the spot size resulting from the 99% rule. In the event that the half-lengths of the flat mirror are unequal in the x and y directions, we utilize (3.4) and specify the spot sizes in the x and y directions separately.

Utilizing the 99% rule to specify the minimum spot size at the flat mirror results in the beam parameter q_0 being purely imaginary. As a result, the energy density of the propagating wave is confined near the optical axis [39]. Accordingly, we specify a to be several multiples of the half-length of M_1 in the x direction. In a similar fashion, we specify b to be several multiples of the half-length of M_1 in the y direction. The outcoupling mirror is then located in the interior of $[-a, a] \times [-b, b]$. Specifying a and b sufficiently large allows us to enforce Dirichlet boundary conditions along the transverse boundary. In particular, we require that the electric field remain at zero along the transverse boundary. The resulting conditions are of the form

$$u(-a, y, z) = 0 = u(a, y, z) \text{ and} \tag{3.6}$$

$$u(x, -b, z) = 0 = u(x, b, z). \tag{3.7}$$

The partial differential equation model above is applied for wave propagation from the horizontal mirror to $z = D$.

We now present several theoretical results for the model of upward propagation. The first result involves the upward model in the absence of atomic gain. Denote Ω according to $\Omega = [-a, a] \times [-b, b] \times [0, D]$. Let $\mathcal{H} = L_2(\Omega)$ and $\mathcal{D}(A_0) = \mathcal{H}_0^1 \cap \mathcal{H}^2$.

Define

$$A_0 : \mathcal{D}(A_0) \subseteq \mathcal{H} \to \mathcal{H} \text{ by} \tag{3.8}$$

$$A_0 u = -\frac{j}{2k} \left(\frac{\partial^2 u}{\partial x^2} + \frac{\partial^2 u}{\partial y^2} \right) - jk(n-1)u. \tag{3.9}$$

THEOREM 3.1.1
The operator A_0 defined by (3.8) and (3.9) generates a C_0-group of unitary operators on $\mathcal{H}$.

Proof.

Consider the operator $F = jA_0$. Define $\mathcal{D}(F) = \mathcal{D}(A_0) = \mathcal{H}_0^1 \cap \mathcal{H}^2$, and observe that

$$Fu = j(A_0 u) \tag{3.10}$$

$$= j\left[-\frac{j}{2k}\left(\frac{\partial^2 u}{\partial x^2} + \frac{\partial^2 u}{\partial y^2}\right) - jk(n-1)u\right] \tag{3.11}$$

$$= \frac{1}{2k}\left(\frac{\partial^2 u}{\partial x^2} + \frac{\partial^2 u}{\partial y^2}\right) + k(n-1)u. \tag{3.12}$$

Since $k > 0$, it follows by direct calculation that $F^* = F$, i.e., F is self-adjoint. Therefore, by Stones Theorem, it follows that A_0 generates a C_0-group of unitary operators on $L_2(\Omega)$.

□

We now consider the case in which atomic gain is present throughout the optical cavity. That is, we now consider the case when $[\alpha_1, \alpha_2] = [0, D]$. Let $f(x, y) \in L_2(\Omega)$, where $f(x, y)$ is defined according to (3.1). Define A_1 on $\mathcal{D}(A_1) = \mathcal{D}(A_0) = \mathcal{H}_0^1 \cap \mathcal{H}^2$ according to

$$A_1 u = A_0 u + f(x, y)Iu. \tag{3.13}$$

Since Ω is a bounded subset of $\mathbb{R}^3$, it follows that the operator $f(x, y)Iu$ is a bounded linear operator on $L_2(\Omega)$. Therefore, $A_1 = A_0 + f(x, y)I$ generates a C_0-semigroup on $L_2(\Omega)$. We summarize this in the following theorem.

THEOREM 3.1.2
The operator $A_1 = A_0 + f(x, y)I$ generates a C_0-semigroup on $L_2(\Omega)$.

We now utilize the results of Theorems 3.1.1 and 3.1.2 to show that the model for upward propagation is well posed in the case where $[\alpha_1, \alpha_2] \subsetneq [0, D]$.

Corollary 3.1.1
The model for upward propagation is well-posed.

Proof.

We proceed by decomposing Ω into the regions in which atomic gain is present or not

present. To this end, let Ω_1, Ω_2, and Ω_3 be defined according to

$$\Omega_1 = [-a, a] \times [-b, b] \times [0, \alpha_1), \tag{3.14}$$

$$\Omega_2 = [-a, a] \times [-b, b] \times [\alpha_1, \alpha_2], \text{ and} \tag{3.15}$$

$$\Omega_3 = [-a, a] \times [-b, b] \times (\alpha_2, D]. \tag{3.16}$$

Atomic gain is not present for all $z \in [0, \alpha_1)$. As a result, Theorem 3.1.1 implies that the model for upward propagation is well-posed on Ω_1.

Positive atomic gain is present for all $z \in [\alpha_1, \alpha_2]$. Applying Theorem 3.1.2 to the case in which $\Omega = \Omega_2$ results in the model for upward propagation being well-posed on Ω_2.

As in the case of Ω_1, no atomic gain is present for $z \in (\alpha_2, D]$. As a result, Theorem 3.1.1 implies that the upward model is well-posed on Ω_3. Therefore, the upward model is well-posed on Ω_1, Ω_2, and Ω_3. As a result, it is well-posed on all of Ω. □

We end this section with a theoretical result describing the influence of the atomic gain function $\alpha(x, y, z)$ on the wave profile $u(x, y, z)$. Define the energy $\mathcal{E}_u(z)$ associated with a wave profile $u(x, y, z)$ by

$$\mathcal{E}_u(z) = \int_{-\infty}^{\infty} \int_{-\infty}^{\infty} |u(x, y, z)|^2 dxdy. \tag{3.17}$$

THEOREM 3.1.3
Consider the dynamical system

$$\frac{\partial}{\partial z} u = A_0 u + \alpha u = Au, \text{ and} \tag{3.18}$$

$$u(x, y, 0) = u_0 \in L_2(\Omega). \tag{3.19}$$

The energy $\mathcal{E}_u(z) = \int_\Omega |u(x, y, z)|^2 dxdy$ *varies according to*

$$\frac{\partial}{\partial z} \mathcal{E}_u(z) = 2 \int_\Omega \alpha(x, y, z) |u(x, y, z)|^2 dxdy.$$

Proof.

The energy of the solution to (3.18)-(3.19) is given by

$$||u(x, y, z)||^2 = \langle u(x, y, z), u(x, y, z) \rangle \tag{3.20}$$

$$= \int_\Omega \bar{u}(x, y, z) u(x, y, z) dxdy. \tag{3.21}$$

If $u_0 \in \mathcal{D}(A_0)$, then $u(\cdot,\cdot,z) \in \mathcal{D}(A_0)$ and $\langle A_0 u, u\rangle = 0$. It follows that

$$\frac{\partial}{\partial z}(\langle u(x,y,z), u(x,y,z)\rangle) = 2\langle u_z(x,y,z), u(x,y,z)\rangle \tag{3.22}$$

$$= 2\langle A_0 u + \alpha u, u\rangle \tag{3.23}$$

$$= 2\langle A_0 u, u\rangle + 2\langle \alpha u, u\rangle \tag{3.24}$$

$$= 2\int_\Omega \bar{\alpha}\bar{u}u dxdy \tag{3.25}$$

$$= 2\int_\Omega \alpha |u|^2 dxdy. \tag{3.26}$$

□

From the result of Theorem 3.1.3, the influence of the atomic gain function $\alpha(x,y,z)$ on the wave profile $u(x,y,z)$ is apparent. If a negative atomic gain function is present, energy in the system is dissipated. In the case of zero atomic gain, the energy of the system is conserved. When a positive atomic gain is present, energy is added to the system.

3.2 Mirror Transformation

Upon arriving at $z = D$, the propagating wave encounters the spherical mirror. Recall that a spherical mirror transforms the complex beam parameter $q(z)$ used in the construction of the Hermite-Gaussian modes. In order to incorporate the appropriate transformation into our model, we expand the solution $u(x,y,D)$ in terms of the Hermite-Gaussian basis functions. That is, we expand $u(x,y,D)$ as

$$u(x,y,D) = \sum_n \sum_m c_{nm}\phi_n(x,D)\phi_m(y,D), \tag{3.27}$$

where ϕ_n and ϕ_m are the Hermite-Gaussian modes given by (2.83). Recall that the coefficients used in the expansion are given by

$$c_{nm} = \int_{-\infty}^{\infty}\int_{-\infty}^{\infty} u(x,y,D)\phi_n^*(x,D)\phi_m^*(y,D)dxdy. \tag{3.28}$$

Denote the value of the complex beam parameter at $z = D$ by

$$q(D) = q_1. \tag{3.29}$$

Then, by utilizing (2.96), the transformed beam parameter q_2 due to reflection is given by

$$\frac{1}{q_2} = \frac{1}{q_1} - \frac{2}{r}, \tag{3.30}$$

The transformed Hermite-Gaussian modes are of the form

$$\tilde{\phi}_n(x,z) = \left(\frac{2}{\pi}\right)^{\frac{1}{4}} \left(\frac{1}{2^n n! w_0}\right)^{\frac{1}{2}} \left(\frac{q_0}{q_2}\right)^{\frac{1}{2}} \left[\frac{q_0 q_2^*}{q_0^* q_2}\right]^{\frac{n}{2}} H_n\left(\frac{\sqrt{2}x}{w(z)}\right) \exp\left[-j\frac{kx^2}{2q_2}\right]. \tag{3.31}$$

Recombining the transformed Hermite-Gaussian modes yields the transformed solution $\tilde{u}(x,y,D)$ due to reflection. The resulting expression for $\tilde{u}(x,y,D)$ is of the form

$$\tilde{u}(x,y,D) = \sum_n \sum_m c_{nm} \tilde{\phi}_n(x,D) \tilde{\phi}_m(y,D). \tag{3.32}$$

3.3 Propagation Toward Decreasing z

Upon reaching the spherical mirror, the propagating wave is reflected. The solution at the spherical mirror is transformed according to (3.32). The transformed wave then propagates toward decreasing values of z. Thus, wave propagation after reflection is described by the downward paraxial wave equation of the form

$$\frac{\partial g}{\partial z} = \frac{j}{2k}\left(\frac{\partial^2 g}{\partial x^2} + \frac{\partial^2 g}{\partial y^2}\right) + [\alpha(x,y,z) + jk(n-1)]g, \ (k<0) \tag{3.33}$$

The transformed solution at $z = D$ is used as the initial data for (3.33). That is, we specify that

$$g(x,y,D) = \tilde{u}(x,y,D). \tag{3.34}$$

As in the case of upward propagation, we require that the electric field remain at zero along the transverse boundary. As a result,

$$g(-a,y,z) = 0 = g(a,y,z), \text{ and} \tag{3.35}$$

$$g(x,-b,z) = 0 = g(x,b,z). \tag{3.36}$$

The theoretical results for the model of upward propagation are also valid in the case of downward propagation. In particular, the results of Theorems 3.1.1 and 3.1.2 are still valid. As a result, the model for downward propagation is well-posed. We summarize this fact in the following corollary.

Corollary 3.3.1
The model for downward propagation is well-posed.

Proof. The proof is identical to that for Corollary 3.1.1. □

3.4 Energy Extraction

After reflecting from the spherical mirror, the wave propagates through decreasing z values until it arrives back at the outcoupling mirror M_1. The modulus of the electric field incident on the outcoupling mirror is given by $|g(x, y, 0)|$. In order to completely describe wave behavior for one round-trip through the optical cavity, we now model the extraction of wave energy that occurs at the outcoupling mirror. In the RADICL device, approximately ten percent of the wave energy is transmitted through the outcoupling mirror. Roughly ninety percent of the wave energy is reflected from the outcoupling mirror back into the optical cavity.

Recall that wave reflection from a spherical mirror transforms the complex beam parameter $q(z)$ used in the specification of the Hermite-Gaussian modes. In particular, the transformation is given by

$$\frac{1}{q_2} = \frac{1}{q_1} - \frac{2}{r}, \tag{3.37}$$

where q_2 is the value of $q(z)$ immediately after reflection and q_1 is the value of $q(z)$ immediately before reflection. As can be seen from (3.37), the parameter $q(z)$ is unchanged in the case of reflection from a mirror with infinite radius of curvature. As a result, to determine the wave profile after one round-trip through the optical cavity, we simply decompose $g(x, y, 0)$ into two parts. The first part is that portion of $g(x, y, 0)$ that is incident on the outcoupling mirror. The second part is the portion of $g(x, y, 0)$ that misses the flat mirror.

To incorporate the transmission of energy through the outcoupling mirror, recall that the energy $\mathcal{E}_u(z)$ associated with a wave profile $u(x, y, z)$ is given by

$$\mathcal{E}_u(z) = \int_{-\infty}^{\infty}\int_{-\infty}^{\infty} |u(x, y, z)|^2 dxdy. \tag{3.38}$$

Define the function $g_M(x, y, 0)$ according to

$$g_M(x, y, 0) = \begin{cases} g(x, y, 0) & \text{if } (x, y) \in \mathcal{D}(M_1); \\ 0, & \text{otherwise,} \end{cases} \tag{3.39}$$

where $\mathcal{D}(M_1)$ is the region in $[-a, a]\times[-b, b]$ occupied by the flat mirror. In a similar fashion, define $g_R(x, y, 0)$ according to

$$g_R(x, y, 0) = \begin{cases} g(x, y, 0) & \text{if } (x, y) \notin \mathcal{D}(M_1); \\ 0, & \text{otherwise.} \end{cases} \tag{3.40}$$

For the sake of simplicity, we assume that energy not incident on the outcoupling mirror is absorbed by the optical cavity wall. As a result, the energy associated with $g_R(x, y)$ is completely absorbed. None of the energy associated with $g_R(x, y)$ is reflected back into the optical cavity.

The requirement that ten percent of the energy of the wave profile incident on M_1 is transmitted through the mirror results in the specification that

$$\int_{-\infty}^{\infty}\int_{-\infty}^{\infty}|u_R(x,y,0)|^2dxdy = 0.9\int_{-\infty}^{\infty}\int_{-\infty}^{\infty}|g_M(x,y,0)|^2dxdy, \tag{3.41}$$

where $u_R(x,y,0)$ is the wave profile after one round-trip through the optical cavity. As a result, the round-trip solution $u_R(x,y,0)$ is found according to

$$u_R(x,y,0) = \sqrt{0.9}g_M(x,y,0). \tag{3.42}$$

Chapter 4

Two Dimensional Optical Cavity

In this chapter we present numerical methods for obtaining approximate solutions to the initial boundary value problem developed in Chapter 3. The model presented in the previous chapter involves two transverse directions, namely x and y. However, much is to be gained by first considering the case of one transverse direction. First, the numerical schemes developed for the case of one transverse direction are much simpler than those required for two transverse directions. In addition, the amount of computation time required to obtain a numerical solution is much greater in the case of two transverse directions. Thus, it can be quickly determined if computational results agree with theoretical results in the case of one transverse direction. As a result, the concern of this chapter is to develop a numerical scheme for the case of one transverse direction. The more general case of two transverse directions is presented in the next chapter.

4.1 Implementation Toward Increasing z

As outlined in Chapter 3, our partial differential equation model is composed of two parts. The first part describes propagation toward increasing values of z.

A uniform grid can be constructed on the problem domain. One of the first steps in constructing a uniform grid is the specification of step-sizes. In the work presented here, the step-size in the x direction is denoted by h. The step-size in the z direction is denoted by Δz. We construct a uniform grid on $[-a, a] \times [0, D]$. This region is illustrated in Figure 4.1.

On our uniform grid, we construct a Crank-Nicholson finite difference scheme. As we are interested in propagation toward increasing values of z, our Crank-Nicholson scheme must

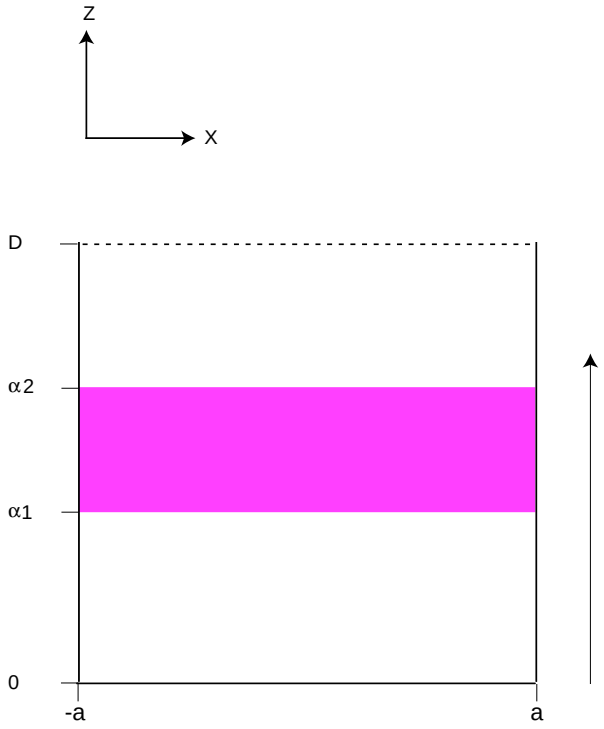

Figure 4.1: Two Dimensional Optical Cavity, Upward Propagation

approximate the model for upward propagation given by

$$\frac{\partial u}{\partial z} = -\frac{j}{2k}\frac{\partial^2 u}{\partial x^2} + [\alpha(x,z) - jk(n-1)]u, \ (k > 0), \tag{4.1}$$

$$u(-a,z) = 0 = u(a,z), \text{ and} \tag{4.2}$$

$$u(x,0) = u_0(x,w_0), \tag{4.3}$$

where w_0 is the minimum spot size discussed in Chapter 2.

In order to construct a finite difference scheme for our problem, it is necessary to discretize the derivatives in (4.1). To this end, we approximate the first order derivative in the z direction as

$$\frac{\partial u(\cdot,z)}{\partial z} \approx \frac{u(\cdot,z+\Delta z) - u(\cdot,z)}{\Delta z}. \tag{4.4}$$

The second order derivative in the x direction is discretized as

$$\frac{\partial^2 u(x,\cdot)}{\partial x^2} \approx \frac{u(x-\Delta x,\cdot) - 2u(x,\cdot) + u(x+\Delta x,\cdot)}{h^2}. \tag{4.5}$$

The Crank-Nicholson scheme is the average of an explicit and an implicit scheme. The explicit finite difference approximation to (4.1) is obtained by substituting (4.4) and (4.5)

into the partial differential equation (4.1) and evaluating the right hand side at $z = z_n$. The resulting difference equation at each evaluation point (x_i, z_n) is of the form

$$\frac{u_i^{n+1} - u_i^n}{\Delta z} = -\frac{j}{2k}\left(\frac{u_{i-1}^n - 2u_i^n + u_{i+1}^n}{h^2}\right) + (\alpha_i^n - jk(n-1))u_i^n. \tag{4.6}$$

To simplify the expression given by (4.6), we specify ν and c_i^n by

$$\nu = \frac{j\Delta z}{2kh^2}, \tag{4.7}$$

$$c_i^n = \Delta z(\alpha_i^n - jk(n-1)) \tag{4.8}$$

$$= \begin{cases} -j\Delta zk(n-1) & \text{if } z_n \notin [\alpha 1, \alpha 2]; \\ \Delta z(\alpha_i^n - jk(n-1)) & \text{otherwise.} \end{cases} \tag{4.9}$$

Then, the explicit scheme given by (4.6) is written as

$$u_i^{n+1} - u_i^n = -\nu(u_{i-1}^n - 2u_i^n + u_{i+1}^n) + c_i^n u_i^n. \tag{4.10}$$

Evaluating the right hand side of (4.10) at $z = z_{n+1}$ yields the implicit finite difference approximation to (4.1). As a result, the implicit scheme is given by

$$u_i^{n+1} - u_i^n = -\nu(u_{i-1}^{n+1} - 2u_i^{n+1} + u_{i+1}^{n+1}) + c_i^{n+1}u_i^{n+1}. \tag{4.11}$$

Adding (4.10) and (4.11) results in the Crank-Nicholson scheme. The resulting finite difference approximation is of the form

$$\nu u_{i-1}^{n+1} + (2 - 2\nu - c_i^{n+1})u_i^{n+1} + \nu u_{i+1}^{n+1} = -\nu u_{i-1}^n + (2 + 2\nu + c_i^n)u_i^n - \nu u_{i+1}^n. \tag{4.12}$$

We now present a convergence theorem for the Crank-Nicholson scheme in the case of zero atomic gain.

THEOREM 4.1.1
In the case of zero atomic gain, the Crank-Nicholson scheme given by (4.12) is unconditionally convergent.

Proof.

A routine Taylor series expansion demonstrates the consistency of (4.12).

To determine the stability of (4.12), we construct a Fourier mode solution of the form $U^n = \eta^n e^{j\theta}$, where η is the amplification factor. Substituting the Fourier mode $\eta^n e^{j\theta}$ into the Crank-Nicholson scheme results in an expression for η of the form

$$\nu\left(\eta e^{-j\theta} + e^{-j\theta}\right) + \left(2 - 2\nu - c_i^{n+1}\right)\eta - (2 + 2\nu + c_i^n) + \nu(\eta e^{j\theta} + e^{j\theta}) = 0. \tag{4.13}$$

Utilizing the identity $e^{j\theta} = \cos(\theta) + j\sin(\theta)$, we can solve (4.13) for the amplification factor η. Doing so results in

$$\eta = -\frac{\nu(\cos\theta - 1) - 1 - \frac{c_i^n}{2}}{\nu(\cos\theta - 1) + 1 - \frac{c_i^{n+1}}{2}}. \tag{4.14}$$

Using the definitions of ν and c_i^n allows us to separate (4.14) into its real and complex components. The resulting expression for η is of the form

$$\eta = -\frac{j\left[\frac{\Delta z}{2kh^2}(\cos\theta - 1) + \Delta z k(n-1)\right] - 1 - \frac{\Delta z \alpha_i^n}{2}}{j\left[\frac{\Delta z}{2kh^2}(\cos\theta - 1) + \Delta z k(n-1)\right] + 1 - \frac{\Delta z \alpha_i^{n+1}}{2}}. \tag{4.15}$$

In the case of zero atomic gain, $\alpha_i^n = \alpha_i^{n+1} = 0$. Thus, in the case of zero atomic gain, the amplification factor η satisfies

$$|\eta| = 1. \tag{4.16}$$

Therefore, by the Lax Equivalence Theorem, the Crank-Nicholson scheme given by (4.12) is unconditionally convergent in the case of zero atomic gain. □

A few remarks are in order regarding Theorem 4.1.1. The addition of positive gain may lead to the modulus of the amplification factor η being much greater than one. As can be seen in (4.15), an atomic gain function with large magnitude requires a reduction in the step size Δz in order to ensure that errors introduced by the numerical scheme are not significantly increased. However, in the results presented in this dissertation, the product $\Delta z \max(\alpha(x, y, z))$ is on the order of 10^{-3}. As a result, the modulus of the amplification factor is still very close to one.

We are now in a position to incorporate boundary condition information into (4.12). By denoting the number of evaluation points in the x direction by M, we see that particular values of $i = 0$ and $i = M + 1$ correspond to the transverse boundary. As a result, the Dirichlet boundary conditions given by (4.2) are incorporated into (4.12) by specifying that

$$u_0^n = 0 = u_{M+1}^n, \text{ and} \tag{4.17}$$

$$u_0^{n+1} = 0 = u_{M+1}^{n+1}. \tag{4.18}$$

Varying i between 1 and M in (4.12) results in a linear system of equations. For notational convenience, define θ_i^n and β_i^n as

$$\theta_i^n = 2 - 2\nu - c_i^n, \text{ and} \tag{4.19}$$

$$\beta_i^n = 2 + 2\nu + c_i^n. \tag{4.20}$$

The system of equations resulting from (4.12) is then written as

$$\begin{bmatrix} \theta_1^{n+1} & \nu & 0 & \dots & 0 & 0 & 0 \\ \nu & \theta_2^{n+1} & \nu & \dots & 0 & 0 & 0 \\ 0 & \nu & \theta_3^{n+1} & & 0 & 0 & 0 \\ & & & \ddots & & & \\ 0 & 0 & 0 & & \theta_{M-2}^{n+1} & \nu & 0 \\ 0 & 0 & 0 & \dots & \nu & \theta_{M-1}^{n+1} & \nu \\ 0 & 0 & 0 & \dots & 0 & \nu & \theta_M^{n+1} \end{bmatrix} \begin{bmatrix} u_1^{n+1} \\ u_2^{n+1} \\ u_3^{n+1} \\ \vdots \\ u_{M-2}^{n+1} \\ u_{M-1}^{n+1} \\ u_M^{n+1} \end{bmatrix} =$$

$$\begin{bmatrix} \beta_1^n & -\nu & 0 & \dots & 0 & 0 & 0 \\ -\nu & \beta_2^n & -\nu & \dots & 0 & 0 & 0 \\ 0 & -\nu & \beta_3^n & & 0 & 0 & 0 \\ & & & \ddots & & & \\ 0 & 0 & 0 & & \beta_{M-2}^n & -\nu & 0 \\ 0 & 0 & 0 & \dots & -\nu & \beta_{M-1}^n & -\nu \\ 0 & 0 & 0 & \dots & 0 & -\nu & \beta_M^n \end{bmatrix} \begin{bmatrix} u_1^n \\ u_2^n \\ u_3^n \\ \vdots \\ u_{M-2}^n \\ u_{M-1}^n \\ u_M^n \end{bmatrix} \tag{4.21}$$

Iterations are done with (4.21) to iterate the initial condition given by (4.3) to the curved mirror at $z = D$.

4.2 Mirror Transformation Implementation

Utilizing the Crank-Nicholson scheme developed in the previous section, a numerical solution is obtained at $z = D$. Upon arriving at $z = D$, the propagating wave encounters the curved mirror. To numerically incorporate the reflection properties of Hermite-Gaussian beams into the numerical approximation, we expand the numerical solution at $z = D$ in terms of the Hermite-Gaussian modes. That is, we expand $u(x_i, D)$ as

$$u(x_i, D) = \sum_{n=0}^{N_m} c_n \phi_n(x_i, D), \tag{4.22}$$

where N_m is the order of the highest order mode used in the expansion. As the numerical solution has support on the interval $[-a, a]$, the coefficients c_n are found according to the formula

$$c_n = \int_{-a}^{a} u(x, D)\phi_n^*(x, D)dx. \tag{4.23}$$

In this work, the integral in (4.23) is numerically evaluated via a trapezoidal rule. The integral on each subinterval $[x_{i-1}, x_i]$ is approximated as

$$\int_{x_{i-1}}^{x_i} u(x, D)\phi_n^*(x, D)dx \approx \frac{h}{2}[u(x_{i-1}, D)\phi_n^*(x_{i-1}, D) + u(x_i, D)\phi_n^*(x_i, D)]. \tag{4.24}$$

Summing over all subintervals $[x_{i-1}, x_i]$ yields the numerical approximation to the integral in (4.23).

Having obtained the coefficients needed in the expansion, the Hermite-Gaussian modes are transformed according to (3.31). Recombining the transformed Hermite-Gaussian modes yields a transformed numerical solution $\tilde{u}(x_i, D)$ of the form

$$\tilde{u}(x_i, D) = \sum_{n=0}^{N_m} c_n \tilde{\phi}_n(x_i, D), \tag{4.25}$$

where $\tilde{\phi}_n$ is the transformed Hermite-Gaussian mode of order n.

4.3 Implementation Toward Decreasing z

Up to now, we have been concerned with propagation toward increasing values of z. Using the numerical schemes outlined in the previous two sections, one obtains a transformed numerical solution $\tilde{u}(x_i, D)$ due to wave reflection at M_2. After reflecting from the curved mirror M_2, the propagating wave begins to propagate toward decreasing values of z. As a result, we now shift our attention to the propagation of the transformed solution $\tilde{u}(x_i, D)$ to the flat mirror M_1. As discussed in Chapter 3, propagation of this sort is governed by the initial boundary value problem

$$\frac{\partial g}{\partial z} = \frac{j}{2k}\frac{\partial^2 g}{\partial x^2} + [\alpha(x,z) + jk(n-1)]g, \ (k<0) \tag{4.26}$$

$$g(-a, z) = 0 = g(a, z), \text{ and} \tag{4.27}$$

$$g(x, D) = \tilde{u}(x, D). \tag{4.28}$$

Downward propagation is equivalent to reversing the sign of the wave number k. Similar to the case of upward propagation, define ν and c_i^n as

$$\nu = \frac{j\Delta z}{2kh^2}, \ (k<0) \tag{4.29}$$

$$c_i^n = \Delta z(\alpha_i^n + jk(n-1)), \ (k<0). \tag{4.30}$$

Then, reversing the sign of k in (4.12) results in a Crank-Nicholson scheme of the form

$$-\nu g_{i-1}^{n+1} + (2 + 2\nu - c_i^{n+1})g_i^{n+1} - \nu g_{i+1}^{n+1} = \nu g_{i-1}^n + (2 - 2\nu + c_i^n)g_i^n + \nu g_{i+1}^n. \tag{4.31}$$

THEOREM 4.3.1
In the case of zero atomic gain, the Crank-Nicholson scheme given by (4.31) is unconditionally convergent.

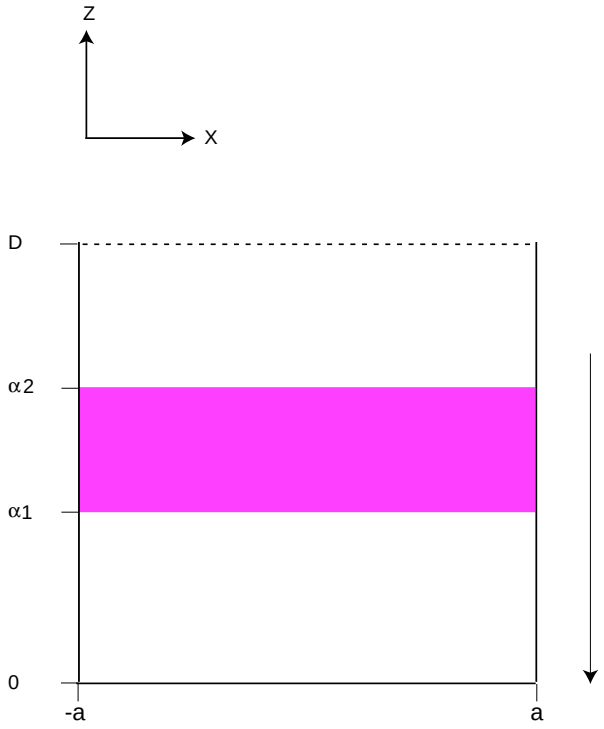

Figure 4.2: Two Dimensional Optical Cavity, Downward Propagation

Proof.

The proof is identical to that of Theorem 4.1.1. □

As in the case of upward propagation, the Dirichlet boundary conditions specified by (4.27) are incorporated into (4.31) by specifying that

$$g_0^n = 0 = g_{M+1}^n, \text{ and} \tag{4.32}$$

$$g_0^{n+1} = 0 = g_{M+1}^{n+1}. \tag{4.33}$$

For notational convenience, define θ_i^n and β_i^n as

$$\theta_i^n = 2 + 2\nu - c_i^n, \text{ and} \tag{4.34}$$

$$\beta_i^n = 2 - 2\nu + c_i^n. \tag{4.35}$$

Allowing i to range between 1 and M results in a linear system of equations of the form

$$\begin{bmatrix} \theta_1^{n+1} & -\nu & 0 & \dots & 0 & 0 & 0 \\ -\nu & \theta_2^{n+1} & -\nu & \dots & 0 & 0 & 0 \\ 0 & -\nu & \theta_3^{n+1} & & 0 & 0 & 0 \\ & & & \ddots & & & \\ 0 & 0 & 0 & & \theta_{M-2}^{n+1} & -\nu & 0 \\ 0 & 0 & 0 & \dots & -\nu & \theta_{M-1}^{n+1} & -\nu \\ 0 & 0 & 0 & \dots & 0 & -\nu & \theta_M^{n+1} \end{bmatrix} \begin{bmatrix} g_1^{n+1} \\ g_2^{n+1} \\ g_3^{n+1} \\ \vdots \\ g_{M-2}^{n+1} \\ g_{M-1}^{n+1} \\ g_M^{n+1} \end{bmatrix} = \tag{4.36}$$

$$\begin{bmatrix} \beta_1^n & \nu & 0 & \dots & 0 & 0 & 0 \\ \nu & \beta_2^n & \nu & \dots & 0 & 0 & 0 \\ 0 & \nu & \beta_3^n & & 0 & 0 & 0 \\ & & & \ddots & & & \\ 0 & 0 & 0 & & \beta_{M-2}^n & \nu & 0 \\ 0 & 0 & 0 & \dots & \nu & \beta_{M-1}^n & \nu \\ 0 & 0 & 0 & \dots & 0 & \nu & \beta_M^n \end{bmatrix} \begin{bmatrix} g_1^n \\ g_2^n \\ g_3^n \\ \vdots \\ g_{M-2}^n \\ g_{M-1}^n \\ g_M^n \end{bmatrix}$$

The remaining iterations are done with (4.36). The transformed numerical solution $\tilde{u}(x_i, D)$ is used as initial data.

4.4 Energy Extraction Implementation

Utilizing the numerical scheme given in the previous section for downward propagation, an approximate solution $g(x_i, 0)$ is obtained. In order to obtain the wave profile after one round-trip through the optical cavity, we decompose $g(x_i, 0)$ into two parts, as described in Chapter 3. The round-trip solution $u_R(x_i, 0)$ is then found according to

$$u_R(x_i, 0) = \sqrt{0.9} g_M(x_i, 0), \tag{4.37}$$

where $g_M(x_i, 0)$ is that portion of $g(x_i, 0)$ incident on the flat mirror.

4.5 Numerical Experiments

We now implement the numerical scheme presented in this chapter to the optical cavity geometry illustrated in Figure 4.3.

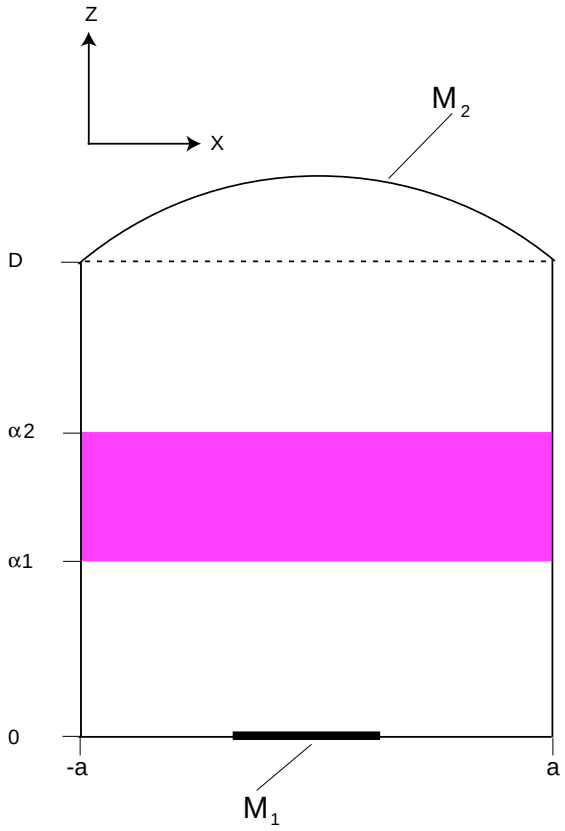

Figure 4.3: Optical Cavity Geometry

The schematic shown in Figure 4.3 depicts two mirrors separated on the left by a value of D. The lower mirror is perfectly horizontal. The upper mirror is an arc of a circle with radius r.

We investigate the influence of the atomic gain function $f(x)$ on the propagating wave in the optical cavity. As an initial investigation, we specify a wave profile at $z = 0$ and propagate through the optical cavity with zero atomic gain. We then propagate the same initial wave profile though the optical cavity with a nonzero atomic gain function $f(x)$.

In the results that follow, we use the 99% rule to initially specify w_0 at the flat mirror M_1. We specify the half-length of the flat mirror at $z = 0$ and then determine w_0 according to

$$w_0 = \frac{2M_r}{\pi}, \tag{4.38}$$

where M_r is the half-length of the flat mirror.

The resulting initial condition we specify is of the form

$$u(x,0) = \frac{10}{q_0} \exp\left(\frac{-jkx^2}{2q_0}\right). \tag{4.39}$$

In the numerical results that follow, we designate the following values:

- D= 7.682,
- $r = 10$,
- $M_r = 1$,
- $n = 1$,
- k = 55,
- $a = 2.5$,
- $\alpha_1 = 3$,
- $\alpha_2 = 5$.

In each numerical experiment, the initial condition, atomic gain function $f(x)$, and the numerical solution after one round-trip through the optical cavity are presented. The untransformed and transformed Hermite-Gaussian expansions at the curved mirror are also presented. In addition, a plot illustrating the difference between the Hermite-Gaussian expansion and the Crank-Nicholson solution at $z = D$ is shown. Fifteen Hermite-Gaussian modes are used to expand the solution at the curved mirror.

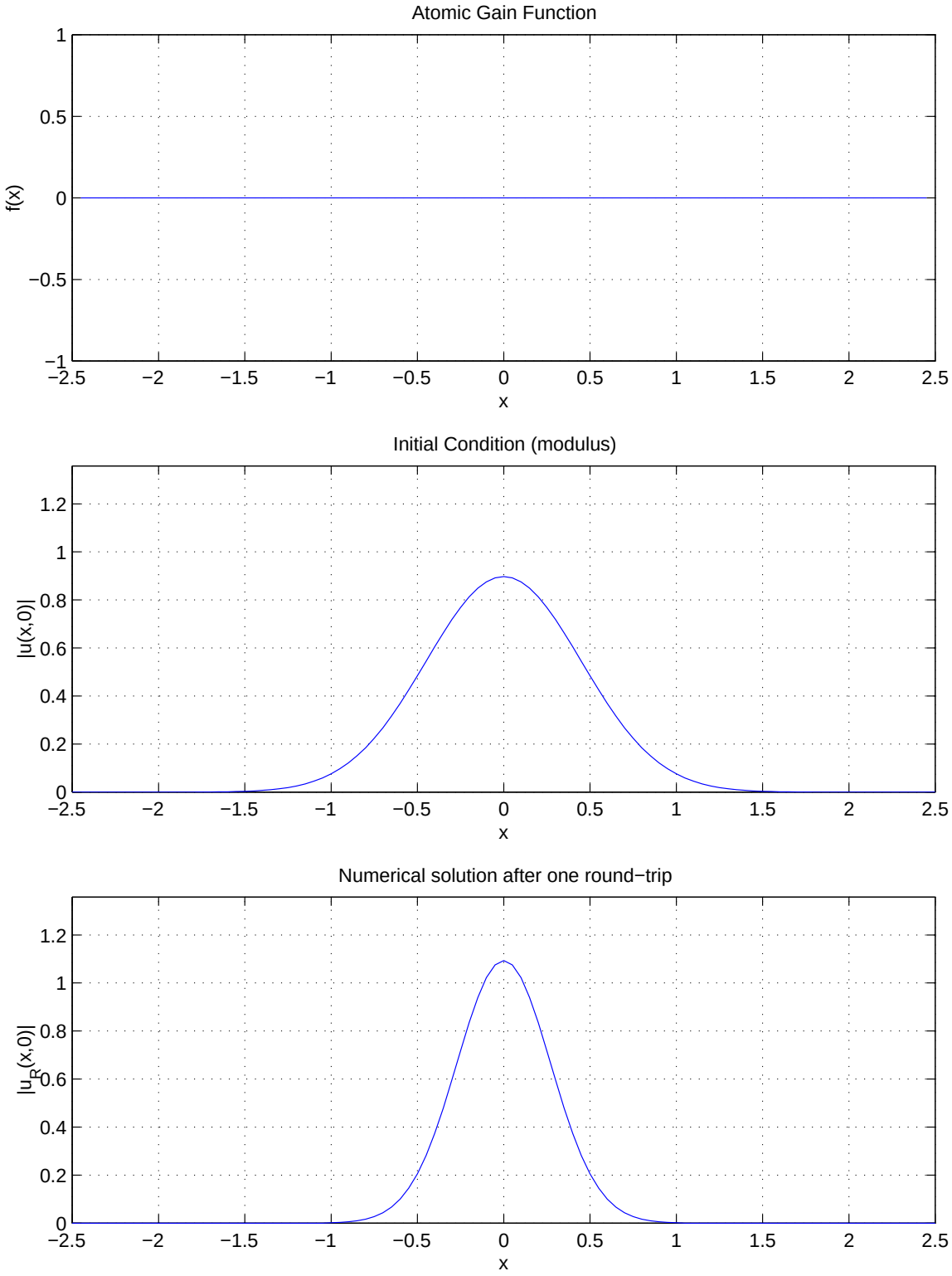

Figure 4.4: Propagation with zero atomic gain.

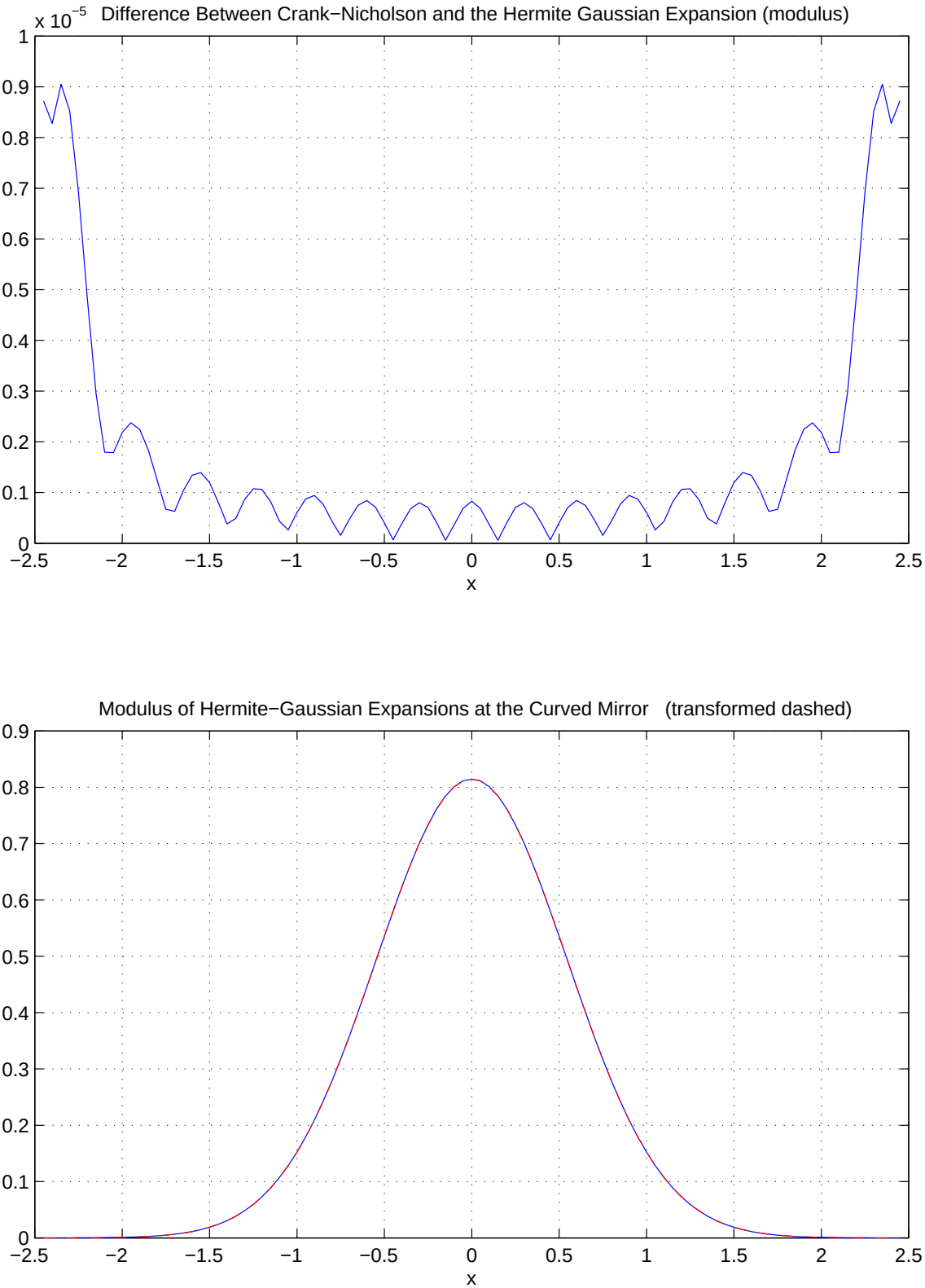

Figure 4.5: Propagation with zero atomic gain (continued).

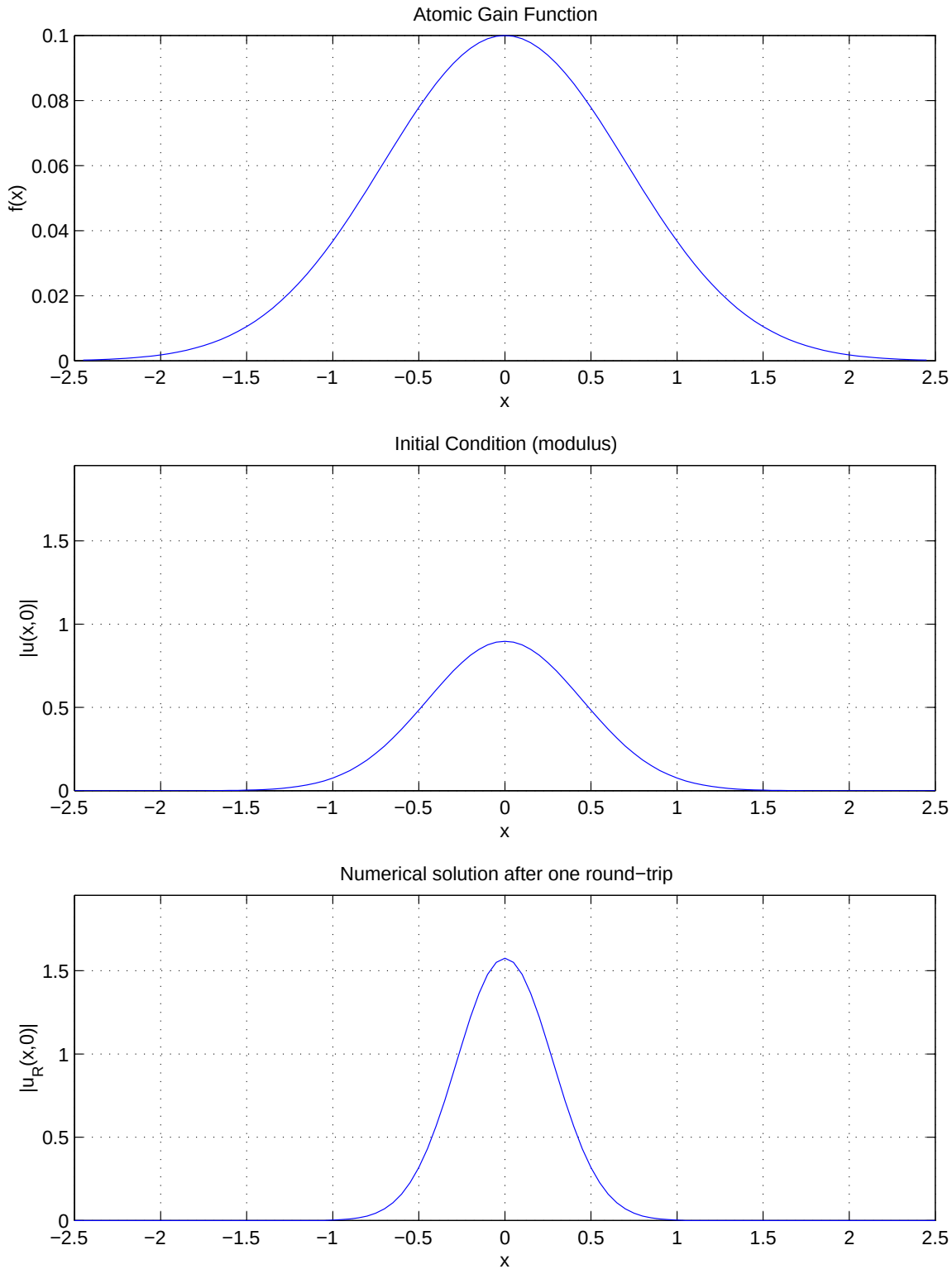

Figure 4.6: Propagation with $f(x) = .1e^{-x^2}$.

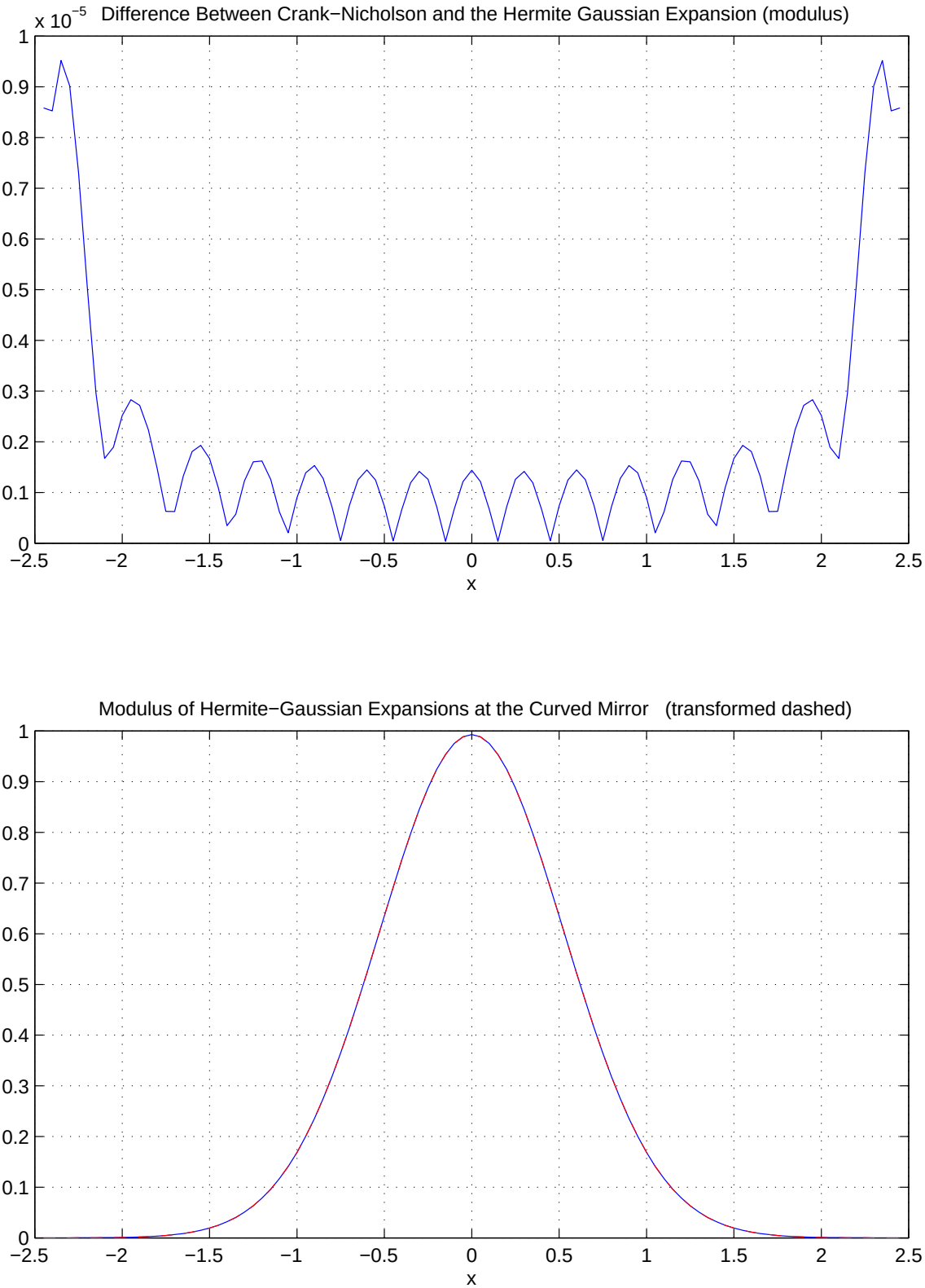

Figure 4.7: Propagation with $f(x) = .1e^{-x^2}$ (continued).

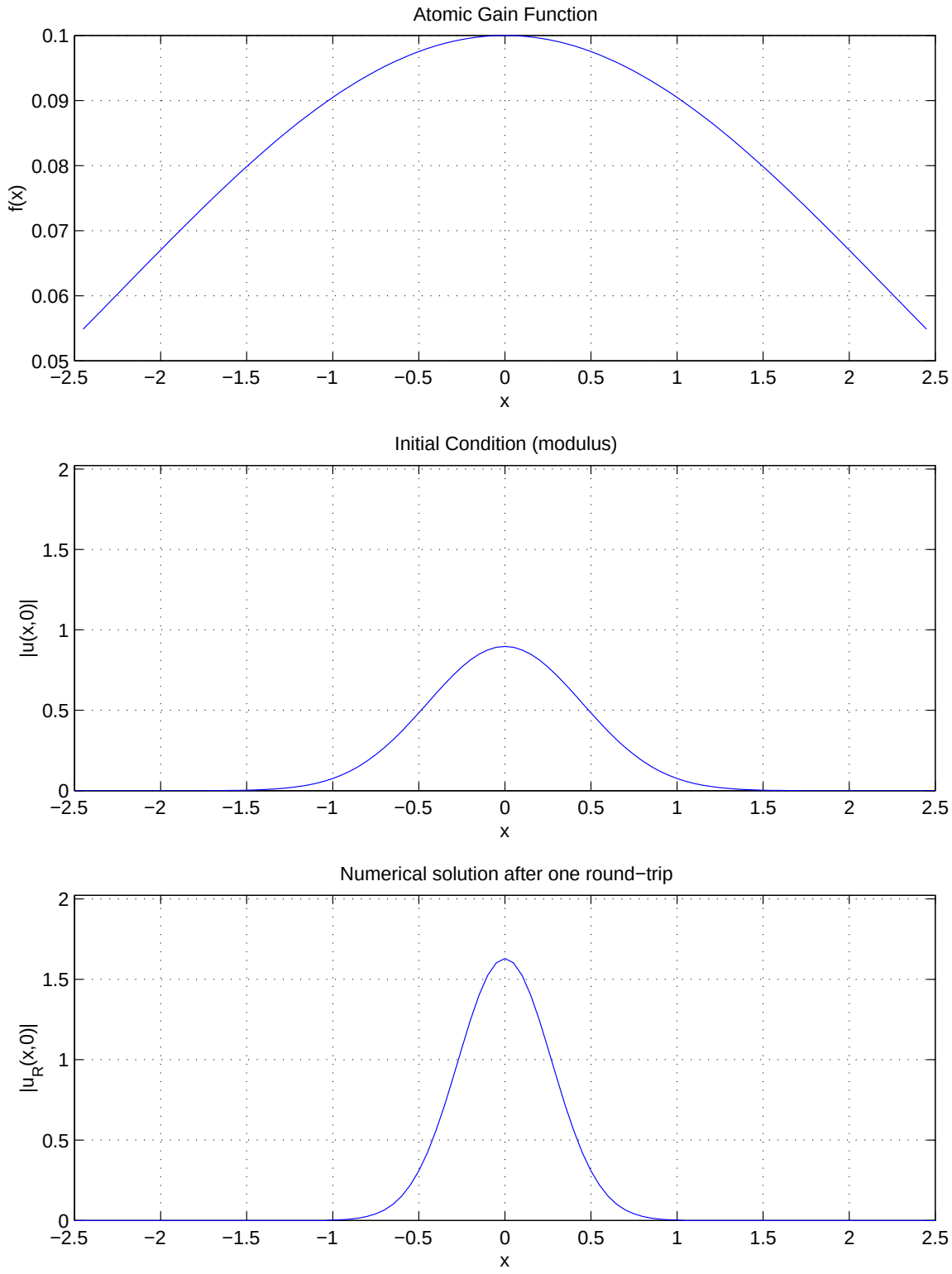

Figure 4.8: Propagation with $f(x) = .1e^{\frac{-x^2}{10}}$.

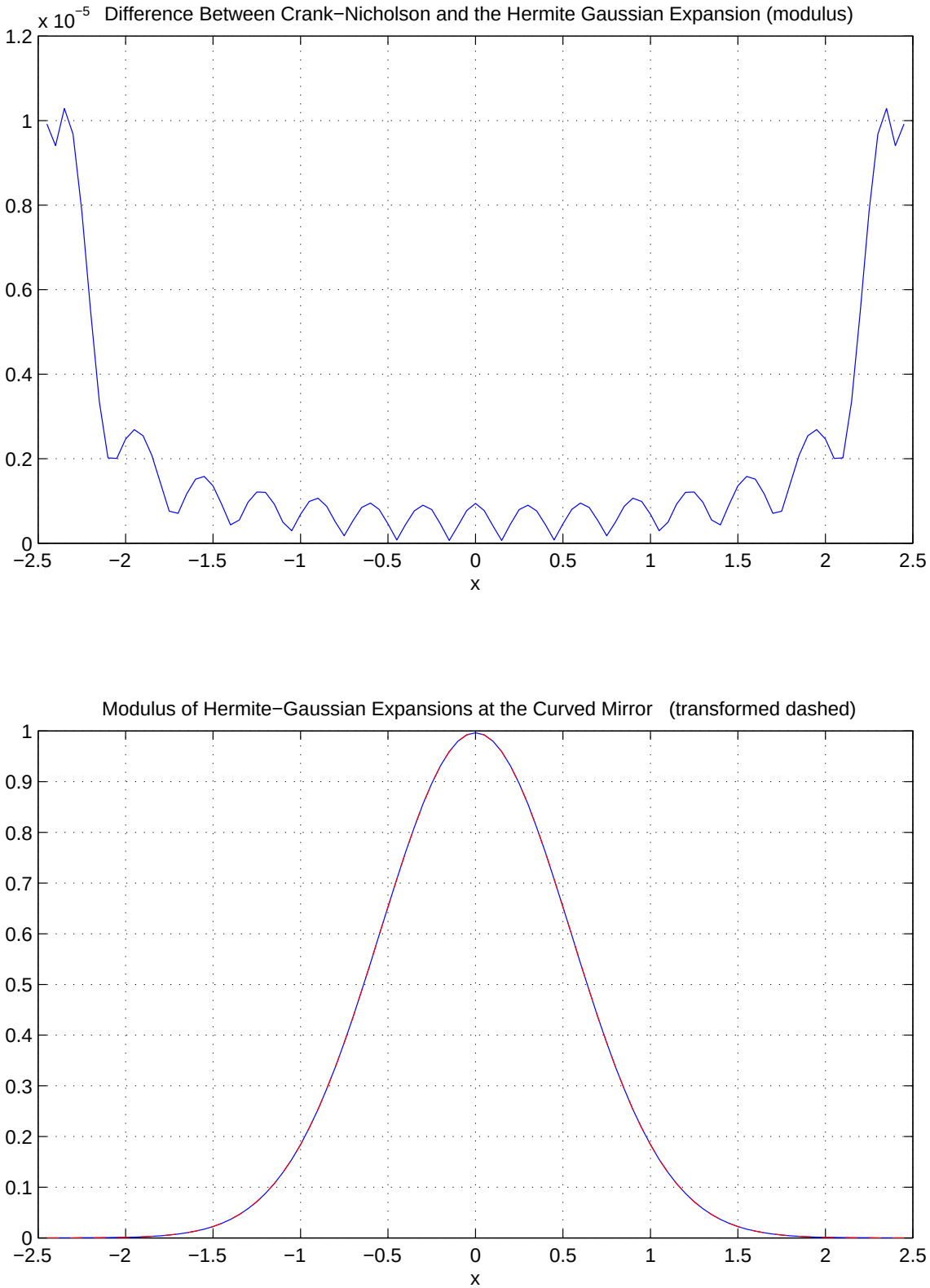

Figure 4.9: Propagation with $f(x) = .1e^{\frac{-x^2}{10}}$ (continued).

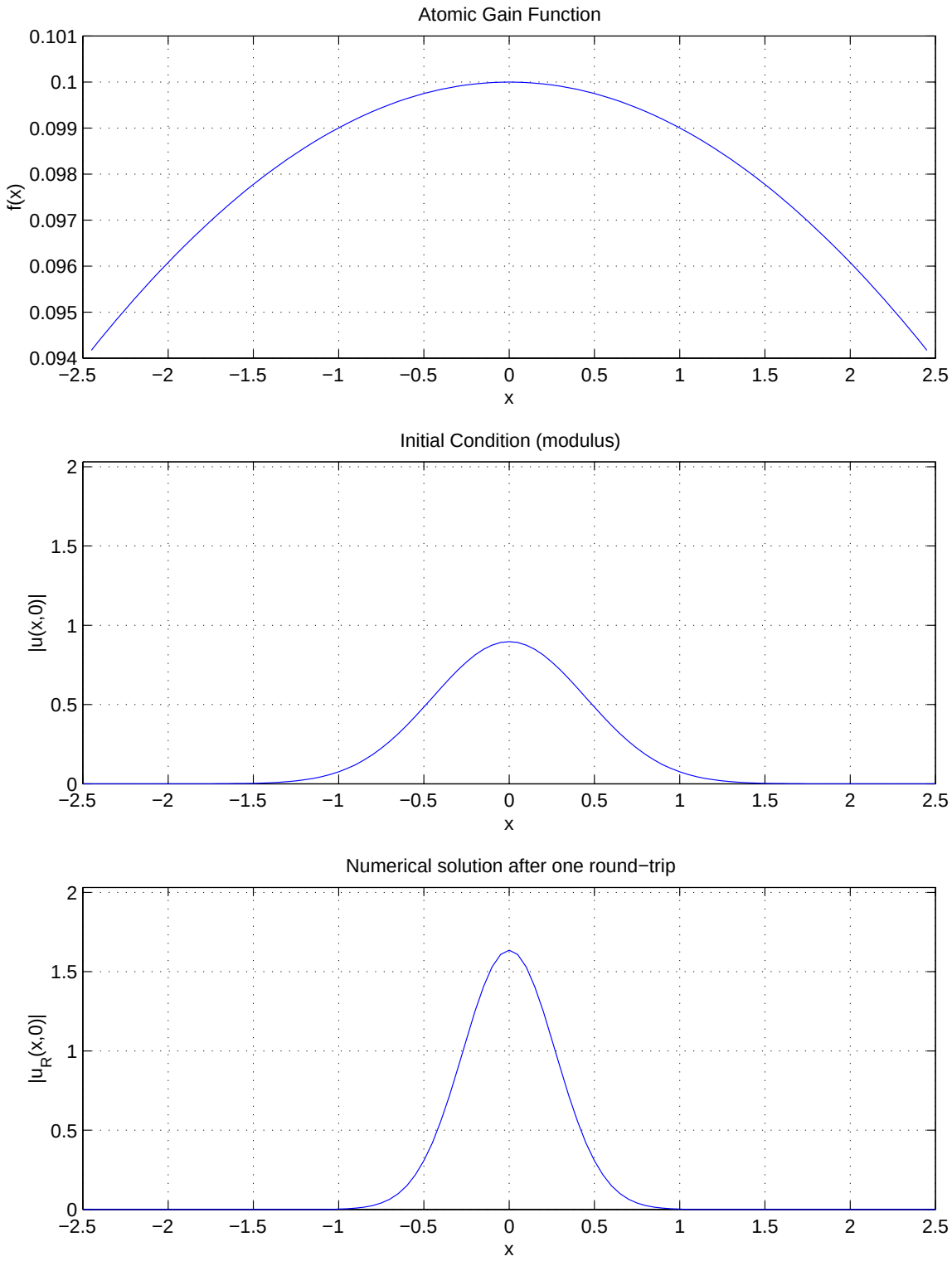

Figure 4.10: Propagation with $f(x) = .1e^{\frac{-x^2}{100}}$.

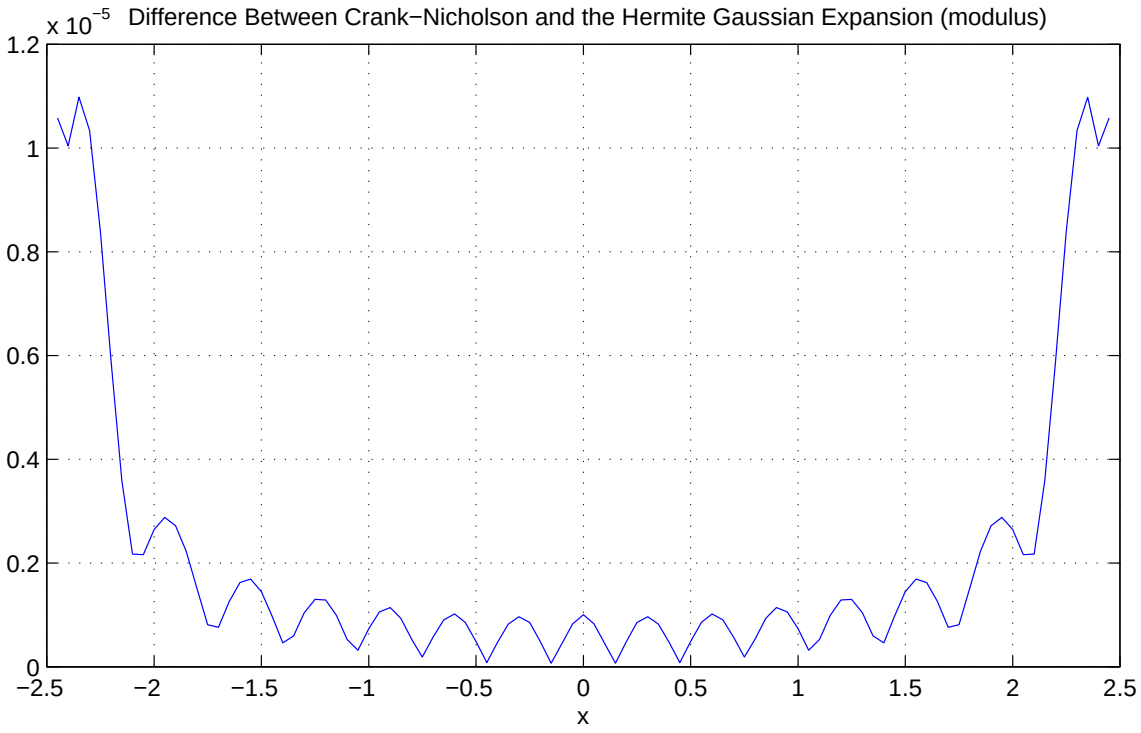

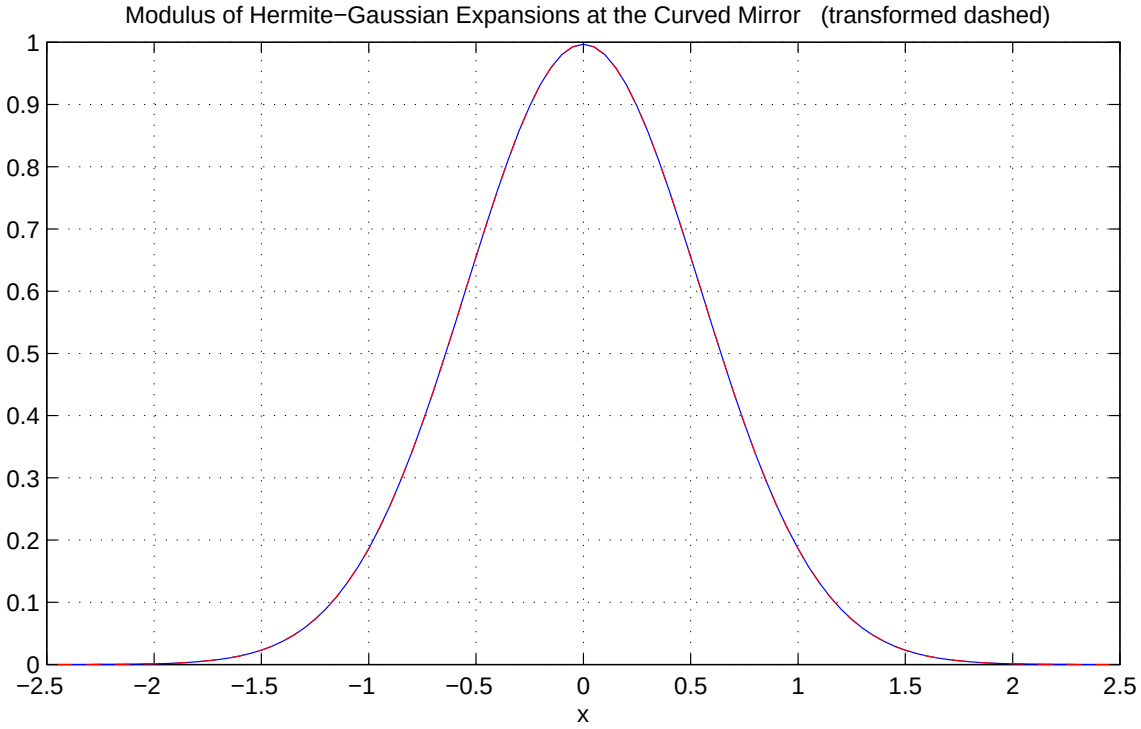

Figure 4.11: Propagation with $f(x) = .1e^{\frac{-x^2}{100}}$ (continued).

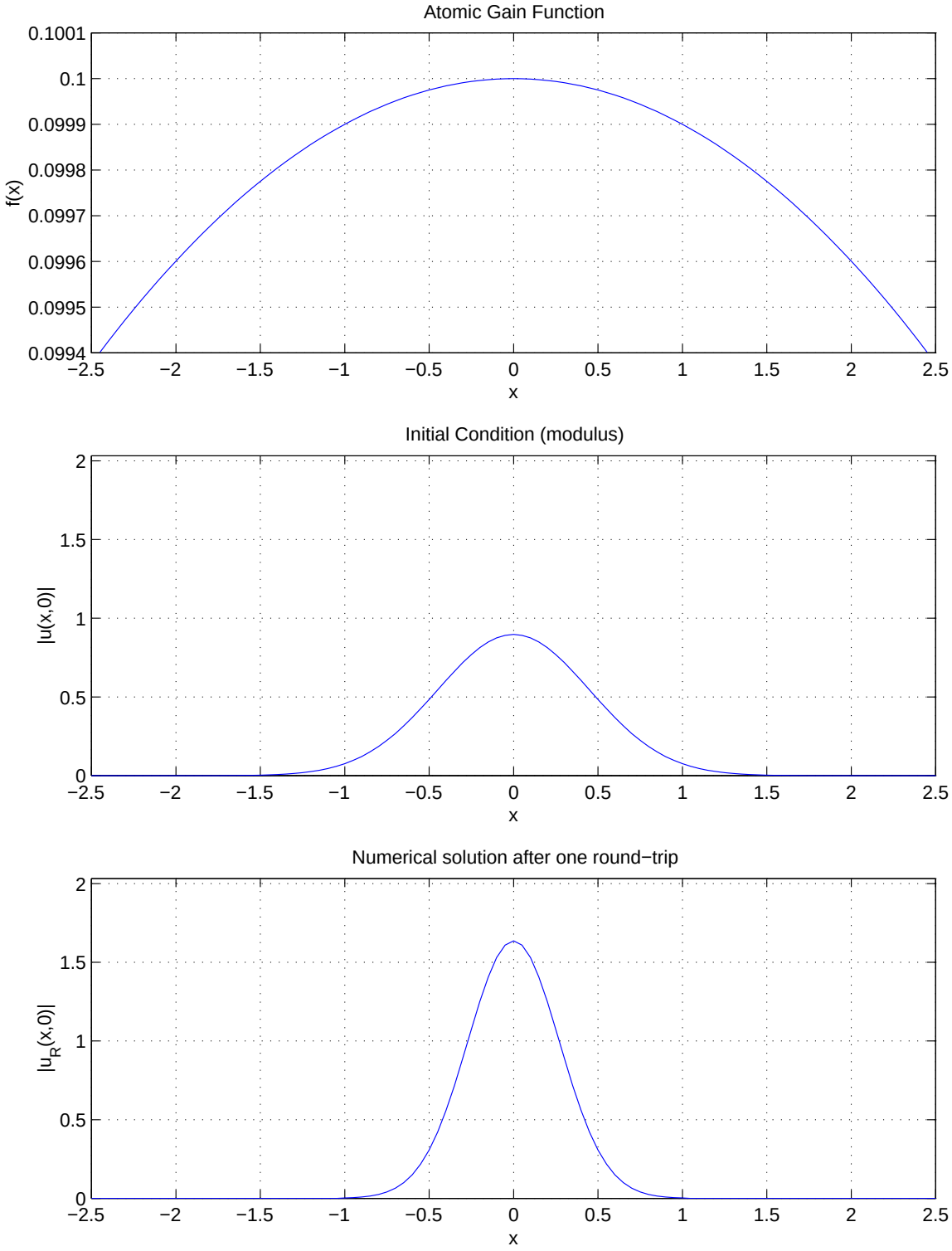

Figure 4.12: Propagation with $f(x) = .1e^{\frac{-x^2}{1000}}$.

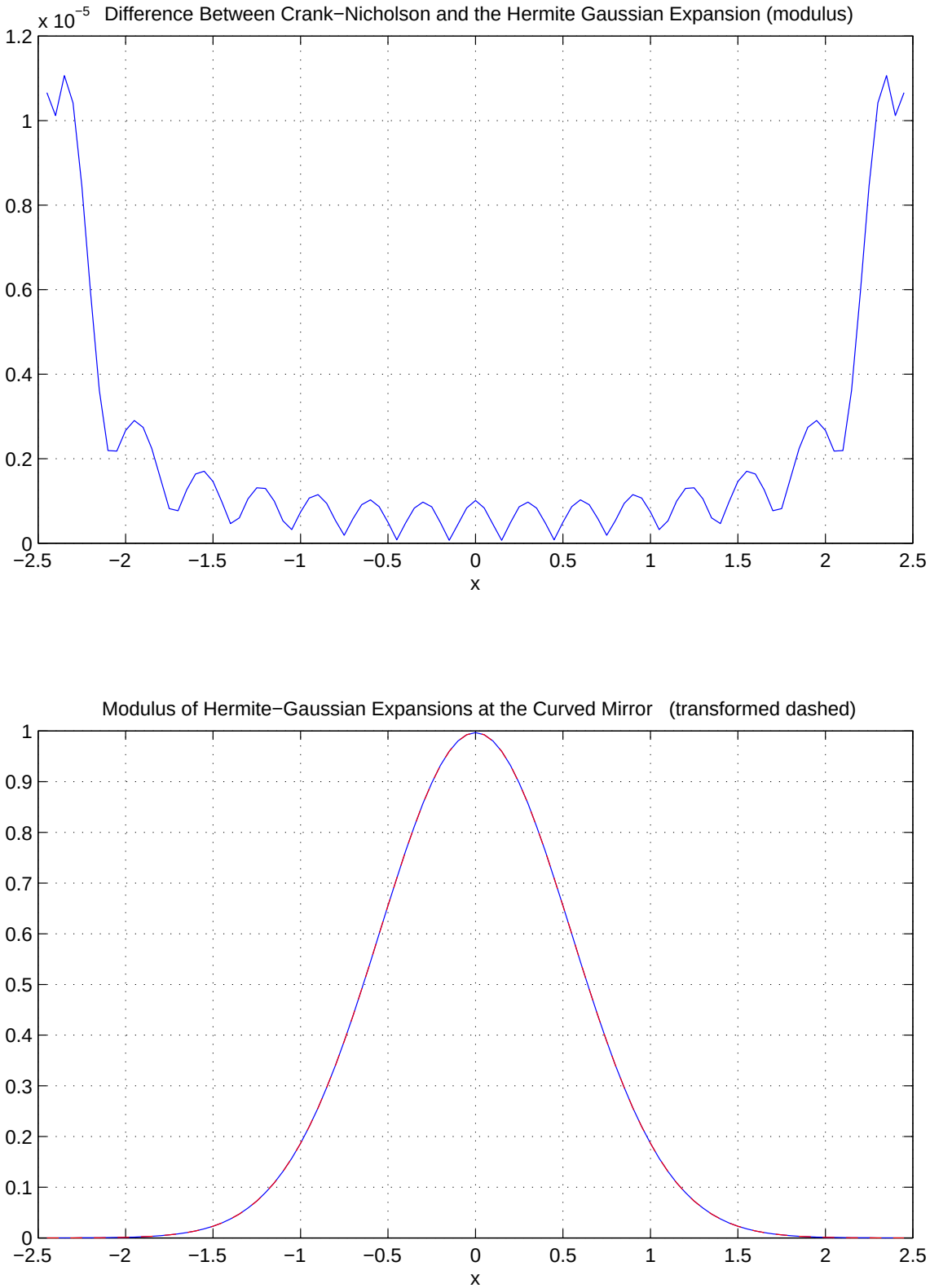

Figure 4.13: Propagation with $f(x) = .1e^{\frac{-x^2}{1000}}$ (continued).

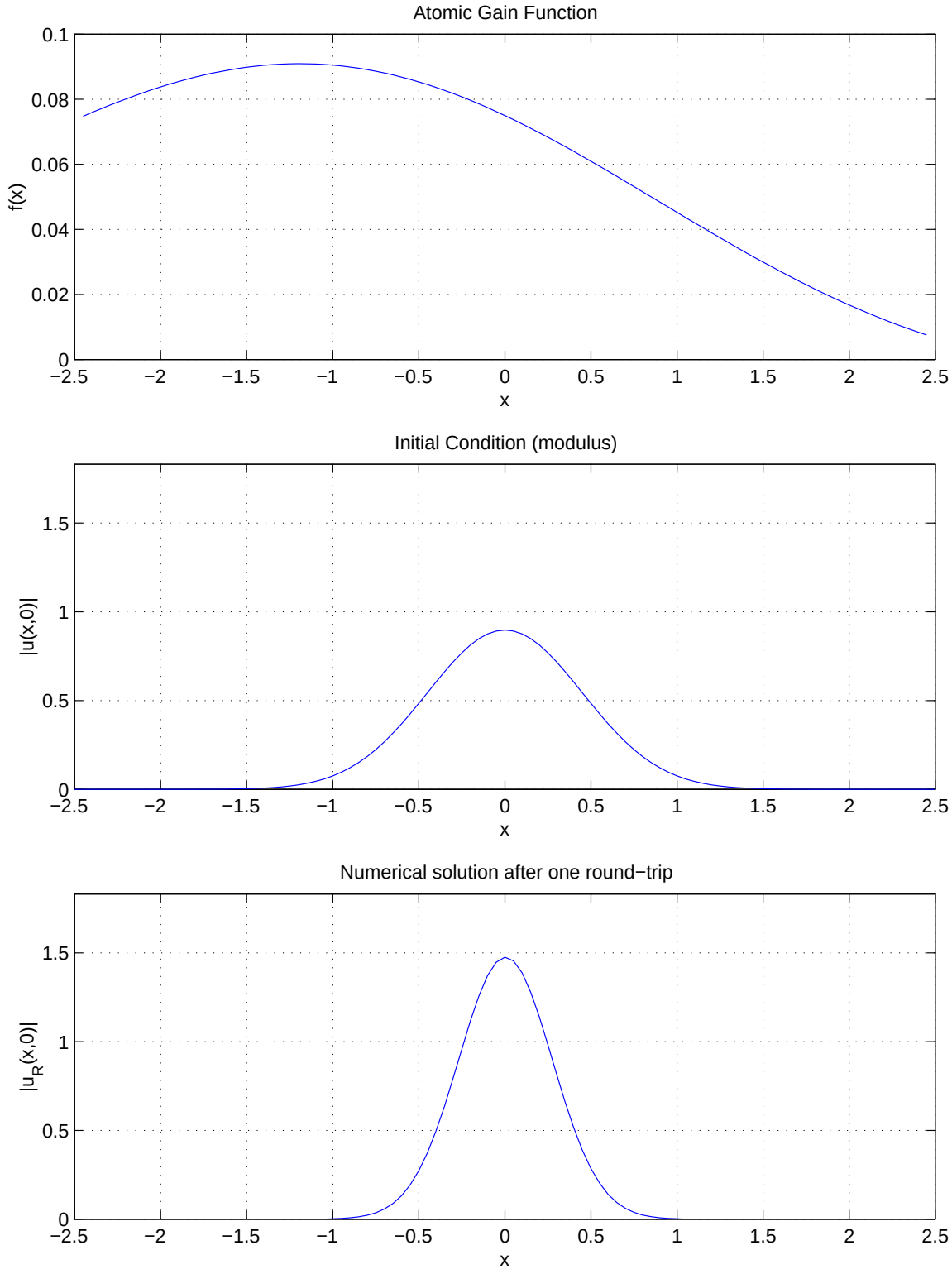

Figure 4.14: Propagation with $f(x) = \frac{3-x}{40} e^{\frac{-x^2}{10}}$.

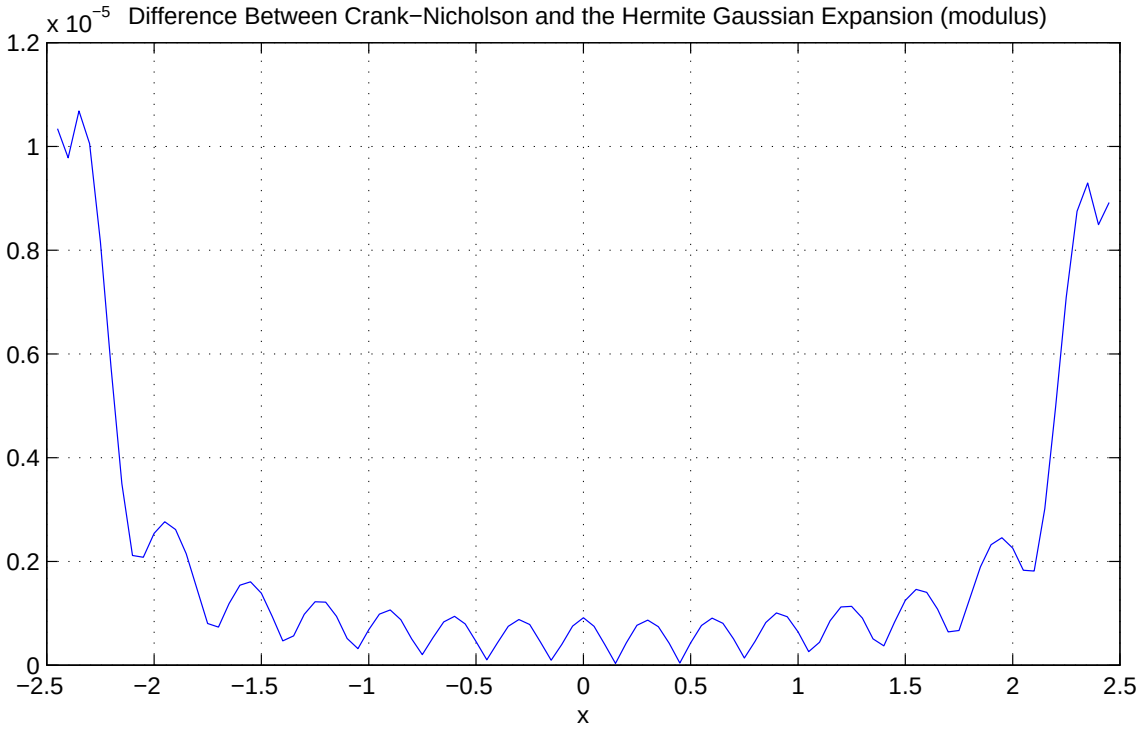

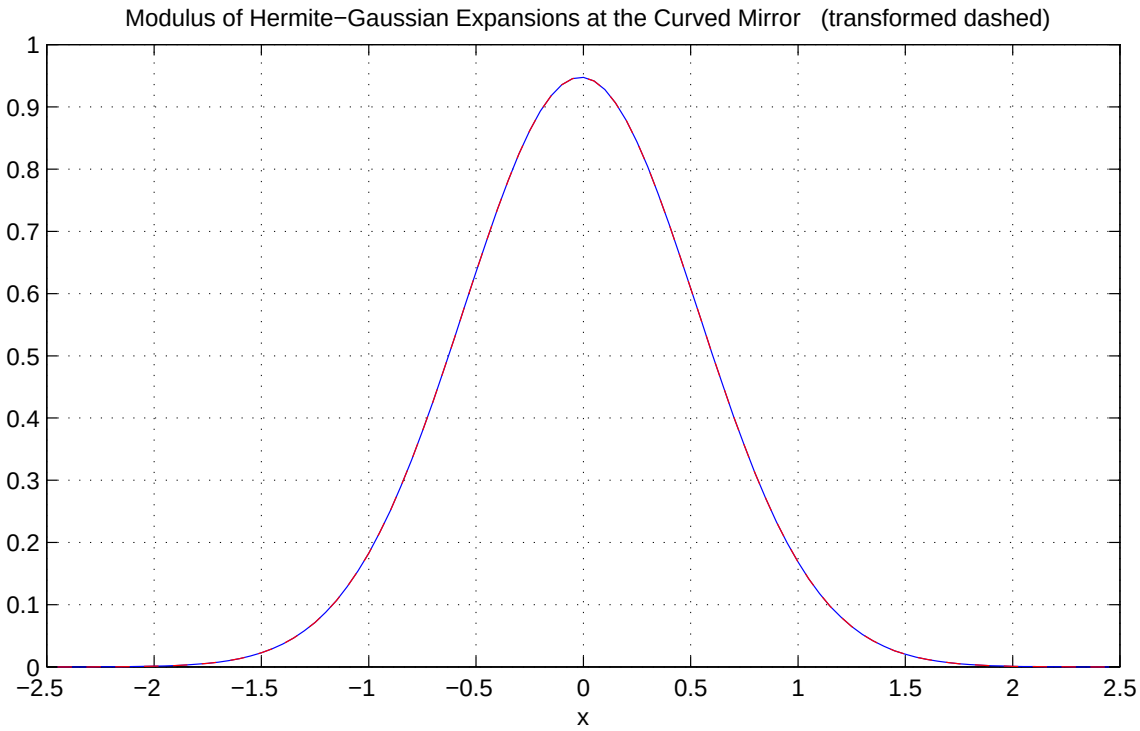

Figure 4.15: Propagation with $f(x) = \frac{3-x}{40} e^{\frac{-x^2}{10}}$ (continued).

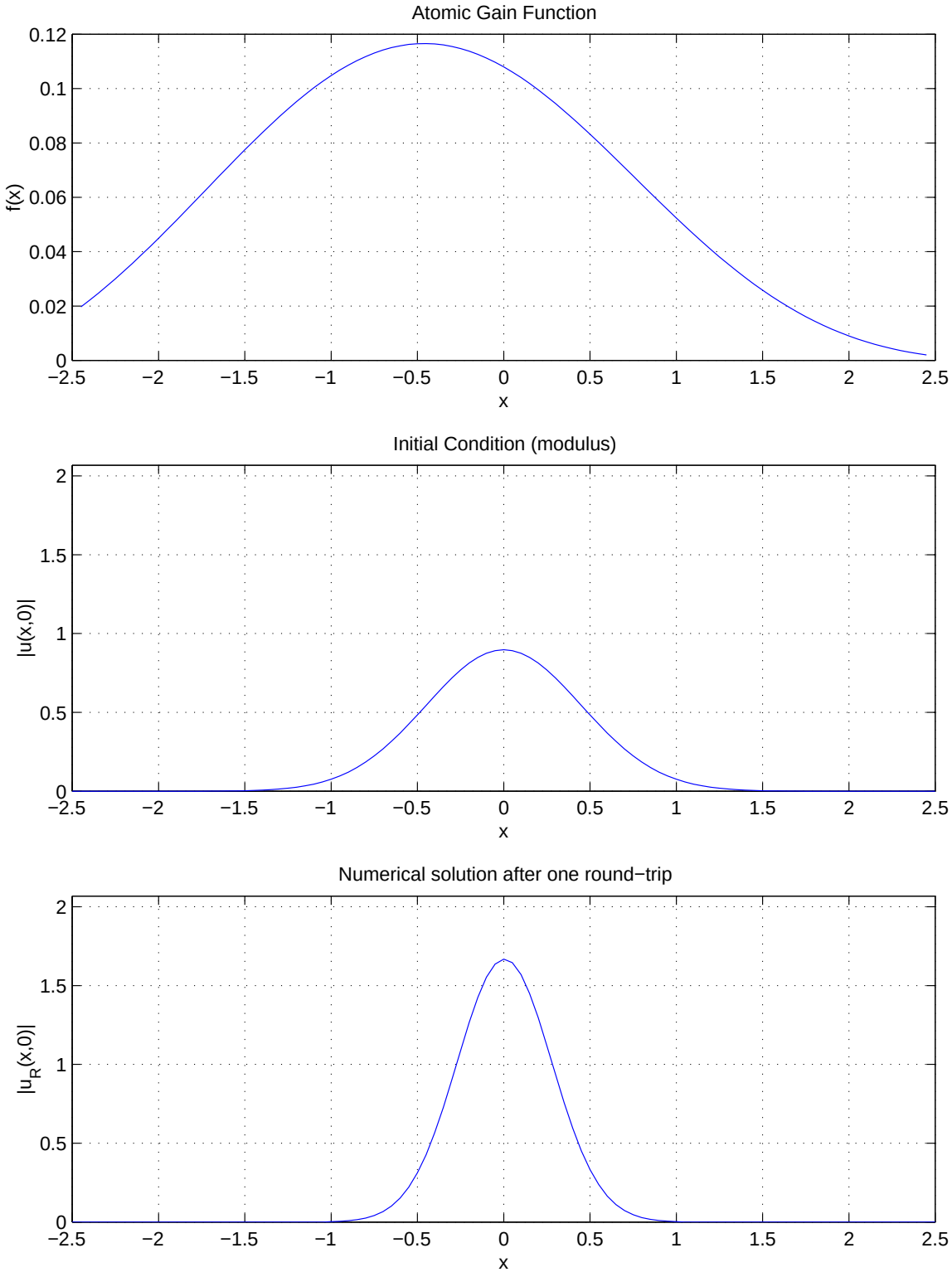

Figure 4.16: Propagation with $f(x) = \frac{(3-x)(9-x^2)}{250} e^{\frac{-x^2}{5}}$.

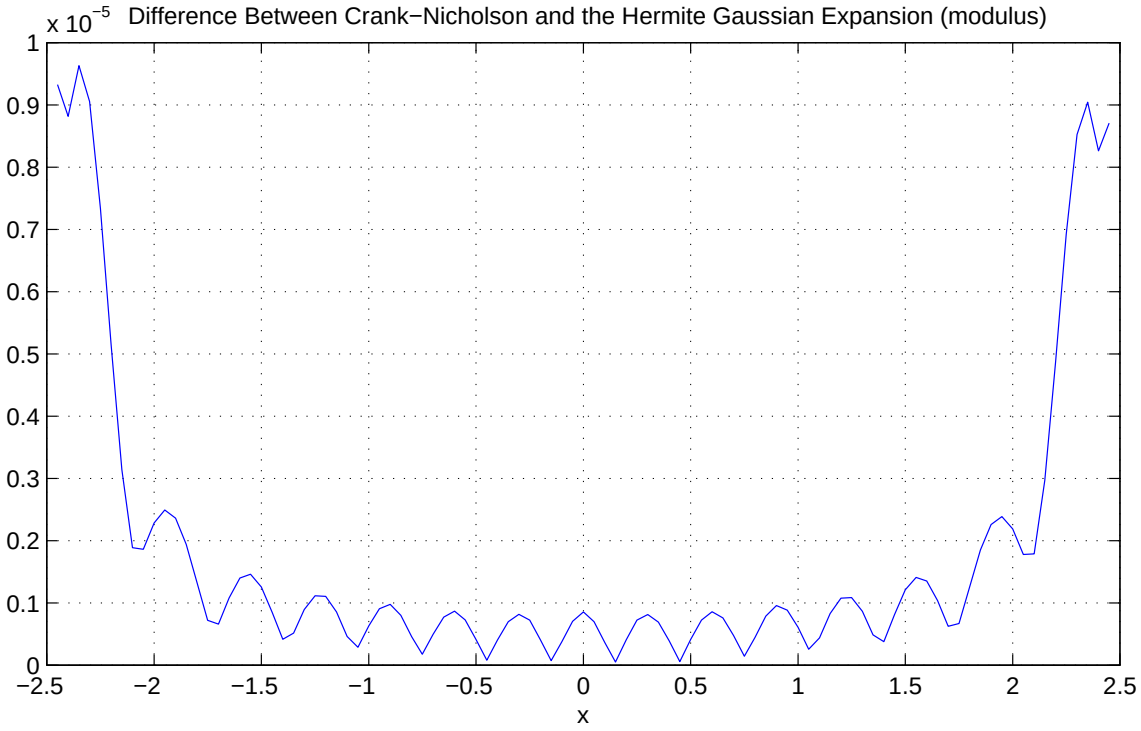

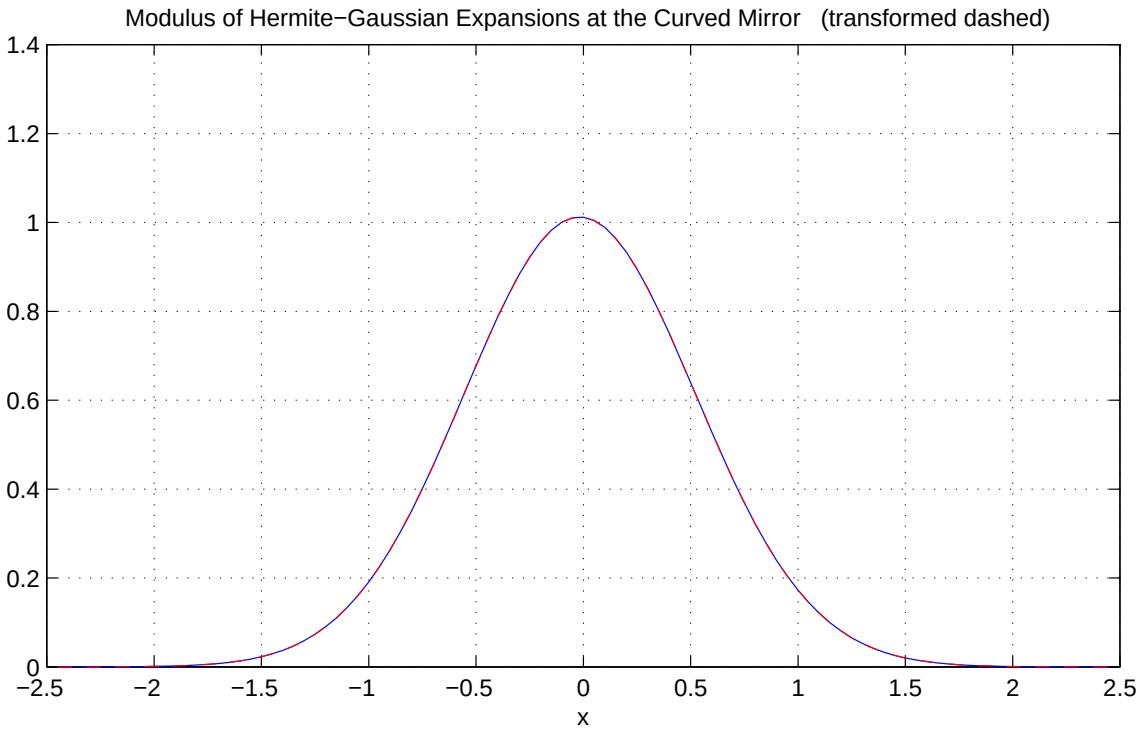

Figure 4.17: Propagation with $f(x) = \frac{(3-x)(9-x^2)}{250} e^{\frac{-x^2}{5}}$ (continued).

By examining the numerical results for the two dimensional optical cavity, the influence of the curved mirror on the propagating wave is apparent. As expected, the curvature of the outer mirror tends to focus the propagating wave. In all of the results, the Gaussian beam has a more slender profile after propagating back and forth through the optical cavity than it did initially. Moreover, the amplitude of the wave is increased.

Utilizing the results of propagation in the presence of zero gain as a reference point, the influence of the atomic gain function $f(x)$ on the propagating wave can be determined. Recall that the energy $\mathcal{E}_u(z)$ associated with a wave profile $u(x,z)$ is given by

$$\mathcal{E}_u(z) = \int_{-\infty}^{\infty} |u(x,z)|^2 dx. \tag{4.40}$$

The energies of the wave profiles obtained numerically are given in Table 4.1 for several locations in the optical cavity.

Table 4.1: Wave Profile Energies for the Two Dimensional Optical Cavity

Gain Function $f(x)$	$\mathcal{E}_u(0)$	$\mathcal{E}_u(D)$	$\mathcal{E}_g(D)$	$\mathcal{E}_g(0)$	$\mathcal{E}_{u_R}(0)$
0	0.6423	0.6423	0.6423	0.6423	0.5781
$.1e^{-x^2}$	0.6423	0.9252	0.9252	1.3663	1.2296
$.1e^{-\frac{x^2}{10}}$	0.6423	0.9571	0.9571	1.4305	1.2874
$.1e^{-\frac{x^2}{100}}$	0.6423	0.9610	0.9610	1.4382	1.2944
$.1e^{-\frac{x^2}{1000}}$	0.6423	0.9614	0.9614	1.4390	1.2951
$\frac{3-x}{40}e^{-\frac{x^2}{10}}$	0.6423	0.8667	0.8667	1.1723	1.0551
$\frac{(3-x)(9-x^2)}{250}e^{-\frac{x^2}{5}}$	0.6423	0.9795	0.9795	1.5087	1.3578

As can be seen from the data in Table 4.1, the numerical results agree with the theoretical results presented in Chapter 3. The Crank-Nicholson scheme preserves the group structure of the system when $f(x) = 0$. In particular, as can be seen in Table 4.1, energy is conserved in the case of propagation with zero atomic gain. The initial energy of the propagating wave is identical to the energy of the wave incident on the outcoupling mirror. As a result, the norm in $L_2(\Omega)$ is preserved. However, the addition of a positive atomic gain function yields an increase in the energy of the propagating wave. Thus, the numerical results also agree with the theoretical result given by Theorem 3.1.3 describing the influence of atomic gain on the energy of a wave profile. In addition, the shape of the gain function influences the quantity and location of energy increase in the wave profile. In all of the cases presented, the curvature of the outer mirror focused the propagating wave in such a way that the vast majority of the energy of the returning wave is incident on the outcoupling mirror. As a

result, a negligible amount of energy is absorbed by the optical cavity wall. The truncation of $g(x, 0)$ led to practically no energy loss.

In this work, the outer mirror is modeled as being completely reflective. As a result, there should be no energy loss at the curved mirror. In other words, the transformation of the complex beam parameter $q(z)$ due to reflection should not influence the energy of the wave profile at the curved mirror. In all of the numerical results, the modulus of the solution $u(x, D)$ and the modulus of the transformed solution $g(x, D)$ are virtually identical. In particular, the maximum difference between $|u(x, D)|$ and $|g(x, D)|$ is on the order of 10^{-16} in every result presented. As a result, the energy associated with the wave profile is virtually unchanged by reflection from the curved mirror.

Finally, recall that the Hermite-Gaussian modes are obtained by way of the paraxial wave equation in free space. However, we obtained satisfactory results utilizing the Hermite-Gaussian modes in the case of propagation in the presence of nonzero gain. The error introduced due to expanding the propagating wave in terms of the Hermite-Gaussian modes is on the order of 10^{-5} in the case of zero atomic gain. The error introduced via the expansion remained on the order of 10^{-5} when a nonzero gain function $f(x)$ was present.

In all of the results presented, the error introduced by the Hermite-Gaussian expansion is slightly greater along the transverse boundary. Recall that the support of the Hermite-Gaussian modes increases with n. In addition, as n is increased, the maximum amplitude of the Hermite-Gaussian mode is located at an increasing distance from the optical axis. In our partial differential equation model, it is specified that the solution remain at zero along the transverse boundary. As a result, the numerical approximation obtained by the Crank-Nicholson scheme satisfies the zero boundary data specified by the model. Any error introduced in the numerical integration procedure needed to expand the Crank-Nicholson solution in terms of the Hermite-Gaussian modes will lead to the expansion being slightly nonzero along the transverse boundary. As a result, the difference between the Crank-Nicholson solution and the Hermite-Gaussian expansion will be greatest along the transverse boundary.

Chapter 5

Three Dimensional Optical Cavity

As demonstrated by the numerical results of the previous chapter, it appears that Gaussian beam reflection is being correctly predicted by our model. Thus, we now investigate electromagnetic wave propagation through a three-dimensional optical cavity. Doing so allows us to investigate laser intensity in geometries similar to the COIL optical cavity. The methods described previously are analogous to those we apply to the 3D case. A uniform finite difference grid is constructed on the physical domain. However, we now have two transverse directions, namely x and y. As a result, the matrix equation used in the iterations is more complex. In addition, the Hermite-Gaussian expansion at the spherical mirror is more complicated in the case of two transverse directions.

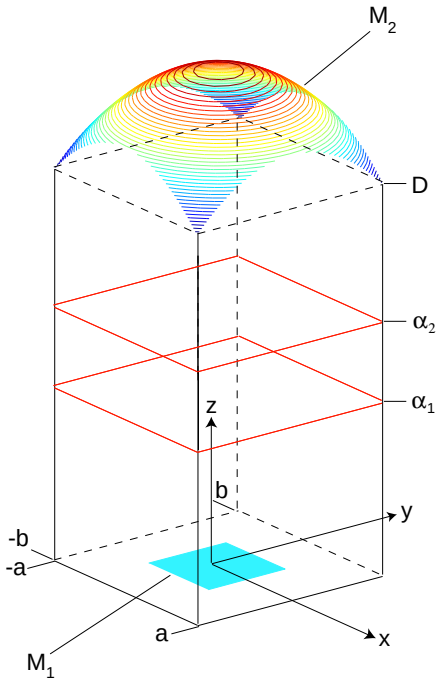

Figure 5.1: Three Dimensional Optical Cavity

In the work presented in this chapter, x values are in the interval $[-a, a]$. Similarly, y values are in the interval $[-b, b]$. We also specify D to be the distance between the mirrors.

As before, we specify a real-valued atomic gain function $\alpha(x, y, z)$ by

$$\alpha(x, y, z) = \begin{cases} f(x, y) & \text{if } z \in [\alpha 1, \alpha 2]; \\ 0, & \text{otherwise.} \end{cases} \tag{5.1}$$

Finally, for notational convenience, we denote s by

$$s = \sqrt{-1}. \tag{5.2}$$

5.1 Propagation Toward Increasing z

We proceed similarly as in the case of the two dimensional optical cavity. First, we consider the case of propagation toward increasing values of z. A uniform finite difference grid is constructed on the rectangle $[-a, a] \times [-b, b] \times [0, D]$. The step-size in the z direction is denoted by Δz. The step-size in the x and y directions is denoted by h. As we are interested in propagation toward increasing values of z, our finite difference scheme must approximate the initial boundary value problem for upward propagation given by

$$\frac{\partial u}{\partial z} = -\frac{s}{2k}\left(\frac{\partial^2 u}{\partial x^2} + \frac{\partial^2 u}{\partial y^2}\right) + [\alpha(x, y, z) - sk(n-1)]u, \ (k > 0) \tag{5.3}$$

$$u(-a, y, z) = 0 = u(a, y, z), \tag{5.4}$$

$$u(x, -b, z) = 0 = u(x, b, z), \text{ and} \tag{5.5}$$

$$u(x, y, 0) = u_0(x, y, w_0). \tag{5.6}$$

As in the case of one transverse direction, the first order derivative in the z direction is approximated as

$$\frac{\partial}{\partial z}u(\cdot, \cdot, z) \approx \frac{u(\cdot, \cdot, z + \Delta z) - u(\cdot, \cdot, z)}{\Delta z}. \tag{5.7}$$

The second order derivatives in the transverse directions are approximated by

$$\frac{\partial^2}{\partial x^2}u(x, \cdot, \cdot) \approx \frac{u(x - h, \cdot, \cdot) - 2u(x, \cdot, \cdot) + u(x + h, \cdot, \cdot)}{h^2}, \text{ and} \tag{5.8}$$

$$\frac{\partial^2}{\partial y^2}u(\cdot, y, \cdot) \approx \frac{u(\cdot, y - h, \cdot) - 2u(\cdot, y, \cdot) + u(\cdot, y + h, \cdot)}{h^2}. \tag{5.9}$$

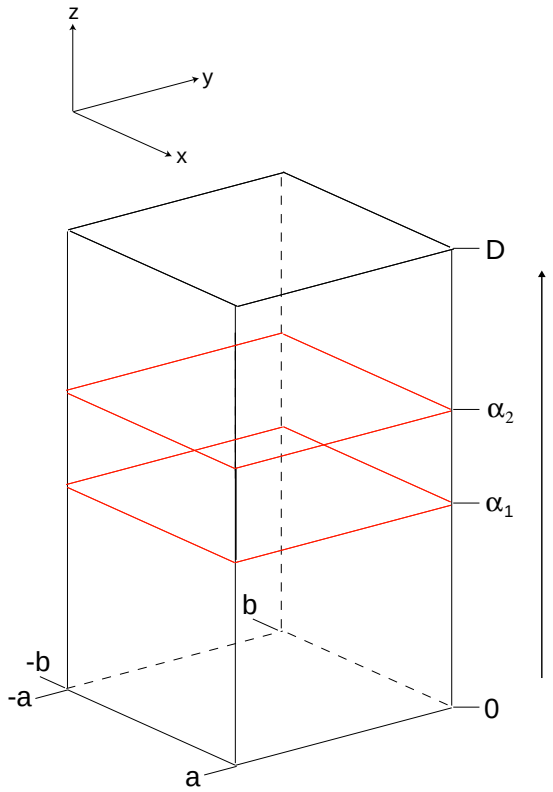

Figure 5.2: Three Dimensional Optical Cavity, Upward Propagation

We proceed as in Chapter 4. An explicit finite difference approximation to the initial boundary value problem is constructed. The analogous implicit scheme is also presented. The explicit and implicit schemes are then added resulting in the semi-implicit Crank-Nicholson scheme. The indices used in the following derivation are i, j, and n. They are indices for the x, y, and z directions, respectively.

The explicit scheme is formed by substituting (5.7) - (5.9) into the upward paraxial wave equation (5.3) and evaluating the right-hand-side at $z = z_n$. At each evaluation point (x_i, y_j, z_n), the resulting explicit finite difference equation is of the form

$$u_{i,j}^{n+1} = u_{i,j}^n - \frac{s\Delta z}{2kh^2}(u_{i-1,j}^n - 2u_{i,j}^n + u_{i+1,j}^n + u_{i,j-1}^n - 2u_{i,j}^n + u_{i,j+1}^n) + \Delta z(\alpha_{i,j}^n - sk(n-1))u_{i,j}^n. \tag{5.10}$$

Evaluating the right hand side of (5.10) at $z = z_{n+1}$ results in an implicit finite difference scheme of the form

$$u_{i,j}^{n+1} = u_{i,j}^n - \frac{s\Delta z}{2kh^2}(u_{i-1,j}^{n+1} - 2u_{i,j}^{n+1} + u_{i+1,j}^{n+1} + u_{i,j-1}^{n+1} - 2u_{i,j}^{n+1} + u_{i,j+1}^{n+1}) + \Delta z(\alpha_{i,j}^{n+1} - sk(n-1))u_{i,j}^{n+1}. \tag{5.11}$$

To simplify the expressions given in (5.10) and (5.11), we introduce the quantities ν and $c_{i,j}^n$ given by

$$\nu = \frac{s\Delta z}{2kh^2}, \text{ and} \tag{5.12}$$

$$c_{i,j}^n = \Delta z(\alpha_{i,j}^n - sk(n-1)). \tag{5.13}$$

The explicit and implicit schemes given by (5.10) and (5.11) are then written as

$$u_{i,j}^{n+1} = -\nu u_{i,j-1}^n - \nu u_{i,j+1}^n + (1 + 4\nu + c_{i,j}^n)u_{i,j}^n - \nu u_{i-1,j}^n - \nu u_{i+1,j}^n, \text{ and} \tag{5.14}$$

$$\nu u_{i,j-1}^{n+1} + \nu u_{i,j+1}^{n+1} + \nu u_{i-1,j}^{n+1} + \nu u_{i+1,j}^{n+1} + (1 - 4\nu - c_{i,j}^{n+1})u_{i,j}^{n+1} = u_{i,j}^n. \tag{5.15}$$

Adding (5.14) and (5.15) results in the Crank-Nicholson finite difference scheme of the form

$$\begin{aligned}[\nu u_{i-1,j}^{n+1} + \nu u_{i+1,j}^{n+1} + (2 - 4\nu - c_{i,j}^{n+1})u_{i,j}^{n+1}] + [\nu u_{i,j-1}^{n+1}] + [\nu u_{i,j+1}^{n+1}] = \\ [-\nu u_{i-1,j}^n - \nu u_{i+1,j}^n + (2 + 4\nu + c_{i,j}^n)u_{i,j}^n] - [\nu u_{i,j-1}^n] - [\nu u_{i,j+1}^n].\end{aligned} \tag{5.16}$$

We now present a convergence theorem for the Crank-Nicholson scheme above in the case of zero atomic gain.

THEOREM 5.1.1
In the case of zero atomic gain, the Crank-Nicholson scheme given by (5.16) is unconditionally convergent.

Proof.

Consistency of (5.16) follows from a routine Taylor series expansion.

To determine the stability of (5.16), we construct a Fourier mode solution of the form $U^n = \eta^n e^{s(\theta+\beta)}$, where η is the amplification factor. Substituting the Fourier mode into the Crank-Nicholson scheme results in an expression for η of the form

$$\begin{aligned}\eta[\nu(e^{-s\theta} + e^{s\theta} + e^{-s\beta} + e^{s\beta}) + (2 - 4\nu + c_{i,j}^{n+1})] = \\ -[\nu(e^{-s\theta} + e^{s\theta} + e^{-s\beta} + e^{s\beta}) - (2 + 4\nu + c_{i,j}^n)].\end{aligned} \tag{5.17}$$

Utilizing the identity, $e^{s\theta} = \cos\theta + s\sin\theta$, we can rewrite (5.17) as

$$\eta\left[\nu(\cos\theta + \cos\beta - 2) + \left(1 - \frac{c_{i,j}^{n+1}}{2}\right)\right] = -\left[\nu(\cos\theta + \cos\beta - 2) - \left(1 + \frac{c_{i,j}^n}{2}\right)\right]. \tag{5.18}$$

Using the definitions of ν and $c_{i,j}^n$ allows us to separate (5.18) into its real and complex components. The resulting expression for η is of the form

$$\eta = -\frac{s\left[\frac{\Delta z}{2kh^2}(\cos\theta + \cos\beta - 2) + \Delta z s k(n-1)\right] - 1 - \frac{\Delta z \alpha_{i,j}^n}{2}}{s\left[\frac{\Delta z}{2kh^2}(\cos\theta + \cos\beta - 2) + \Delta z s k(n-1)\right] + 1 - \frac{\Delta z \alpha_{i,j}^{n+1}}{2}}. \tag{5.19}$$

In the case of zero atomic gain, $\alpha_{i,j}^n = \alpha_{i,j}^{n+1} = 0$. Thus, in the case of zero atomic gain, the amplification factor satisfies

$$|\eta| = 1. \tag{5.20}$$

Therefore, by the Lax Equivalence Theorem, the Crank-Nicholson scheme given by (5.16) is unconditionally convergent in the case of zero atomic gain. □

As in the case of the two dimensional optical cavity, the addition of positive gain may lead to the modulus of the amplification factor η being much greater than one. As can be seen in (5.19), an atomic gain function with large magnitude requires a reduction in the step size Δz in order to ensure that errors introduced by the numerical scheme do not dramatically increase. As mentioned earlier, in this work the product $\Delta z \max(\alpha(x,y,z))$ is on the order of 10^{-3}. As a result, the modulus of the amplification factor is still very close to one.

To further simplify the Crank-Nicholson scheme, we define the quantities $\theta_{i,j}^n$ and $\beta_{i,j}^n$ as

$$\theta_{i,j}^n = 2 - 4\nu - c_{i,j}^n, \text{ and} \tag{5.21}$$

$$\beta_{i,j}^n = 2 + 4\nu + c_{i,j}^n. \tag{5.22}$$

The Crank-Nicholson scheme is then written simply as

$$\begin{aligned}[\nu u_{i-1,j}^{n+1} + \nu u_{i+1,j}^{n+1} + \theta_{i,j}^{n+1} u_{i,j}^{n+1}] + [\nu u_{i,j-1}^{n+1}] + [\nu u_{i,j+1}^{n+1}] = \\ [-\nu u_{i-1,j}^n - \nu u_{i+1,j}^n + \beta_{i,j}^n u_{i,j}^n] - [\nu u_{i,j-1}^n] - [\nu u_{i,j+1}^n].\end{aligned} \tag{5.23}$$

We are now in a position to incorporate the Dirichlet boundary conditions given by (5.4) and (5.5) into the Crank-Nicholson approximation (5.23). Define M as the number of evaluation points in the x direction. Similarly, specify N as the number of evaluation points in the y direction. Then, particular values of $i = 0$ and $i = M+1$ correspond to the transverse boundary in the x direction. As a result, the boundary data given by (5.4) is incorporated into (5.23) by specifying that

$$u_{0,\cdot}^n = 0 = u_{M+1,\cdot}^n \text{ and} \tag{5.24}$$

$$u_{0,\cdot}^{n+1} = 0 = u_{M+1,\cdot}^{n+1}\ . \tag{5.25}$$

In a similar fashion, particular values of $j = 0$ and $j = N+1$ correspond to the transverse boundary in the y direction. As a result, the boundary conditions given by (5.5) require the specification that

$$u^n_{\cdot,0} = 0 = u^n_{\cdot,N+1} \text{ and} \tag{5.26}$$

$$u^{n+1}_{\cdot,0} = 0 = u^{n+1}_{\cdot,N+1} \ . \tag{5.27}$$

We can now construct the overall matrix equation used in the iterations. Allow i to vary between 1 and M for each fixed value of $j \in \{1, 2, 3, 4, ..., N\}$. Define the vector U^n_j and the matrices V, A^n_j, and B^n_j as

$$U^n_j = \begin{bmatrix} u^n_{1,j} \\ u^n_{2,j} \\ \vdots \\ u^n_{M-1,j} \\ u^n_{M,j} \end{bmatrix}_{M\times 1}, \ V = \begin{bmatrix} \nu & 0 & \dots & 0 & 0 \\ 0 & \nu & \dots & 0 & 0 \\ & & \ddots & & \\ 0 & 0 & \dots & \nu & 0 \\ 0 & 0 & \dots & 0 & \nu \end{bmatrix}_{M\times M}, \tag{5.28}$$

$$A^n_j = \begin{bmatrix} \theta^n_{1,j} & \nu & 0 & \dots & 0 & 0 & 0 \\ \nu & \theta^n_{2,j} & \nu & \dots & 0 & 0 & 0 \\ 0 & \nu & \theta^n_{3,j} & & 0 & 0 & 0 \\ & & & \ddots & & & \\ 0 & 0 & 0 & & \theta^n_{M-2,j} & \nu & 0 \\ 0 & 0 & 0 & \dots & \nu & \theta^n_{M-1,j} & \nu \\ 0 & 0 & 0 & \dots & 0 & \nu & \theta^n_{M,j} \end{bmatrix}_{M\times M}, \text{ and} \tag{5.29}$$

$$B^n_j = \begin{bmatrix} \beta^n_{1,j} & -\nu & 0 & \dots & 0 & 0 & 0 \\ -\nu & \beta^n_{2,j} & -\nu & \dots & 0 & 0 & 0 \\ 0 & -\nu & \beta^n_{3,j} & & 0 & 0 & 0 \\ & & & \ddots & & & \\ 0 & 0 & 0 & & \beta^n_{M-2,j} & -\nu & 0 \\ 0 & 0 & 0 & \dots & -\nu & \beta^n_{M-1,j} & -\nu \\ 0 & 0 & 0 & \dots & 0 & -\nu & \beta^n_{M,j} \end{bmatrix}_{M\times M}. \tag{5.30}$$

The Crank-Nicholson scheme (5.23) results in a matrix equation for each $j \in \{1, 2, 3, 4, ..., N\}$. Specifying the boundary values given by (5.24) and (5.25) results in a matrix equation of the form

$$VU^{n+1}_{j-1} + VU^{n+1}_{j+1} + A^{n+1}_j U^{n+1}_j = -VU^n_{j-1} - VU^n_{j+1} + B^n_j U^n_j. \tag{5.31}$$

The system of matrix equations given by (5.31) is now written in block diagonal form. Enforcing the boundary conditions given by (5.26) and (5.27) results in a linear system of the form

$$\begin{bmatrix} A_1^{n+1} & V & 0 & \dots & 0 & 0 & 0 \\ V & A_2^{n+1} & V & \dots & 0 & 0 & 0 \\ 0 & V & A_3^{n+1} & & 0 & 0 & 0 \\ & & & \ddots & & & \\ 0 & 0 & 0 & & A_{N-2}^{n+1} & V & 0 \\ 0 & 0 & 0 & \dots & V & A_{N-1}^{n+1} & V \\ 0 & 0 & 0 & \dots & 0 & V & A_N^{n+1} \end{bmatrix} \begin{bmatrix} U_1^{n+1} \\ U_2^{n+1} \\ U_3^{n+1} \\ \vdots \\ U_{N-2}^{n+1} \\ U_{N-1}^{n+1} \\ U_N^{n+1} \end{bmatrix} =$$

$$\begin{bmatrix} B_1^{n} & -V & 0 & \dots & 0 & 0 & 0 \\ -V & B_2^{n} & -V & \dots & 0 & 0 & 0 \\ 0 & -V & B_3^{n} & & 0 & 0 & 0 \\ & & & \ddots & & & \\ 0 & 0 & 0 & & B_{N-2}^{n} & -V & 0 \\ 0 & 0 & 0 & \dots & -V & B_{N-1}^{n} & -V \\ 0 & 0 & 0 & \dots & 0 & -V & B_N^{n} \end{bmatrix} \begin{bmatrix} U_1^{n} \\ U_2^{n} \\ U_3^{n} \\ \vdots \\ U_{N-2}^{n} \\ U_{N-1}^{n} \\ U_N^{n} \end{bmatrix}. \tag{5.32}$$

Iterations are done using (5.32). The iterations are started using the initial condition $u_0(x, y, w_0)$.

5.2 Mirror Transformation Implementation

Utilizing the Crank-Nicholson scheme of the previous section, one obtains a numerical solution to the initial boundary value problem describing upward wave propagation. At an axial distance of $z = D$, the propagating wave encounters the spherical mirror M_2. Thus, we now transform the solution at $z = D$ in order to incorporate the properties of Gaussian beam reflection into the numerical approximation. That is, we expand the solution $u(x_i, y_j, D)$ in terms of the Hermite-Gaussian modes as

$$u(x_i, y_j, D) = \sum_{n=0}^{N_m} \sum_{m=0}^{N_m} c_{nm} \phi_n(x_i, D) \phi_m(y_j, D), \tag{5.33}$$

where N_m is the order of the highest order mode used in the expansion. As the numerical solution has support on the rectangle $[-a, a] \times [-b, b]$, the coefficients c_{nm} are found according to

$$c_{nm} = \int_{-b}^{b} \int_{-a}^{a} u(x, y, D) \phi_n^*(x, D) \phi_m^*(y, D) dx dy. \tag{5.34}$$

In the case of the three-dimensional optical cavity, the integral in (5.34) is approximated via a double Riemann sum. The integral over each uniform square $[x_{i-1}, x_i] \times [y_{j-1}, y_j]$ is

approximated as

$$\int_{y_{j-1}}^{y_j}\int_{x_{i-1}}^{x_i} u(x,y,D)\phi_n^*(x,D)\phi_m^*(y,D)dxdy \approx h^2 u(x_i,y_j,D)\phi_n^*(x_i,D)\phi_m^*(y_j,D), \tag{5.35}$$

where h is the transverse step-size. Summing over all squares $[x_{i-1},x_i]\times[y_{j-1},y_j]$ yields the approximation to (5.34). The resulting expression for c_{nm} is of the form

$$c_{nm} \approx h^2 \sum_{i=1}^{M}\sum_{j=1}^{N} u(x_i,y_j,D)\phi_n^*(x_i,D)\phi_m^*(y_j,D). \tag{5.36}$$

Having obtained the coefficients c_{nm} needed in the expansion, the Hermite-Gaussian modes are transformed according to (3.31). Recombining the transformed Hermite-Gaussian modes yields a transformed numerical solution $\tilde{u}(x_i,y_j,D)$ of the form

$$\tilde{u}(x_i,y_j,D) = \sum_{n=0}^{N_m}\sum_{m=0}^{N_m} c_{nm}\tilde{\phi}_n(x_i,D)\tilde{\phi}_m(y_j,D), \tag{5.37}$$

where $\tilde{\phi}_n$ is the transformed mode of order n.

5.3 Propagation Toward Decreasing z

Utilizing the numerical schemes discussed thus far, one obtains a transformed numerical solution at the spherical mirror M_2. Upon arriving at M_2, the wave is reflected. As a result, the electromagnetic wave propagates downward after reflection. We therefore shift our attention to approximating solutions for waves traveling toward decreasing values of z. The numerical scheme must approximate the initial boundary value problem given by

$$\frac{\partial g}{\partial z} = \frac{s}{2k}\left(\frac{\partial^2 g}{\partial x^2}+\frac{\partial^2 g}{\partial y^2}\right) + [\alpha(x,y,z)+sk(n-1)]g, \ (k<0) \tag{5.38}$$

$$g(-a,y,z) = 0 = g(a,y,z), \tag{5.39}$$

$$g(x,-b,z) = 0 = g(x,b,z), \text{ and} \tag{5.40}$$

$$g(x,y,D) = \tilde{u}(x,y,D). \tag{5.41}$$

The numerical scheme needed for downward propagation is easily obtained by reversing the sign of k.

Similar to the case of upward propagation, we define the quantities ν and $c_{i,j}^n$ by

$$\nu = \frac{s\Delta z}{2kh^2}, (k<0), \tag{5.42}$$

$$c_{i,j}^n = \Delta z(\alpha_{i,j}^n + sk(n-1)), (k<0). \tag{5.43}$$

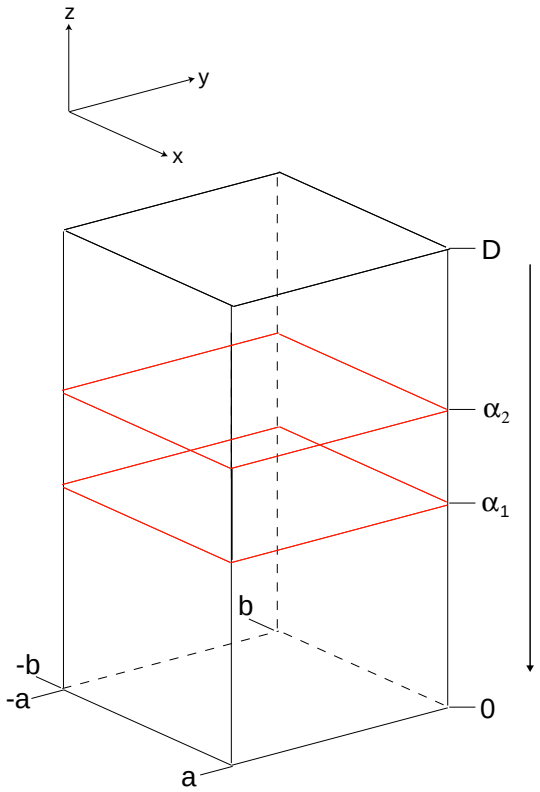

Figure 5.3: Three-Dimensional Optical Cavity, Downward Propagation

Reversing the sign of k in (5.16) results in a Crank-Nicholson scheme of the form

$$[-\nu g^{n+1}_{i-1,j} + -\nu g^{n+1}_{i+1,j} + (2 + 4\nu - c^{n+1}_{i,j})g^{n+1}_{i,j}] - [\nu g^{n+1}_{i,j-1}] - [\nu g^{n+1}_{i,j+1}] = \\ [\nu g^{n}_{i-1,j} + \nu g^{n}_{i+1,j} + (2 - 4\nu + c^{n}_{i,j})g^{n}_{i,j}] + [\nu g^{n}_{i,j-1}] + [\nu g^{n}_{i,j+1}]. \tag{5.44}$$

THEOREM 5.3.1
In the case of zero atomic gain, the Crank-Nicholson scheme given by (5.44) is unconditionally convergent.

Proof.

The proof is identical to that of Theorem 5.1.1. □

As in the case of upward propagation, the Dirichlet boundary conditions specified by (5.39) and (5.40) are incorporated into (5.44) by specifying that

$$g^{n}_{0,\cdot} = 0 = g^{n}_{M+1,\cdot} \quad , \quad g^{n+1}_{0,\cdot} = 0 = g^{n+1}_{M+1,\cdot}, \tag{5.45}$$

$$g^{n}_{\cdot,0} = 0 = g^{n}_{\cdot,N+1} \quad , \text{ and } \quad g^{n+1}_{\cdot,0} = 0 = g^{n+1}_{\cdot,N+1} \ . \tag{5.46}$$

For notational convenience, define the quantities $\theta_{i,j}^n$ and $\beta_{i,j}^n$ as

$$\theta_{i,j}^n = 2 + 4\nu - c_{i,j}^n, \text{ and} \tag{5.47}$$

$$\beta_{i,j}^n = 2 - 4\nu + c_{i,j}^n. \tag{5.48}$$

We can now construct the overall matrix equation used to propagate the transformed solution $u(x_i, y_j, D)$ to the flat mirror M_1. Define the vector G_j^n and the matrices V, A_j^n and B_j^n by

$$G_j^n = \begin{bmatrix} g_{1,j}^n \\ g_{2,j}^n \\ \vdots \\ g_{M-1,j}^n \\ g_{M,j}^n \end{bmatrix}_{M\times 1}, V = \begin{bmatrix} \nu & 0 & \dots & 0 & 0 \\ 0 & \nu & \dots & 0 & 0 \\ & & \ddots & & \\ 0 & 0 & \dots & \nu & 0 \\ 0 & 0 & \dots & 0 & \nu \end{bmatrix}_{M\times M}, \tag{5.49}$$

$$A_j^n = \begin{bmatrix} \theta_{1,j}^n & -\nu & 0 & \dots & 0 & 0 & 0 \\ -\nu & \theta_{2,j}^n & -\nu & \dots & 0 & 0 & 0 \\ 0 & -\nu & \theta_{3,j}^n & & 0 & 0 & 0 \\ & & & \ddots & & & \\ 0 & 0 & 0 & & \theta_{M-2,j}^n & -\nu & 0 \\ 0 & 0 & 0 & \dots & -\nu & \theta_{M-1,j}^n & -\nu \\ 0 & 0 & 0 & \dots & 0 & -\nu & \theta_{M,j}^n \end{bmatrix}_{M\times M}, \text{ and} \tag{5.50}$$

$$B_j^n = \begin{bmatrix} \beta_{1,j}^n & \nu & 0 & \dots & 0 & 0 & 0 \\ \nu & \beta_{2,j}^n & \nu & \dots & 0 & 0 & 0 \\ 0 & \nu & \beta_{3,j}^n & & 0 & 0 & 0 \\ & & & \ddots & & & \\ 0 & 0 & 0 & & \beta_{M-2,j}^n & \nu & 0 \\ 0 & 0 & 0 & \dots & \nu & \beta_{M-1,j}^n & \nu \\ 0 & 0 & 0 & \dots & 0 & \nu & \beta_{M,j}^n \end{bmatrix}_{M\times M}. \tag{5.51}$$

Then, the matrix equation resulting from (5.44) is of the form

$$\begin{bmatrix} A_1^{n+1} & -V & 0 & \dots & 0 & 0 & 0 \\ -V & A_2^{n+1} & -V & \dots & 0 & 0 & 0 \\ 0 & -V & A_3^{n+1} & & 0 & 0 & 0 \\ & & & \ddots & & & \\ 0 & 0 & 0 & & A_{N-2}^{n+1} & -V & 0 \\ 0 & 0 & 0 & \dots & -V & A_{N-1}^{n+1} & -V \\ 0 & 0 & 0 & \dots & 0 & -V & A_N^{n+1} \end{bmatrix} \begin{bmatrix} G_1^{n+1} \\ G_2^{n+1} \\ G_3^{n+1} \\ \vdots \\ G_{N-2}^{n+1} \\ G_{N-1}^{n+1} \\ G_N^{n+1} \end{bmatrix} = \begin{bmatrix} B_1^n & V & 0 & \dots & 0 & 0 & 0 \\ V & B_2^n & V & \dots & 0 & 0 & 0 \\ 0 & V & B_3^n & & 0 & 0 & 0 \\ & & & \ddots & & & \\ 0 & 0 & 0 & & B_{N-2}^n & V & 0 \\ 0 & 0 & 0 & \dots & V & B_{N-1}^n & V \\ 0 & 0 & 0 & \dots & 0 & V & B_N^n \end{bmatrix} \begin{bmatrix} G_1^n \\ G_2^n \\ G_3^n \\ \vdots \\ G_{N-2}^n \\ G_{N-1}^n \\ G_N^n \end{bmatrix}. \tag{5.52}$$

The remaining iterations are done with (5.52). The transformed numerical solution $\tilde{u}(x_i, y_j, D)$ due to reflection is used as initial data.

5.4 Energy Extraction Implementation

Utilizing the numerical scheme given in the previous section for downward propagation, an approximate solution $g(x_i, y_j, 0)$ is obtained. In order to obtain the wave profile after one round-trip through the optical cavity, we decompose $g(x_i, y_j, 0)$ into two parts, as described in Chapter 3. The round-trip solution $u_R(x_i, y_j, 0)$ is then found according to

$$u_R(x_i, y_j, 0) = \sqrt{0.9} g_M(x_i, y_j, 0), \tag{5.53}$$

where $g_M(x_i, y_j, 0)$ is that portion of $g(x_i, y_j, 0)$ incident on the flat mirror.

5.5 Numerical Experiments

We now implement the numerical scheme presented in this chapter to the optical cavity geometry illustrated in Figure 5.4.

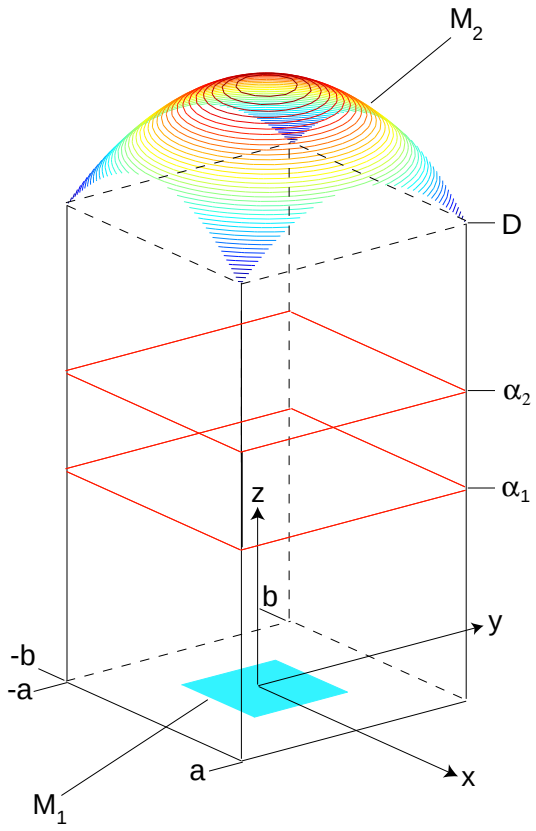

Figure 5.4: Optical Cavity Geometry

The schematic shown in Figure 5.4 depicts two mirrors separated on the left by a distance D. The lower mirror is perfectly horizontal. The upper mirror is a surface patch of a sphere with radius r.

We investigate the influence of the atomic gain function $f(x, y)$ on the propagating wave in the optical cavity. As an initial investigation, we specify a wave profile at M_1 and propagate through the optical cavity with zero atomic gain. We then propagate the same initial wave profile through the optical cavity with a nonzero atomic gain function $f(x, y)$.

Some care needs to be taken in the specification of the initial condition in the case of two transverse directions. The half-length of the flat mirror in the x direction is not necessarily equal to the half-length in the y direction. For this reason, we specify the spot size at the flat mirror by applying the 99% rule to the x and y directions separately. Denoting the half-length of the flat mirror in the x direction by M_x, we specify the minimum spot size in

the x direction by

$$w_{0x} = \frac{2M_x}{\pi}. \tag{5.54}$$

In a similar fashion, the minimum spot size in the y direction is specified according to

$$w_{0y} = \frac{2M_y}{\pi}, \tag{5.55}$$

where M_y is the half-length of the flat mirror in the y direction.

The resulting initial condition we specify is of the form

$$u(x, y, 0) = \frac{10}{\sqrt{q_{0x} q_{0y}}} \exp\left[\frac{-sk}{2}\left(\frac{x^2}{q_{0x}} + \frac{y^2}{q_{0y}}\right)\right], \tag{5.56}$$

where q_{0x} and q_{0y} correspond to the parameter defined by (2.58) applied to the x and y directions separately.

In the results that follow, we specify the following values:

- $D = 7.731$,
- $r = 15$,
- $n = 1$,
- $k = 55$,
- $a = 2$,
- $b = 2$,
- $\alpha_1 = 3$,
- $\alpha_2 = 5$,
- $N_m = 15$.

In each numerical experiment, the initial condition, atomic gain function $f(x, y)$, and the numerical solution after one round-trip through the optical cavity are presented. A plot of the difference in magnitude between the transformed and untransformed Hermite-Gaussian expansions at the spherical mirror is also shown. In addition, a plot illustrating the magnitude of the difference between the Hermite-Gaussian expansion and the Crank-Nicholson solution at $z = D$ is presented.

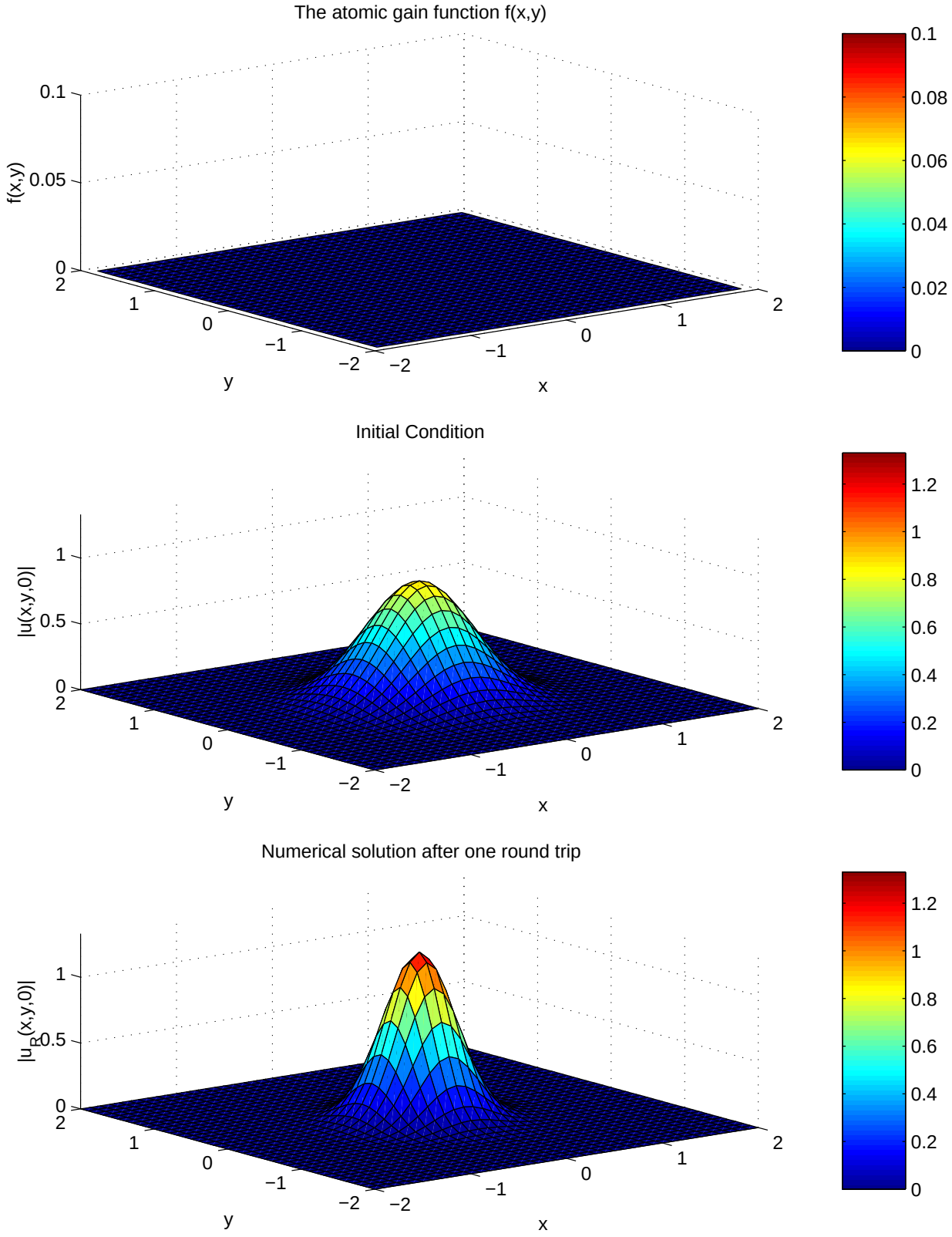

Figure 5.5: Propagation with zero atomic gain, $M_x = M_y = 1$.

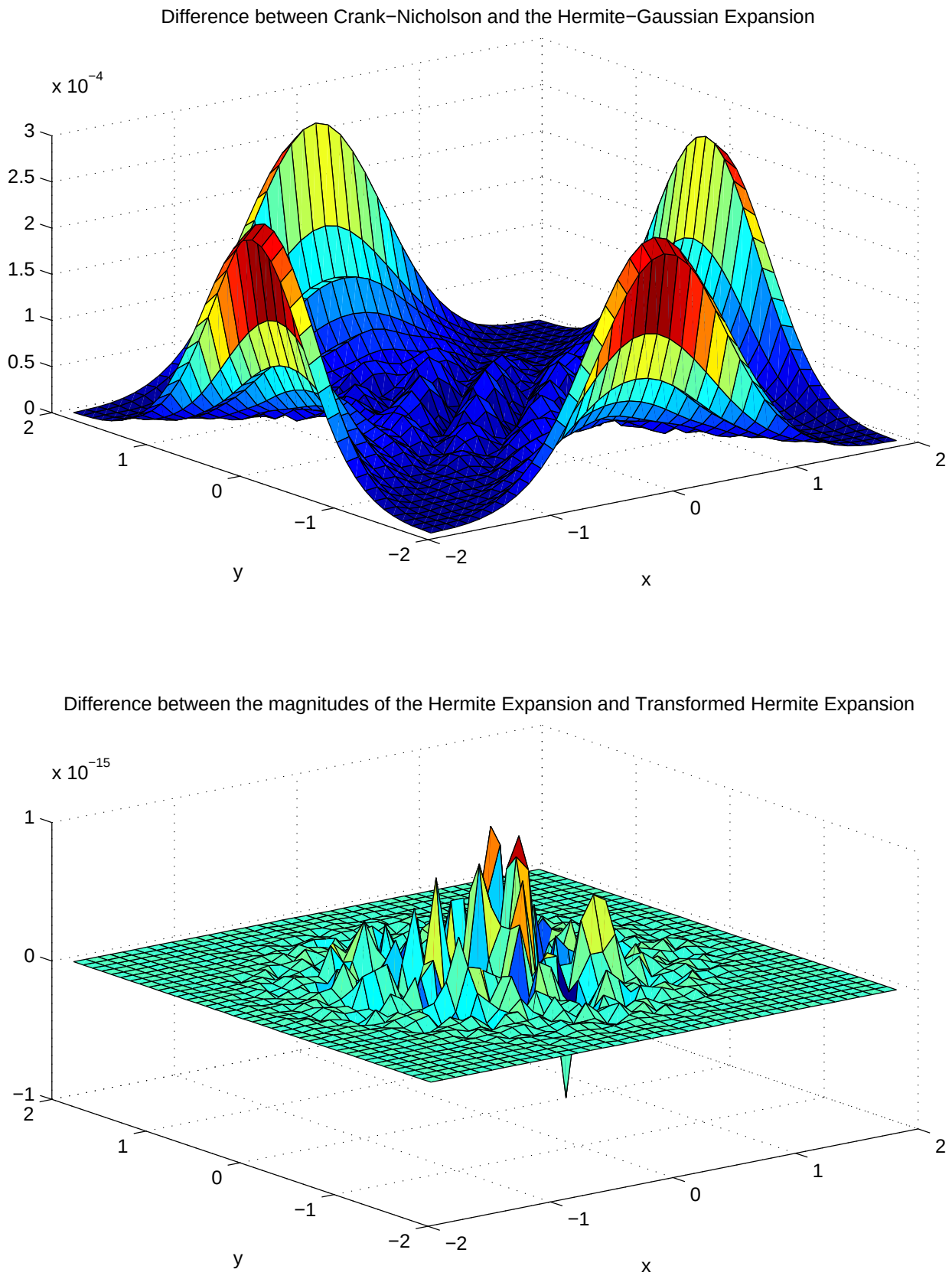

Figure 5.6: Propagation with zero atomic gain, $M_x = M_y = 1$ (continued).

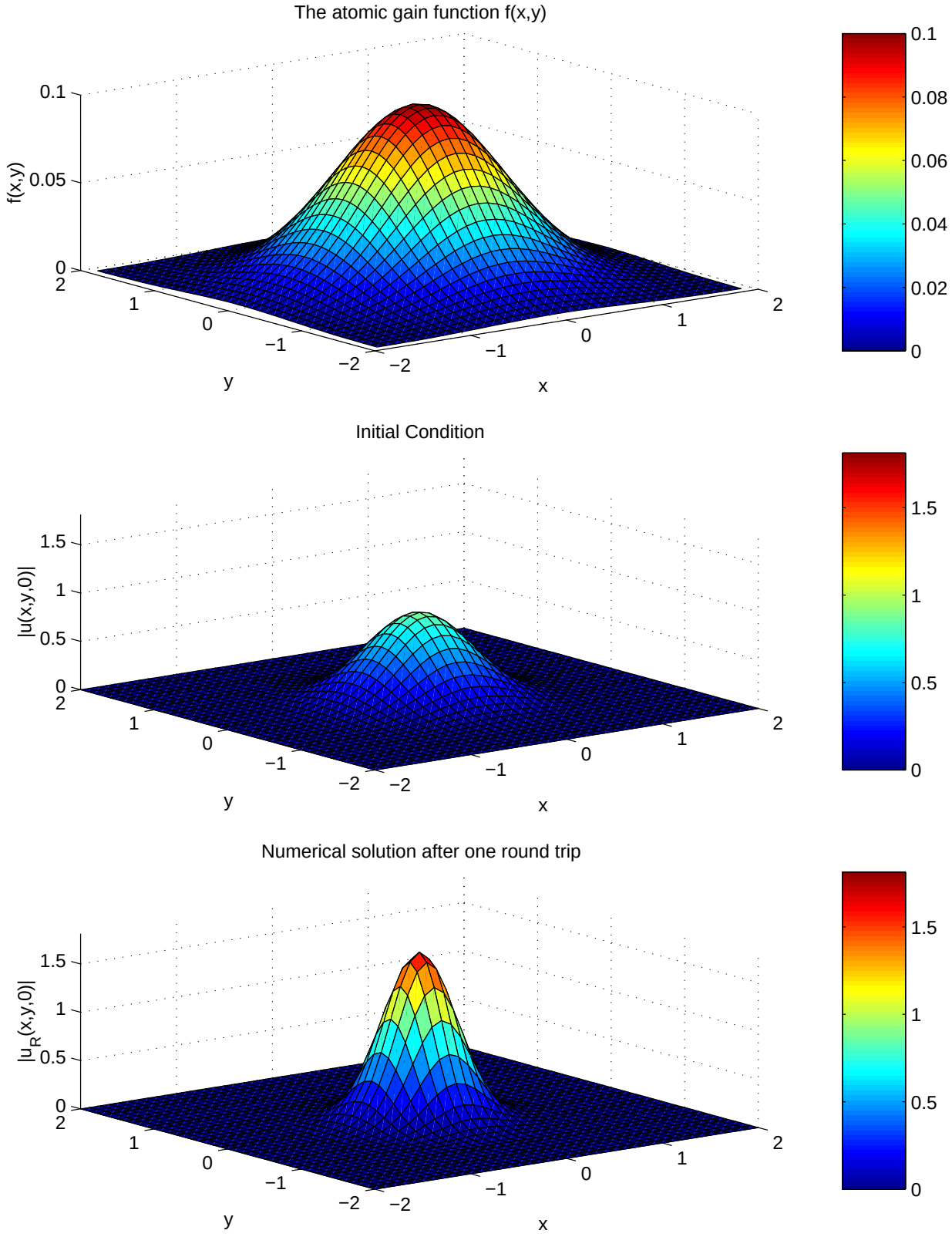

Figure 5.7: Propagation with $f(x,y) = .1e^{-(x^2+y^2)}$, $M_x = M_y = 1$.

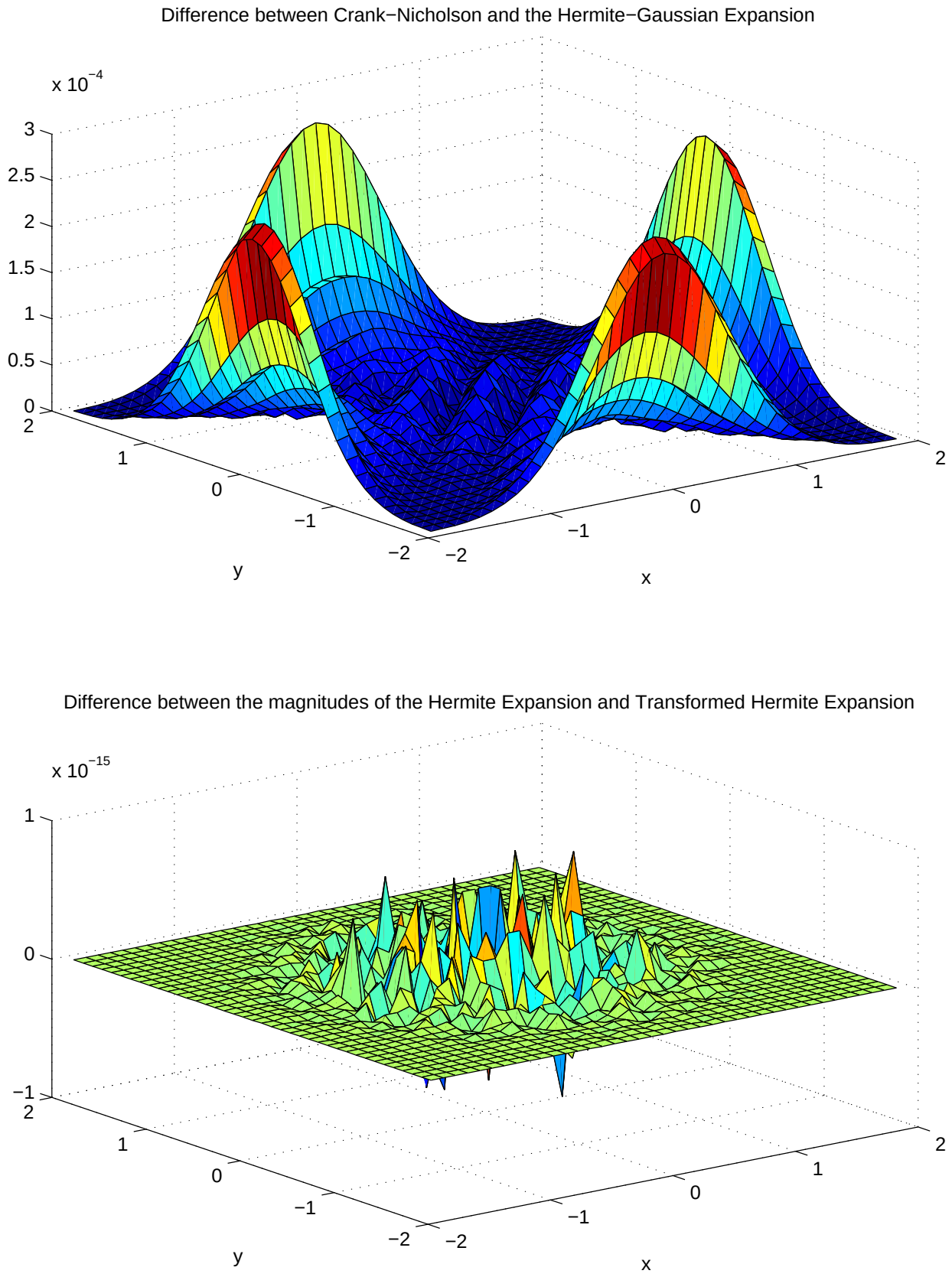

Figure 5.8: Propagation with $f(x,y) = .1e^{-(x^2+y^2)}$, $M_x = M_y = 1$ (continued).

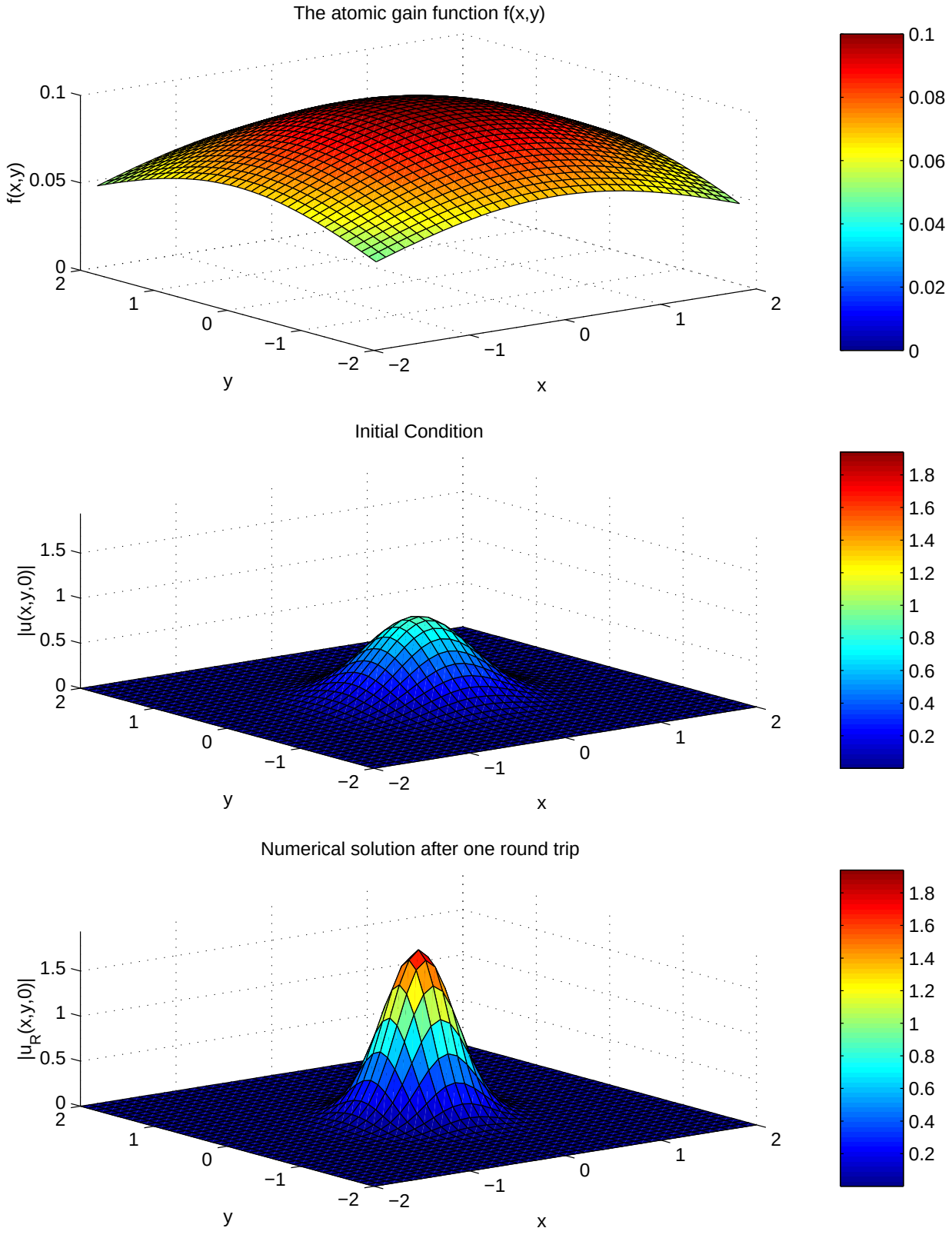

Figure 5.9: Propagation with $f(x,y) = .1e^{-\frac{x^2+y^2}{10}}$, $M_x = M_y = 1$.

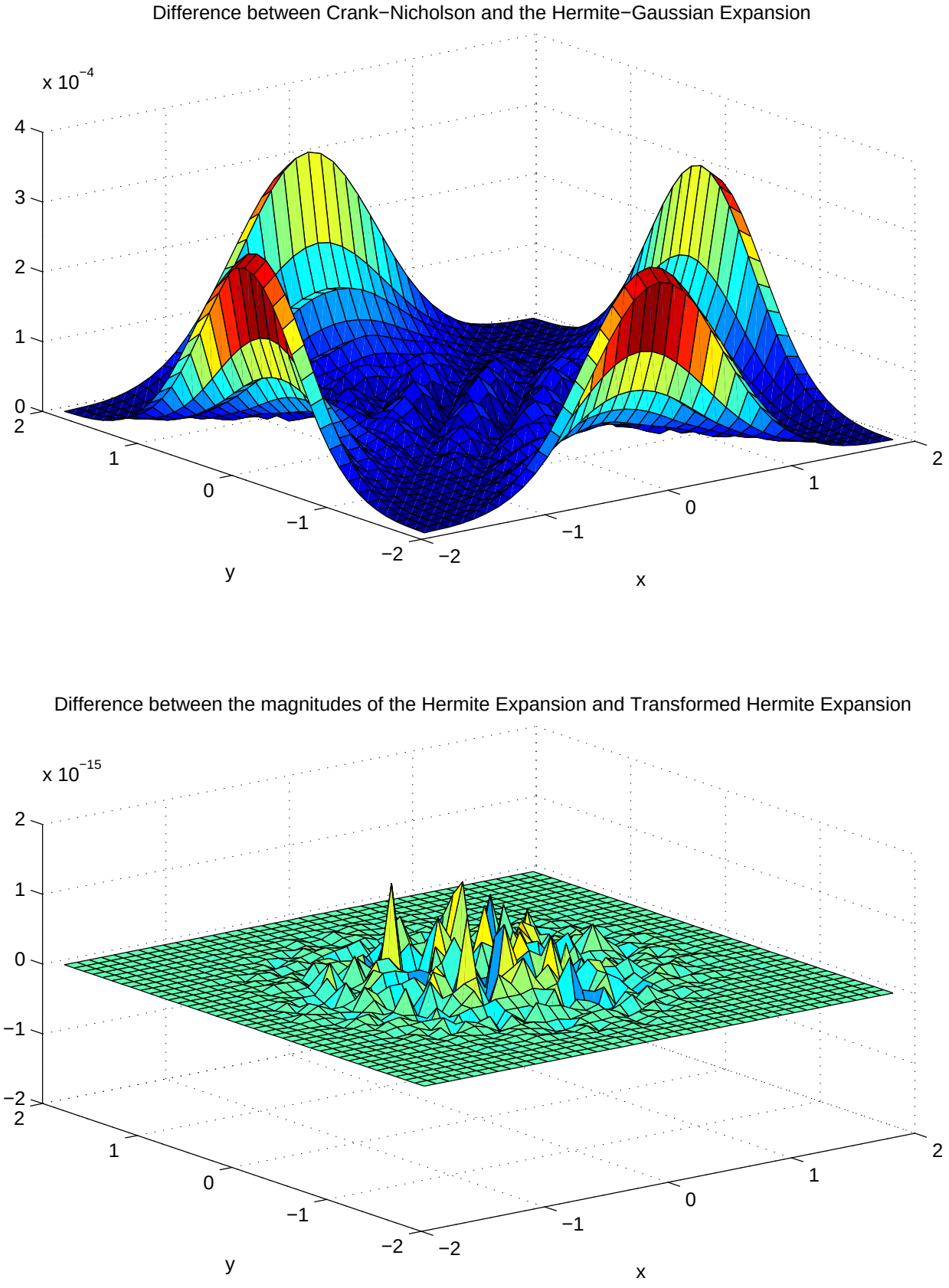

Figure 5.10: Propagation with $f(x,y) = .1e^{-\frac{x^2+y^2}{10}}$, $M_x = M_y = 1$ (continued).

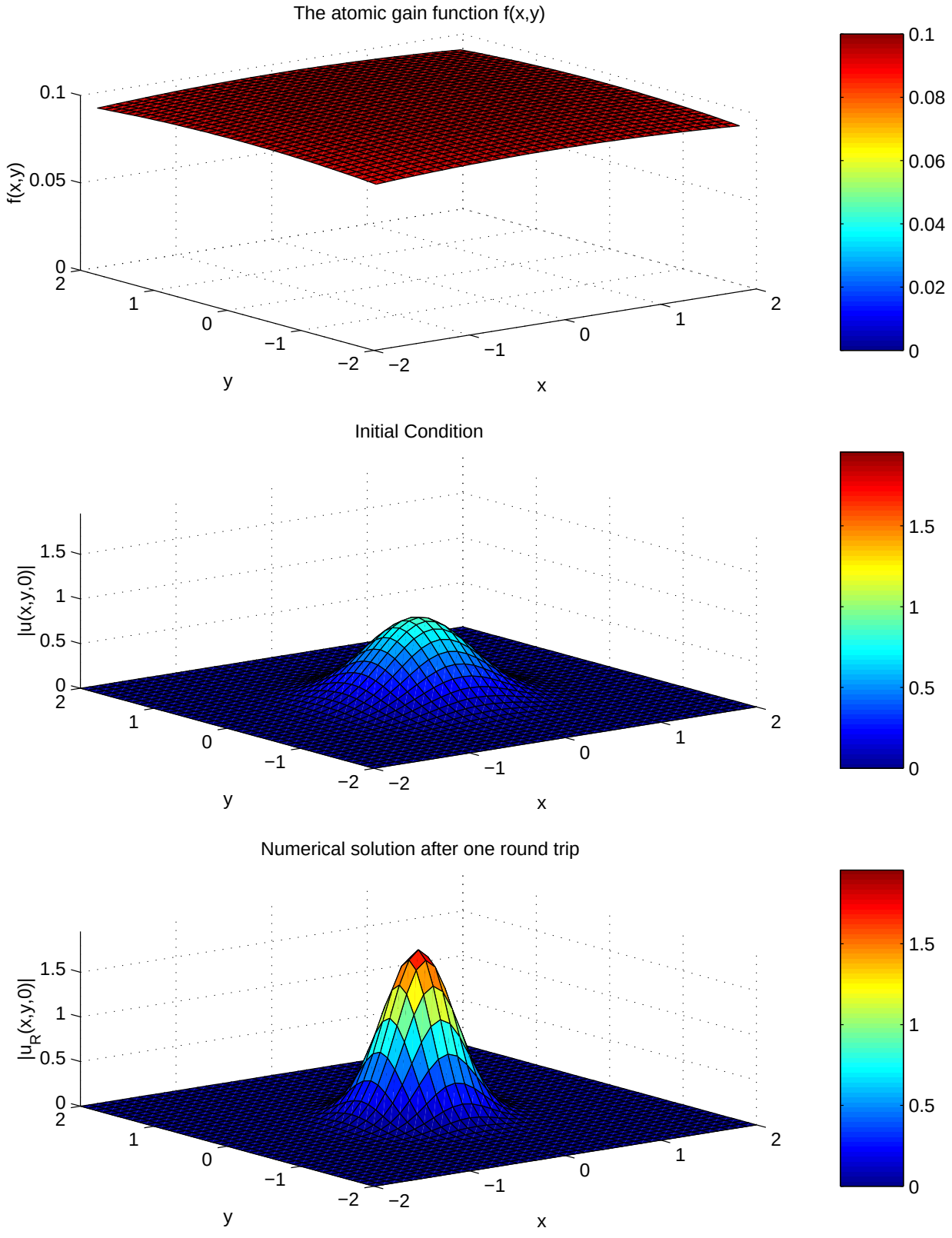

Figure 5.11: Propagation with $f(x,y) = .1e^{-\frac{x^2+y^2}{100}}$, $M_x = M_y = 1$.

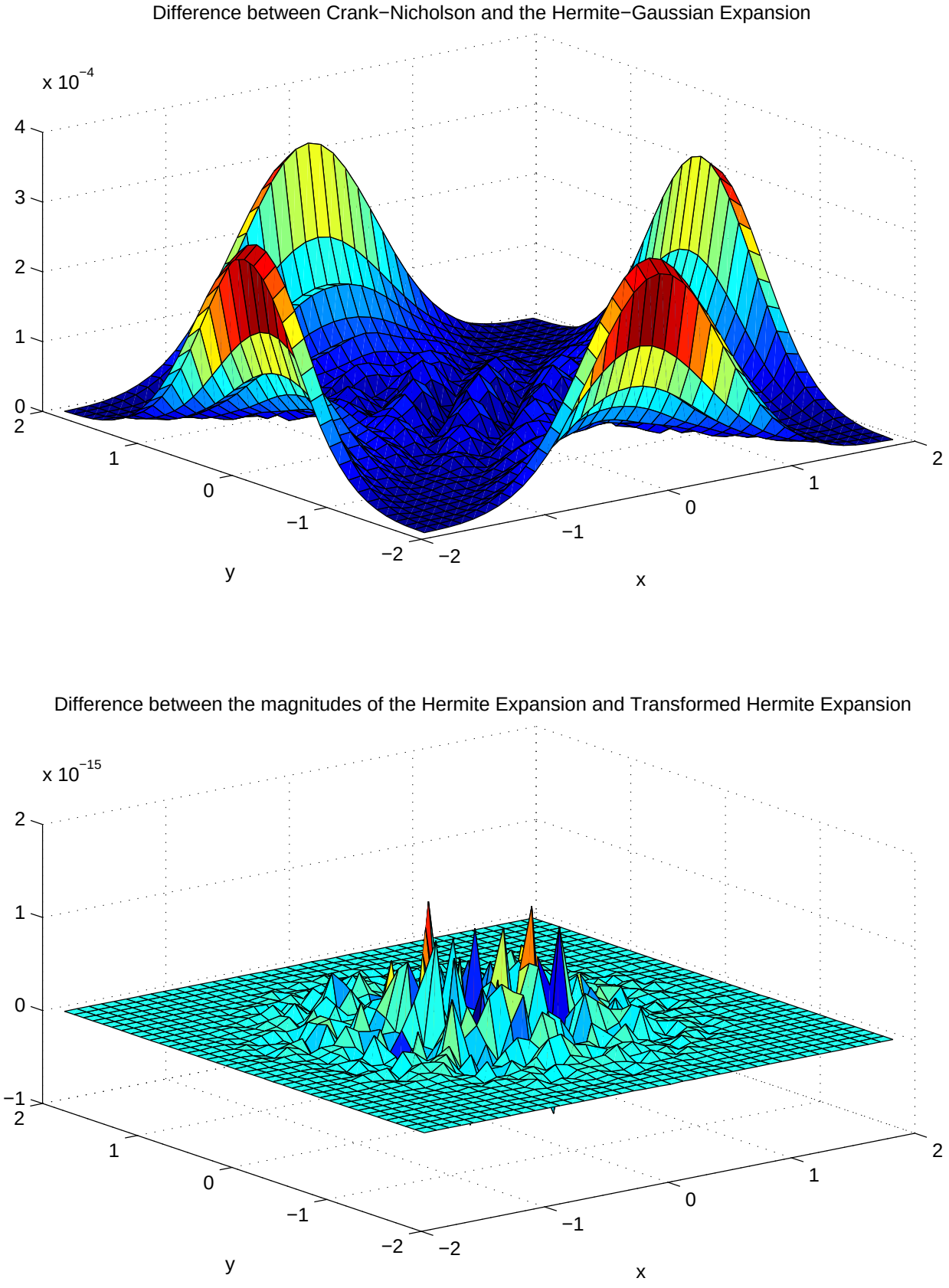

Figure 5.12: Propagation with $f(x,y) = .1e^{-\frac{x^2+y^2}{100}}$, $M_x = M_y = 1$ (continued).

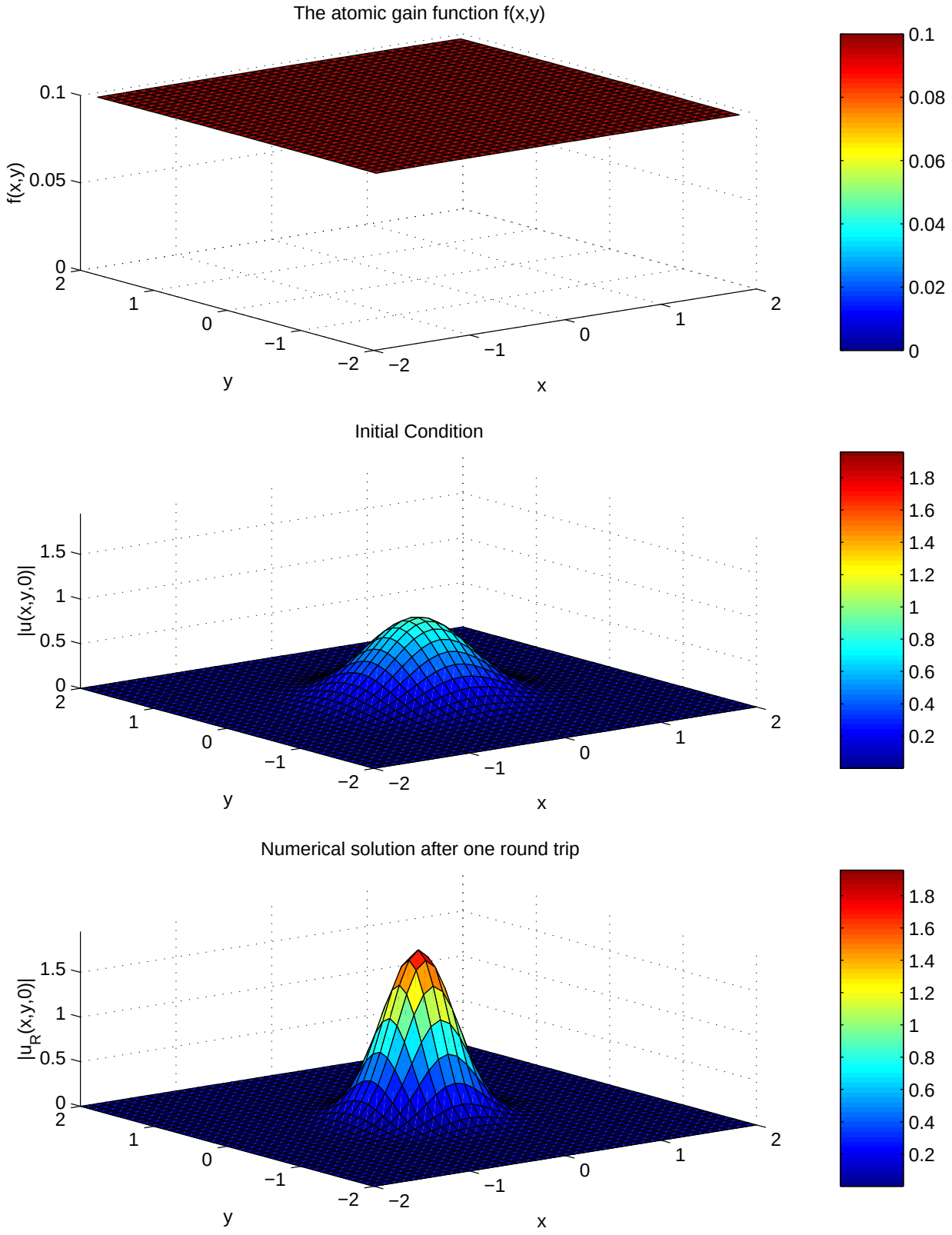

Figure 5.13: Propagation with $f(x,y) = .1e^{-\frac{x^2+y^2}{1000}}$, $M_x = M_y = 1$.

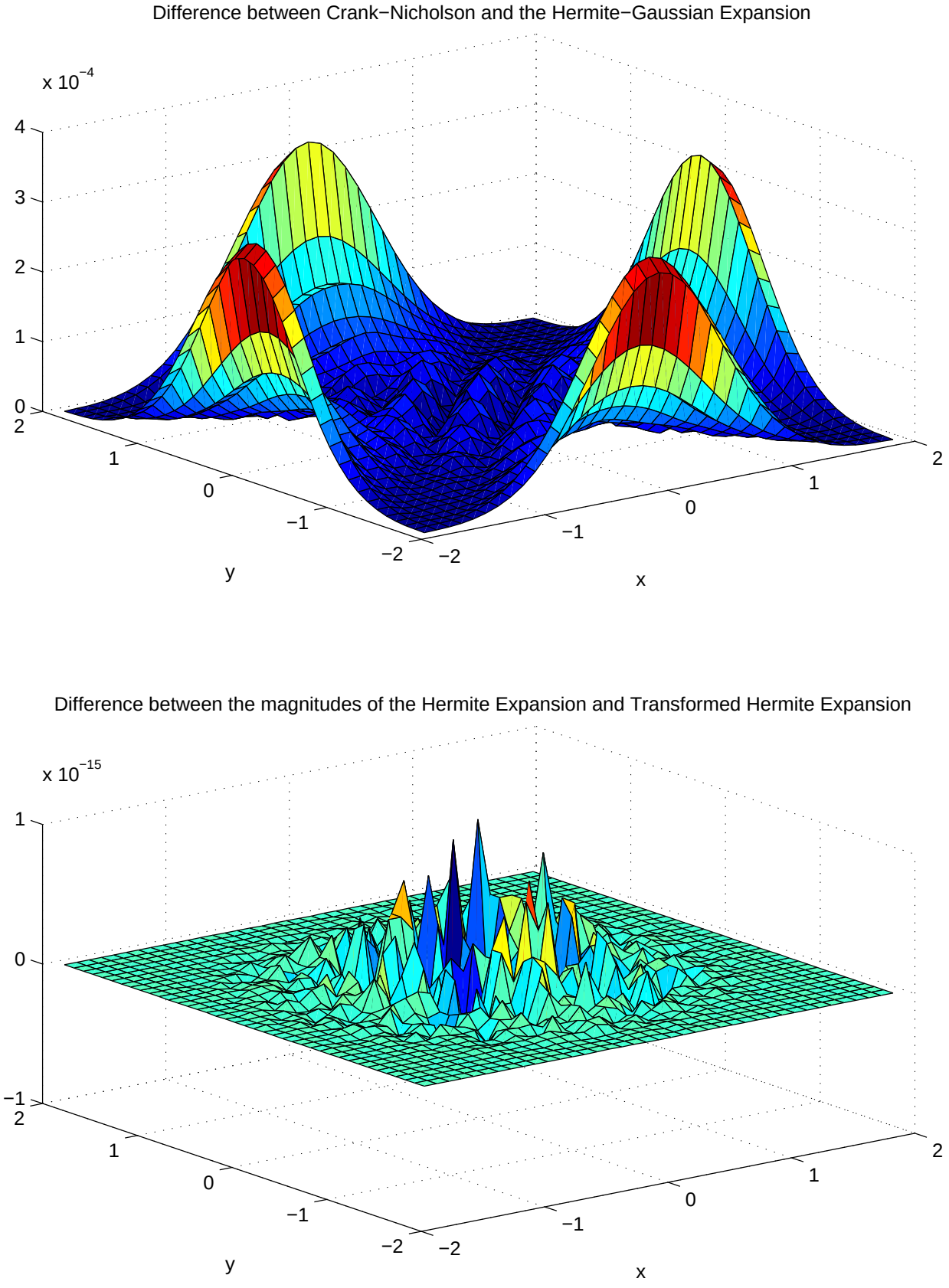

Figure 5.14: Propagation with $f(x,y) = .1e^{-\frac{x^2+y^2}{1000}}$, $M_x = M_y = 1$ (continued).

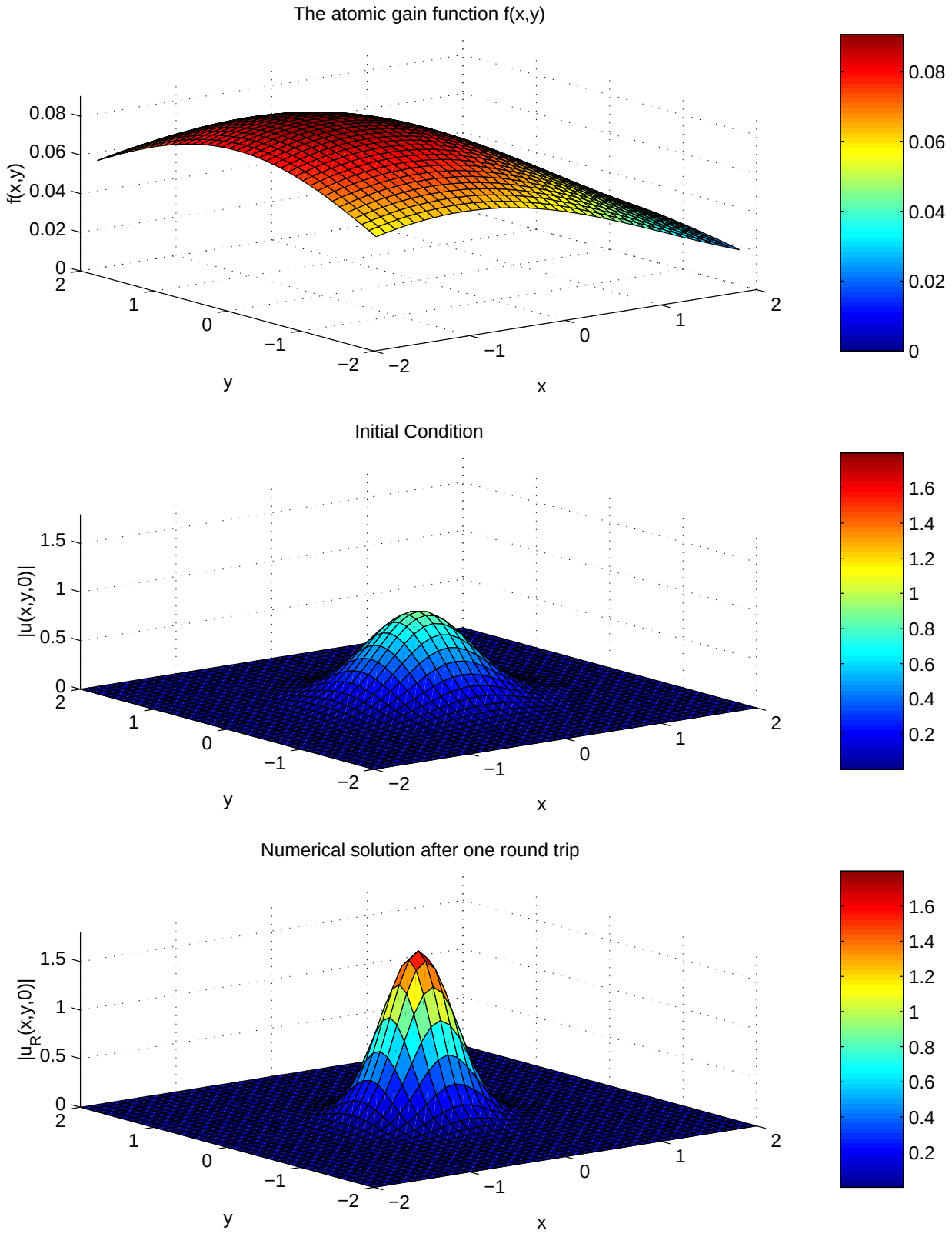

Figure 5.15: Propagation with $f(x,y) = \frac{4-x}{50}e^{-\frac{x^2+y^2}{10}}$, $M_x = 1, M_y = 1$.

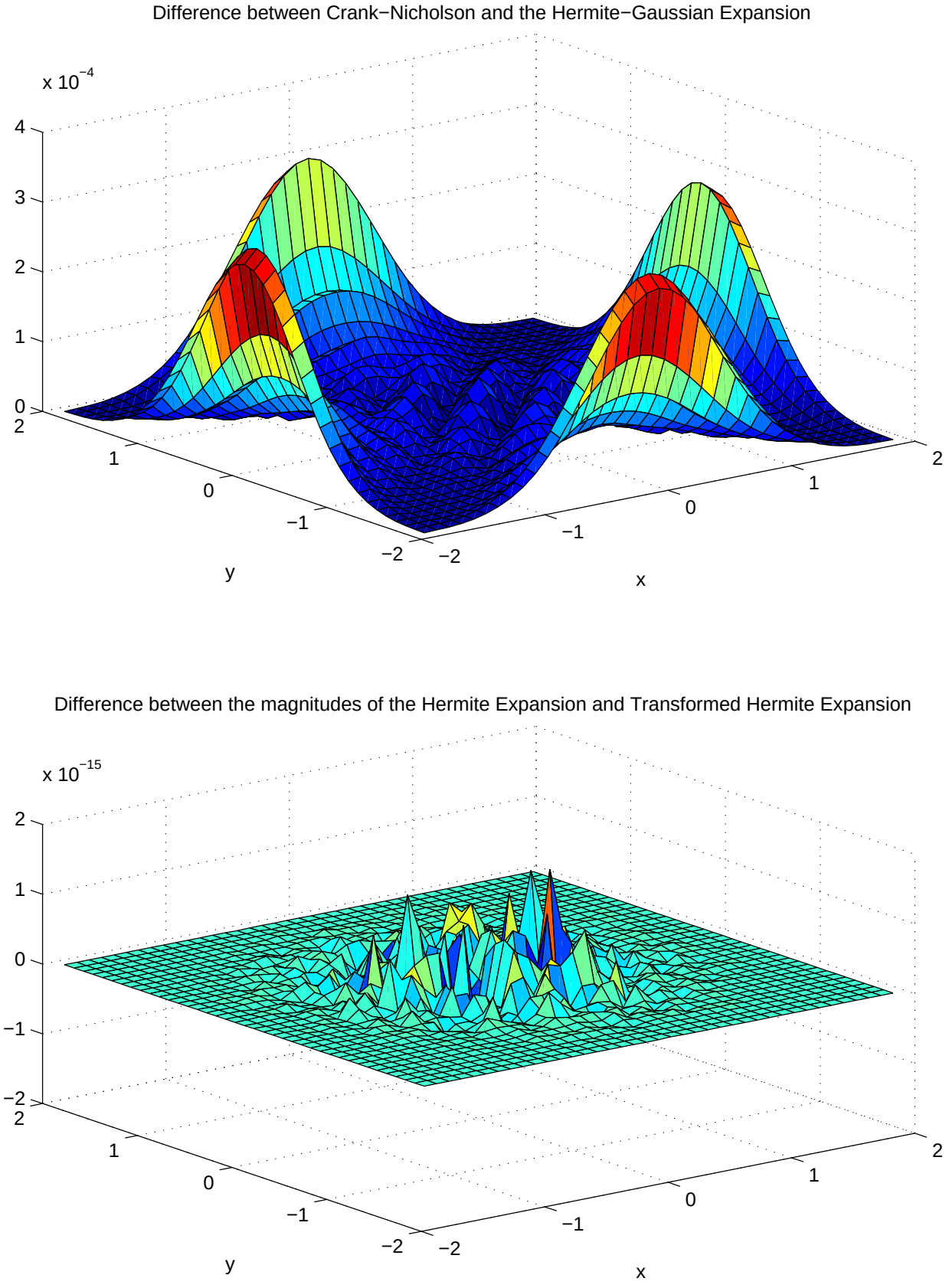

Figure 5.16: Propagation with $f(x,y) = \frac{4-x}{50}e^{-\frac{x^2+y^2}{10}}$, $M_x = 1, M_y = 1$ (continued).

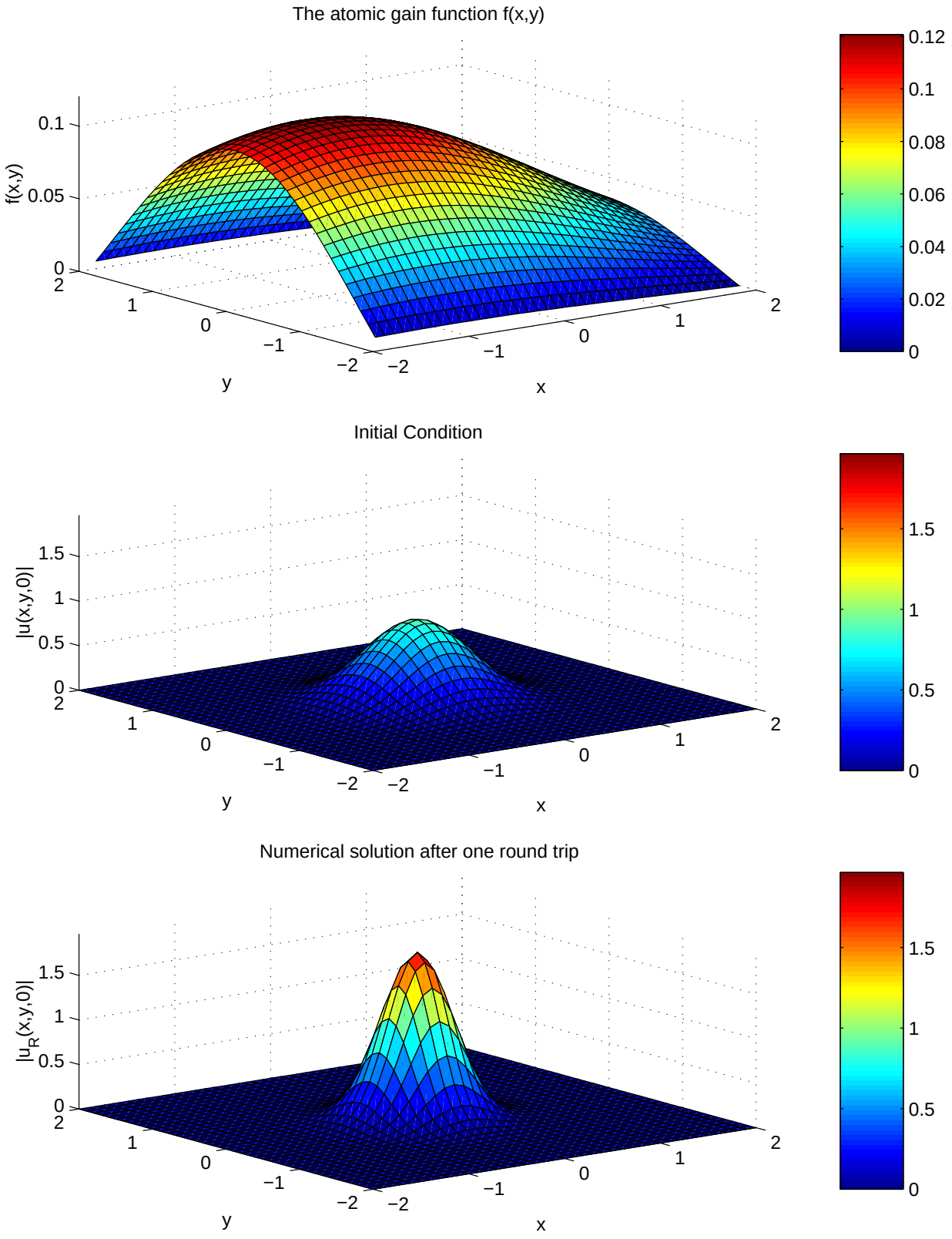

Figure 5.17: Propagation with $f(x,y) = \frac{(4-x)(4-y^2)}{150} e^{-\frac{x^2+y^2}{10}}$, $M_x = 1, M_y = 1$.

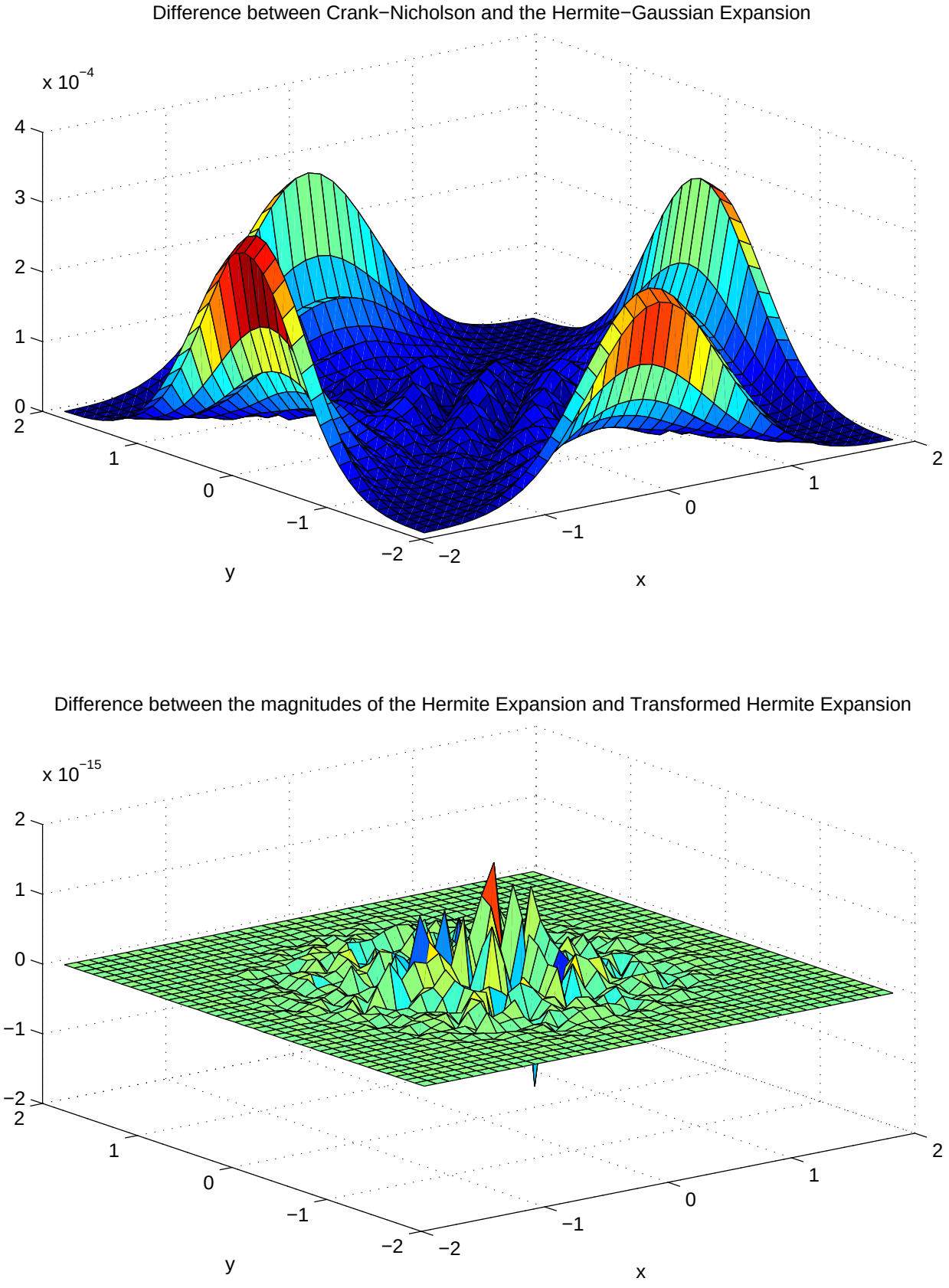

Figure 5.18: Propagation with $f(x,y) = \frac{(4-x)(4-y^2)}{150} e^{-\frac{x^2+y^2}{10}}$, $M_x = 1, M_y = 1$ (continued).

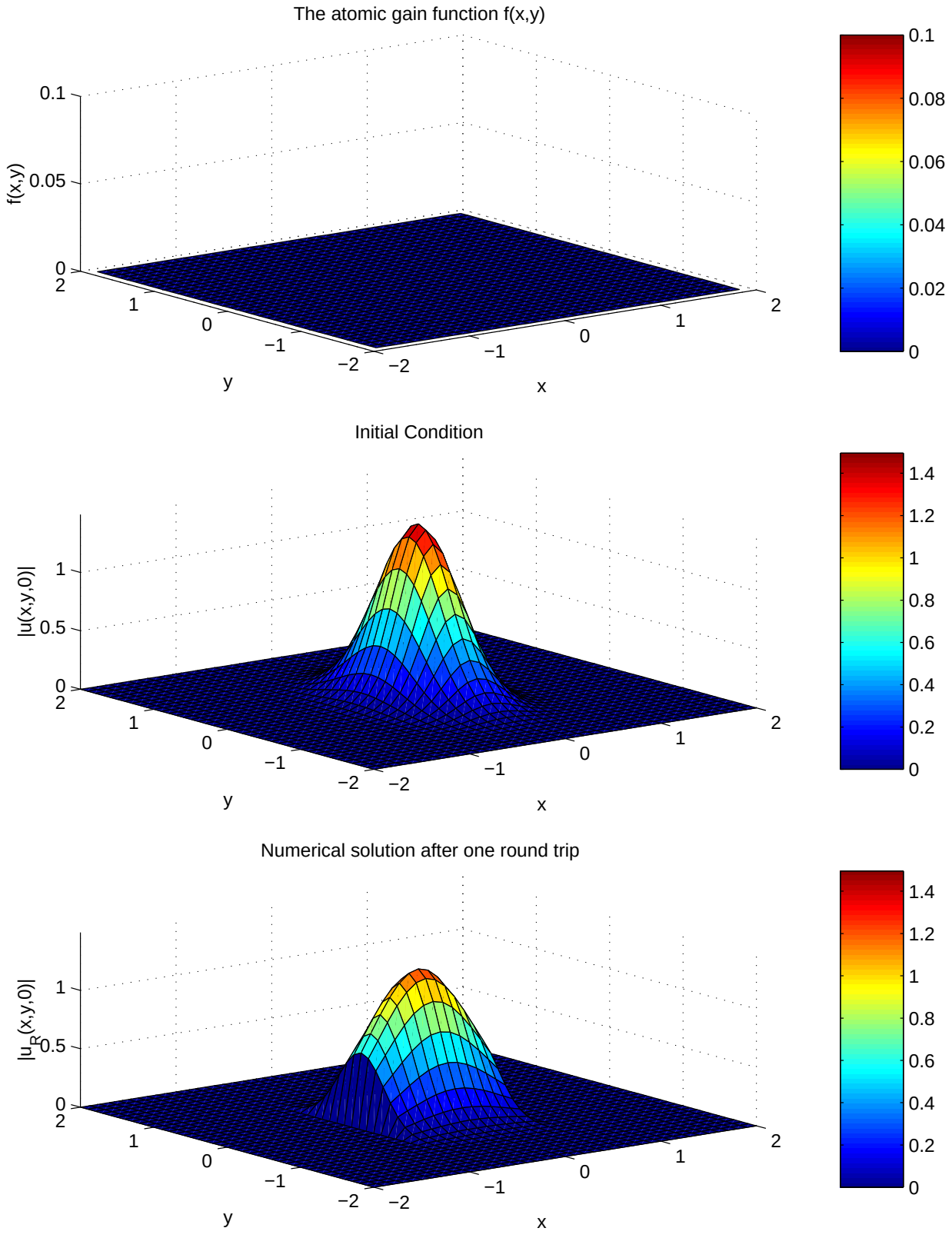

Figure 5.19: Propagation with zero atomic gain, $M_x = .6, M_y = 1$.

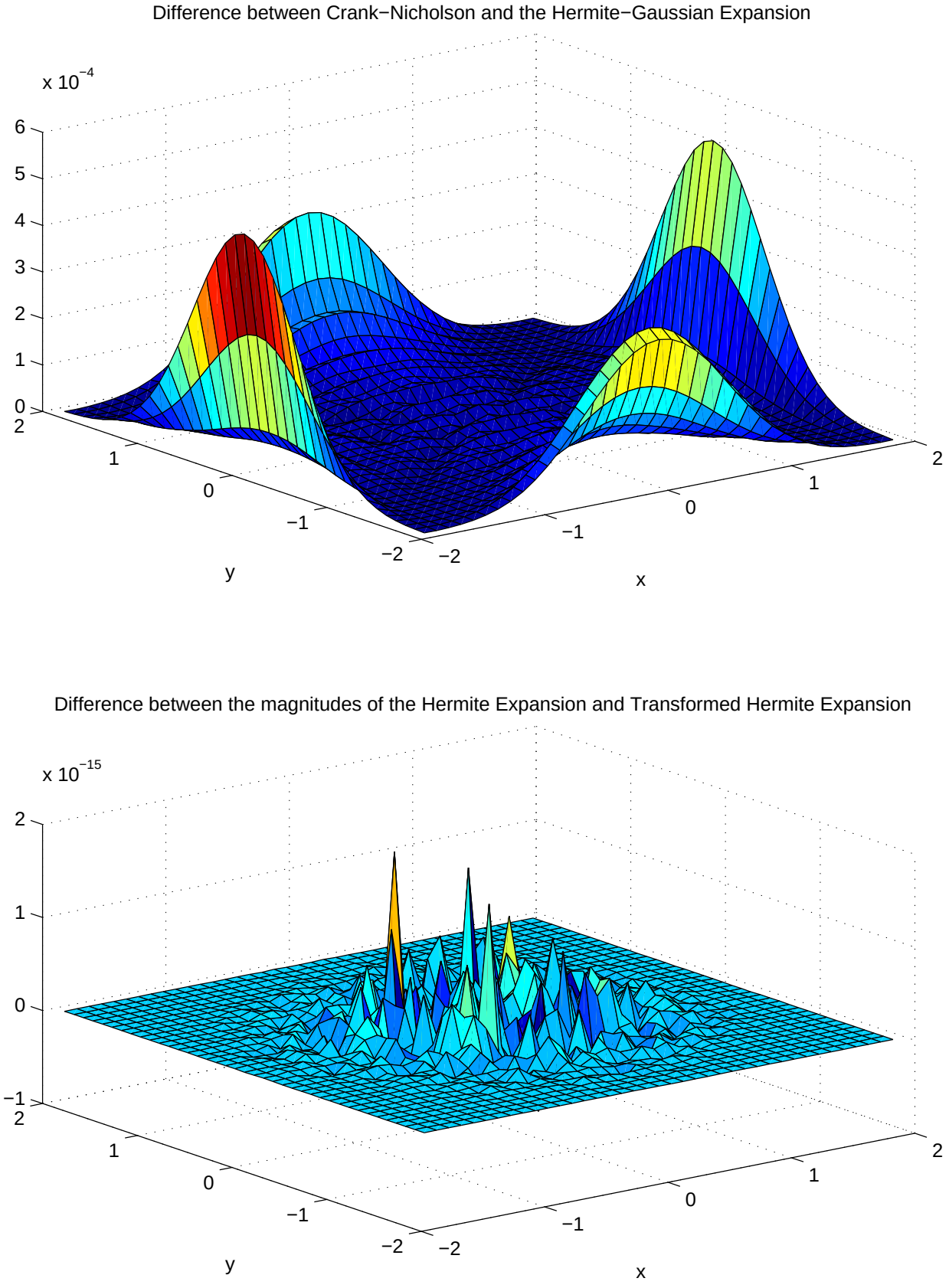

Figure 5.20: Propagation with zero atomic gain, $M_x = .6, M_y = 1$ (continued).

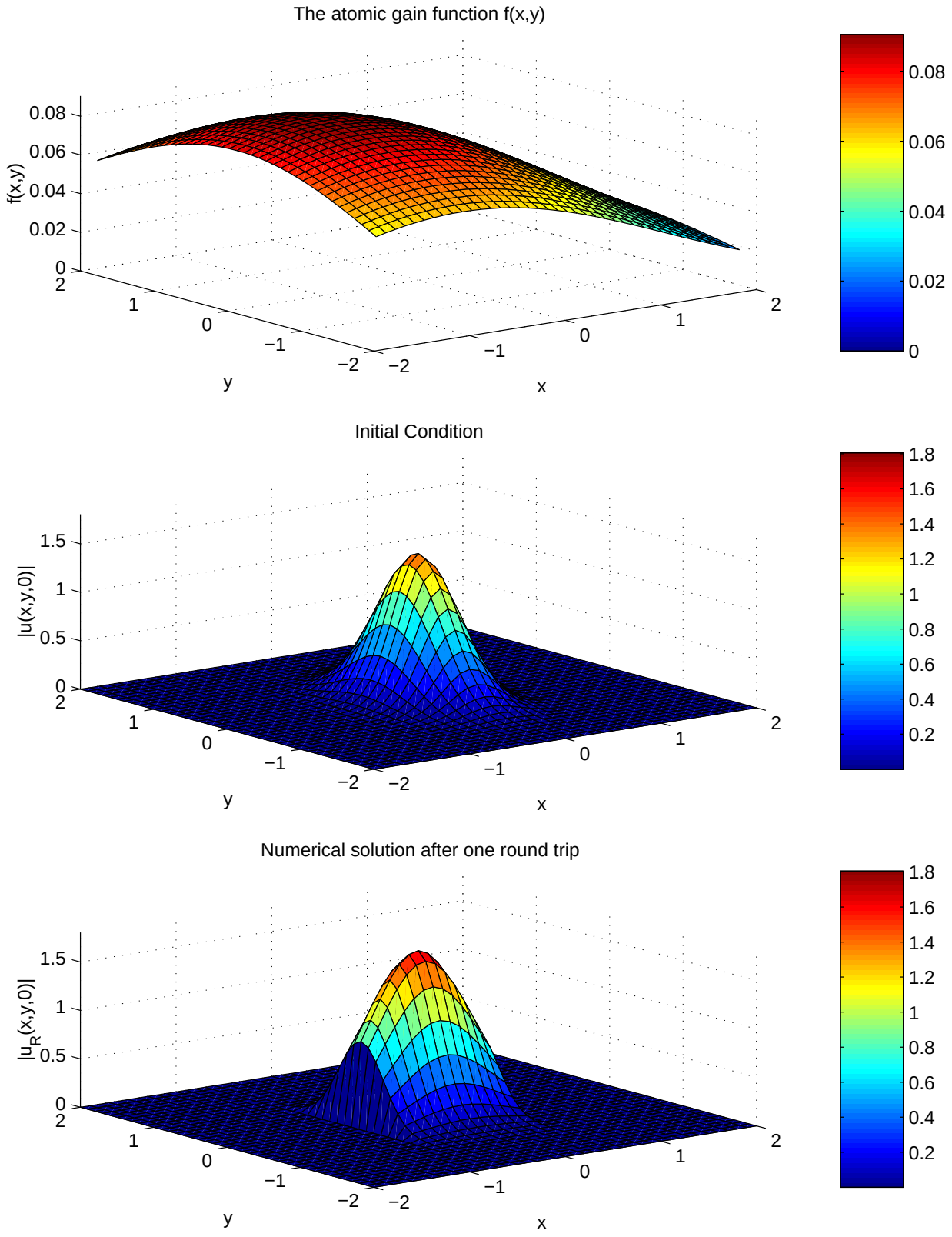

Figure 5.21: Propagation with $f(x,y) = \frac{4-x}{50}e^{-\frac{x^2+y^2}{10}}$, $M_x = .6, M_y = 1$.

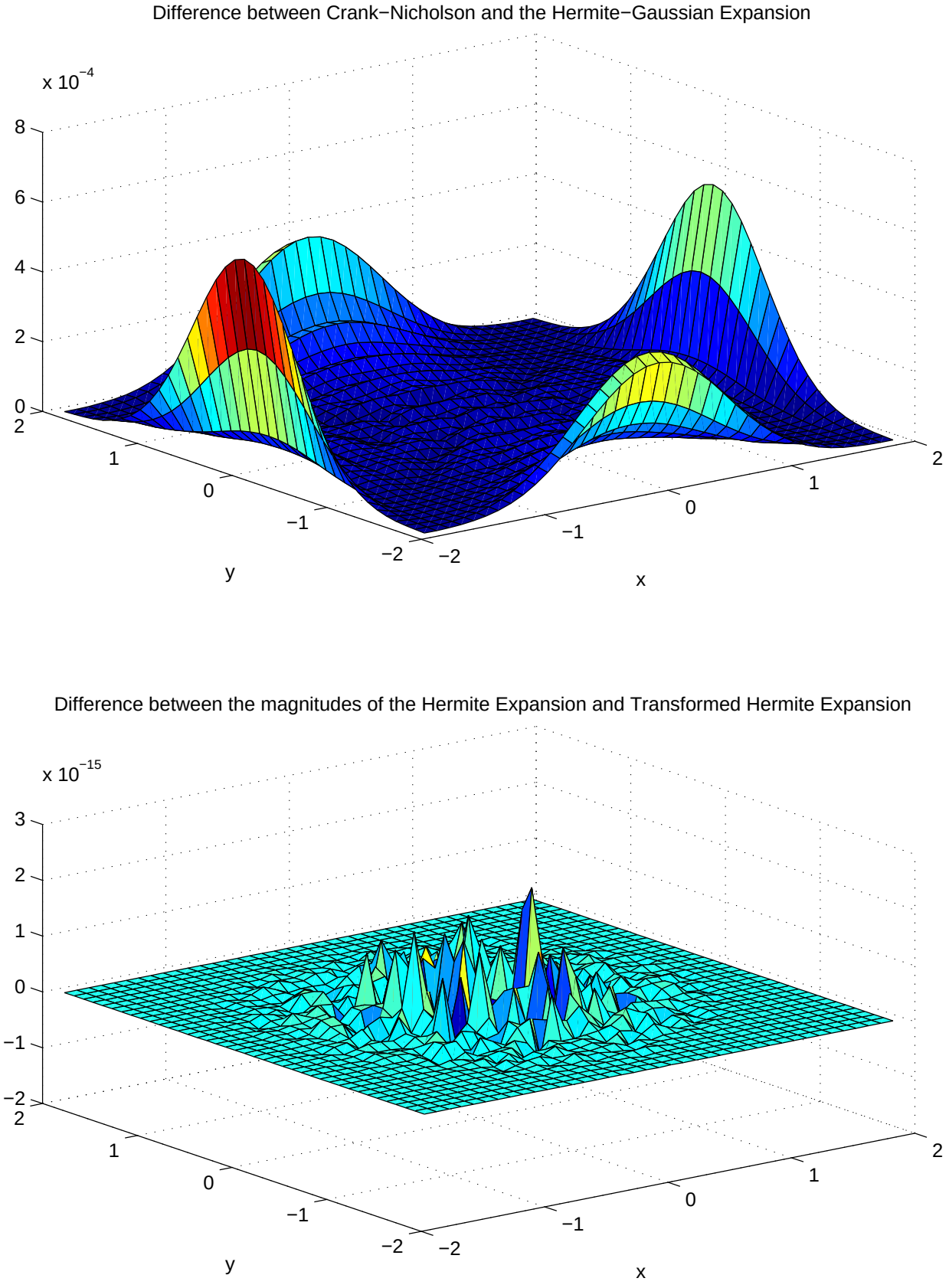

Figure 5.22: Propagation with $f(x,y) = \frac{4-x}{50} e^{-\frac{x^2+y^2}{10}}$, $M_x = .6, M_y = 1$ (continued).

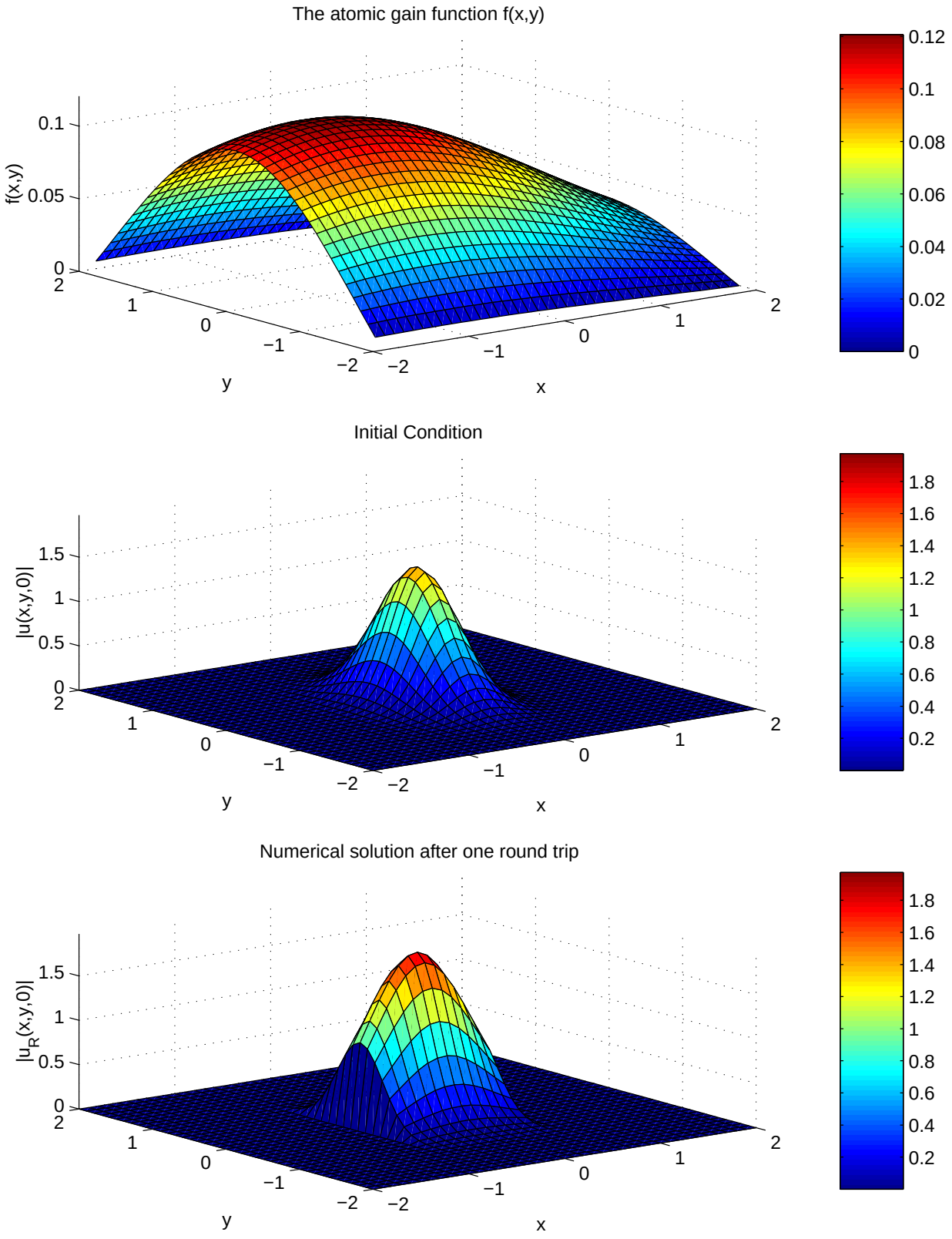

Figure 5.23: Propagation with $f(x,y) = \frac{(4-x)(4-y^2)}{150} e^{-\frac{x^2+y^2}{10}}$, $M_x = .6, M_y = 1$.

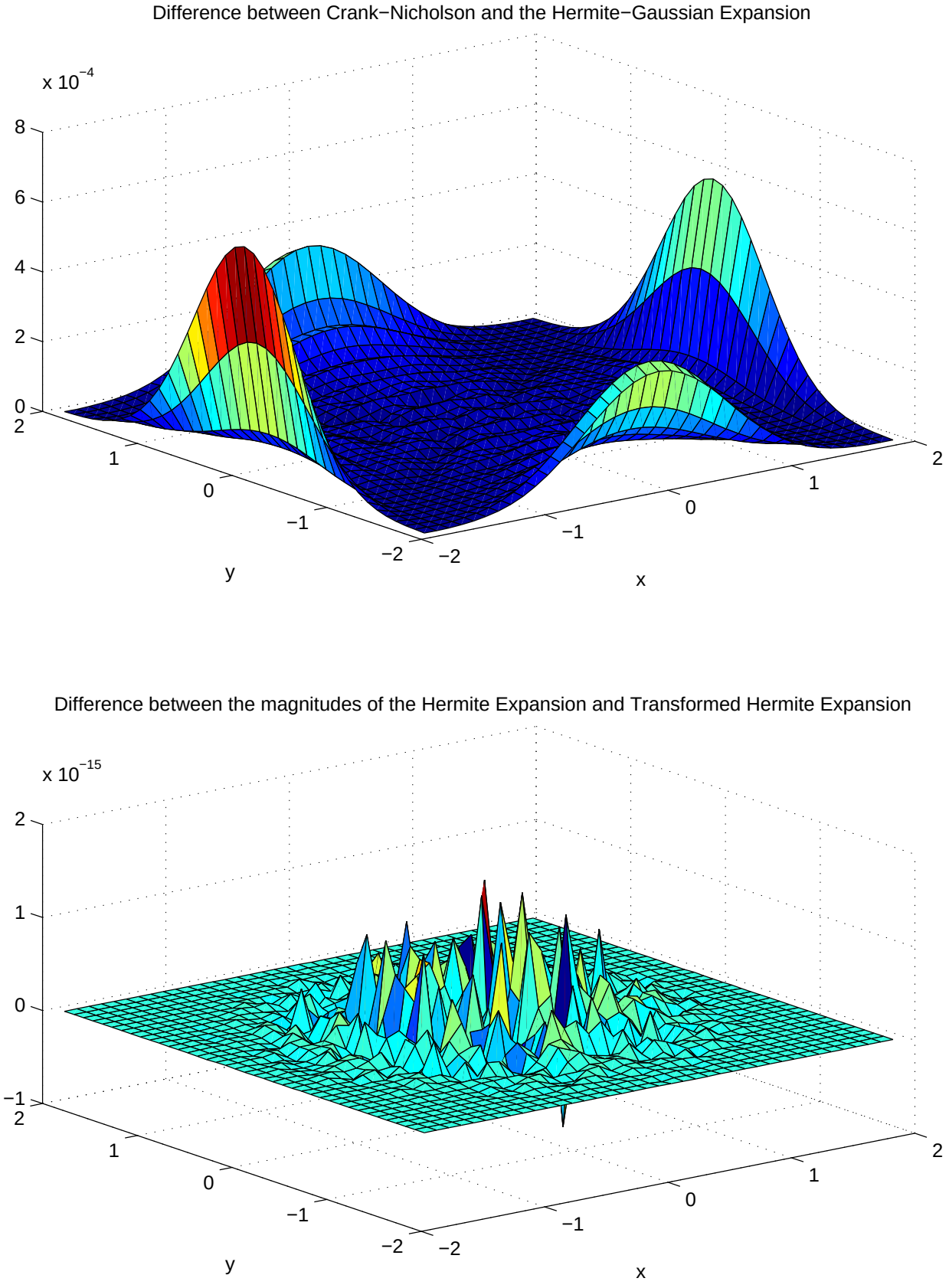

Figure 5.24: Propagation with $f(x,y) = \frac{(4-x)(4-y^2)}{150} e^{-\frac{x^2+y^2}{10}}$, $M_x = .6, M_y = 1$ (continued).

The results for the case of the three dimensional optical cavity are similar to those found for the two dimensional optical cavity. The curvature of the spherical mirror tends to focus the propagating wave. In the cases in which $M_x = M_y = 1$, the Gaussian beam has a more slender profile after propagating back and forth through the optical cavity than it did initially. Moreover, the amplitude of the wave is increased.

Particularly interesting results are those for which the half-lengths of the flat mirror are chosen to be unequal in the x and y directions. In the results of Figure 5.19 - Figure 5.24, the specification that $M_x = 0.6$ and $M_y = 1$ led to a somewhat unintuitive result. The propagating wave initially has a smaller spot size in the x direction than in the y direction. However, after one round trip through the optical cavity, the spot size in the x direction is greater than that in the y direction. This is due to the fact that a smaller value of w_{0x} leads to faster beam spreading in the x direction [29]. As a result, upon arriving at the spherical mirror, the propagating wave has a greater spot size in the x direction than in the y direction. The wave is then reflected from the spherical mirror and propagates back to the flat mirror at $z = 0$ with a larger spot size in the x direction. As a result, a significant portion of the returning wave overlaps the outcoupling mirror. Accordingly, some of the wave energy is lost due to absorption from the optical cavity wall.

Table 5.1: Wave Profile Energies for the Three Dimensional Optical Cavity

$f(x,y)$	(M_x, M_y)	$\mathcal{E}_u(0)$	$\mathcal{E}_u(D)$	$\mathcal{E}_g(D)$	$\mathcal{E}_g(0)$	$\mathcal{E}_{u_R}(0)$
0	(1,1)	0.5125	0.5125	0.5125	0.5125	0.4612
$.1e^{-(x^2+y^2)}$	(1,1)	0.5125	0.7032	0.7032	0.9863	0.8876
$.1e^{-\frac{x^2+y^2}{10}}$	(1,1)	0.5125	0.7479	0.7479	1.0946	0.9851
$.1e^{-\frac{x^2+y^2}{100}}$	(1,1)	0.5125	0.7537	0.7537	1.1087	0.9978
$.1e^{-\frac{x^2+y^2}{1000}}$	(1,1)	0.5125	0.7543	0.7543	1.1101	0.9991
$\frac{4-x}{50}e^{-\frac{x^2+y^2}{10}}$	(1,1)	0.5125	0.6936	0.6936	0.9413	0.8472
$\frac{(4-x)(4-y^2)}{150}e^{-\frac{x^2+y^2}{10}}$	(1,1)	0.5125	0.7589	0.7589	1.1323	1.0191
0	(.6,1)	0.8542	0.8542	0.8542	0.8542	0.7166
$\frac{4-x}{50}e^{-\frac{x^2+y^2}{10}}$	(.6,1)	0.8542	1.1574	1.1574	1.5681	1.3165
$\frac{(4-x)(4-y^2)}{150}e^{-\frac{x^2+y^2}{10}}$	(.6,1)	0.8542	1.2667	1.2667	1.8861	1.5836

Utilizing the results of propagation in the presence of zero gain as a reference point, the influence of the atomic gain function $f(x,y)$ on the propagating wave can be determined.

Recall that the energy $\mathcal{E}_u(z)$ associated with a wave profile $u(x, y, z)$ is defined by

$$\mathcal{E}_u(z) = \int_{-\infty}^{\infty} \int_{-\infty}^{\infty} |u(x, y, z)|^2 dxdy. \tag{5.57}$$

As can be seen from the data in Table 5.1, the numerical results agree with the theoretical results presented in Chapter 3. The Crank-Nicholson scheme preserves the group structure of the system when $f(x, y) = 0$. In particular, as can be seen in Table 5.1, energy is conserved in the cases of propagation with zero atomic gain. The initial energy of the propagating wave is identical to the energy of the wave incident on the outcoupling mirror. As a result, the norm in $L_2(\Omega)$ is preserved. As in the case of one transverse direction, the addition of a nonzero atomic gain function yields an increase in the energy of the propagating wave. In addition, the shape of the gain function influences the quantity and location of energy increase in the wave profile.

As was previously the case, the transformation due to reflection of the complex beam parameter $q(z)$ does not alter the energy of the propagating wave. In all cases shown, the maximum difference between $|u(x, y, D)|$ and $|g(x, y, D)|$ is on the order of 10^{-15}. As a result, the energy associated with the wave profile is virtually unchanged by reflection from the curved mirror.

In the results demonstrated for the three dimensional optical cavity, satisfactory numerical solutions are obtained utilizing the Hermite-Gaussian modes in cases of propagation in the presence of atomic gain. The error introduced due to expanding the propagating wave in terms of the Hermite-Gaussian modes is on the order of 10^{-4} in the case of zero atomic gain. The error introduced via the expansion remained on the order of 10^{-4} when a nonzero gain function $f(x, y)$ was present.

In all of the results presented, the error introduced by the Hermite-Gaussian expansion is slightly greater along the transverse boundary. The explanation for the slight increase in error is the same as it was for the case of the two dimensional optical cavity.

Chapter 6

Conclusions and Future Research

There are primarily three main aspects in this dissertation regarding optical activity of the chemical oxygen-iodine laser. The first aspect deals with the nature and behavior of electromagnetic wave propagation inside the optical cavity of the COIL. As a result, the topics of paraxial wave optics and Gaussian beam theory were presented in depth. The theory of paraxial wave optics provides a partial differential equation describing wave propagation in an atomic medium. The theory of Gaussian beams provides a means of specifying the influence of the spherical optical cavity mirror on the propagating wave.

Utilizing results of paraxial wave optics and Gaussian beam theory, a partial differential equation model describing wave propagation in the optical cavity was developed. This partial differential equation model comprises the second aspect of optical activity studied in this dissertation. As a propagating wave travels toward increasing and decreasing radial values, the partial differential equation model is composed of two parts. The first part describes propagation toward increasing radial values. Conversely, the second part describes propagation toward decreasing radial values. Upon arriving at the spherical mirror of the optical cavity, the propagating wave is transformed in order to account for reflection from the mirror.

The third aspect developed in this dissertation is the development of a numerical scheme used to obtain approximate solutions to the partial differential equation model in the case of one and two transverse directions. A semi-implicit Crank-Nicholson finite difference scheme was presented. In addition, the method used to numerically implement the mirror transformation of propagating wave was discussed. Several numerical results were presented.

In order to mathematically describe the influence of the spherical optical cavity mirror on the propagating wave, the wave is expanded in terms of Hermite-Gaussian basis functions. The basis functions are transformed and recombined resulting in a transformed solution due to reflection. The Hermite-Gaussian modes used in the expansion are derived from the paraxial wave equation for free space propagation. However, we obtained satisfactory numerical results utilizing these modes in the cases of nonzero atomic gain as well. The error

introduced in expanding the propagating wave at the curved mirror was roughly identical in the cases of zero and nonzero atomic gain. Moreover, the energy of the wave profile was unchanged by the mode expansion. As a result, the principle of conservation of energy was not transgressed by the transformation due to reflection from the spherical mirror.

There are several avenues of future work involved with the initial boundary value problem developed in this dissertation. First, there is a more general problem underlying the problem described here. The more general problem involves describing the influence of an arbitrarily shaped reflective mirror on a propagating wave of arbitrary profile. At this stage, there appears to be a lack of theory regarding this aspect of wave propagation. As the theory is developed, the algebraic transformation technique may prove to be a useful method in obtaining numerical solutions. For this reason, in Appendix A we include a brief description of the algebraic transformation method applied to a partial differential equation model similar to that presented in this dissertation.

Another interesting aspect of future research involves the application of the continuous sensitivity equation method to the partial differential equation model presented here. There are several parameters influencing the behavior of the propagating wave. One parameter is the minimum spot size w_0. In this work, we used a design criteria called the 99% rule to specify the minimum spot size at the flat mirror. Sensitivity analysis may provide a more suitable means of specifying w_0.

Finally, another important aspect of future research involves coupling the model presented here describing optical activity in the COIL to a chemically reacting fluid flow model. In this work, the atomic gain function $\alpha(x, y, z)$ is chosen somewhat arbitrarily. However, the gain is a result of a chemically reacting fluid flow. As a result, coupling the optical model to a fluid model will provide a more realistic atomic gain function. Moreover, the evolution of the propagating wave to an equilibrium state can be investigated.

Appendix A

Algebraic Grid Transformation

The methods described in this thesis provide a means to calculate the laser intensity inside the optical cavity of the COIL. There is a more general problem underlying the methods described here. In order to incorporate the influence of the reflective spherical mirror on the propagating wave, we had to utilize properties of Gaussian beams. The fact that the outer mirror of the COIL optical cavity is spherical also simplified the problem somewhat. However, one could pose a more general problem as to how a wave with arbitrary profile reflects from a mirror that is not necessarily spherical. Our first investigation of this problem led us to the method of algebraic grid transformation. The physical domain was transformed to a rectangle, and the governing initial boundary value problem was transformed accordingly. However, it became apparent that is is exceedingly difficult to specify a boundary condition at the curved mirror that adequately describes wave reflection. Moreover, there appears to be a surprising lack of theory regarding general wave reflection. However, the algebraic grid transformation method may prove to be a useful technique in the future for numerically calculating wave reflection from reflective surfaces. Thus, in this appendix we include the algebraic grid transformation method applied to an initial boundary value problem similar to that of Chapter 3.

Suppose a propagating paraxial wave begins at a flat mirror M_1 and propagates to a curved mirror M_2. Free space propagation from M_1 to M_2 is governed by the initial boundary value problem

$$\frac{\partial u}{\partial z} = -\frac{j}{2k}\left(\frac{\partial^2 u}{\partial x^2} + \frac{\partial^2 u}{\partial y^2}\right), \ (k > 0), \tag{A.1}$$

$$u(-a, y, z) = 0 = u(a, y, z) \tag{A.2}$$

$$u(x, -b, z) = 0 = u(x, b, z), \text{ and} \tag{A.3}$$

$$u(M_1) = u_0(x, y), \tag{A.4}$$

where $(x, y) \in [-a, a] \times [-b, b]$.

Upon arriving at the curved mirror, the propagating wave is reflected. Thus, the wave begins to propagate toward decreasing values of z. As a result, free space propagation from M_2 to M_1 us governed by the initial boundary value problem

$$\frac{\partial g}{\partial z} = \frac{j}{2k}\left(\frac{\partial^2 g}{\partial x^2} + \frac{\partial^2 g}{\partial y^2}\right), \ (k < 0), \tag{A.5}$$

$$g(-a, y, z) = 0 = g(a, y, z) \tag{A.6}$$

$$g(x, -b, z) = 0 = g(x, b, z), \text{ and} \tag{A.7}$$

$$g(M_2) = R(u(M_2)), \tag{A.8}$$

where $R(u)$ is a reflection operator transforming the propagating wave to account for reflection from M_2.

To illustrate the algebraic grid transformation technique, denote $\Pi(x, y)$ as the equation describing the shape of the curved mirror M_2. In the discussion that follows, $\Pi(x, y)$ must be twice differentiable. Define the distance D by

$$D = \Pi(a, b). \tag{A.9}$$

A uniform grid can not be constructed on the physical domain due to the shape of the curved mirror M_2. The algebraic grid transformation method provides a means of transforming the physical domain to a convenient computational domain. A uniform grid can then be constructed on the computational domain. A transformation which maps the physical domain $[-a, a] \times [-b, b] \times [0, M_2]$ to the rectangle $[-a, a] \times [-b, b] \times [0, D]$ is of the form

$$\xi = x, \tag{A.10}$$

$$\rho = y, \tag{A.11}$$

$$\eta = \frac{zD}{\Pi(x, y)}. \tag{A.12}$$

In order to implement a numerical scheme on the rectangle resulting from the change of coordinates, it is necessary to transform the governing initial boundary value problem. In the case of upward propagation, we must first transform the governing equation given by (A.1). Utilizing the chain rule, we can write spatial derivatives in the original coordinates (x, y, z) as functions of derivatives in the new coordinates (ξ, ρ, η).

Applying the chain rule results in an expression for $\frac{\partial u}{\partial z}$ of the form

$$\frac{\partial u}{\partial z} = \frac{\partial \bar{u}}{\partial \xi}\frac{\partial \xi}{\partial z} + \frac{\partial \bar{u}}{\partial \rho}\frac{\partial \rho}{\partial z} + \frac{\partial \bar{u}}{\partial \eta}\frac{\partial \eta}{\partial z}, \tag{A.13}$$

where $\bar{u}$ is the transformed state.

Evaluating the derivatives given in (A.13) results in an expression for $\frac{\partial u}{\partial z}$ of the form

$$\frac{\partial u}{\partial z} = \left(\frac{D}{\Pi(\xi,\rho)}\right)\frac{\partial \bar{u}}{\partial \eta}. \tag{A.14}$$

Applying the chain rule twice results in an expression for $\frac{\partial^2 u}{\partial x^2}$ of the form

$$\frac{\partial^2 u}{\partial x^2} = \frac{\partial^2 \bar{u}}{\partial \xi^2}\left(\frac{\partial \xi}{\partial x}\right)^2 + \frac{\partial \bar{u}}{\partial \xi}\frac{\partial^2 \xi}{\partial x^2} + \frac{\partial^2 \bar{u}}{\partial \rho^2}\left(\frac{\partial \rho}{\partial x}\right)^2 + \frac{\partial \bar{u}}{\partial \rho}\frac{\partial^2 \rho}{\partial x^2} + \frac{\partial^2 \bar{u}}{\partial \eta^2}\left(\frac{\partial \eta}{\partial x}\right)^2 + \frac{\partial \bar{u}}{\partial \eta}\frac{\partial^2 \eta}{\partial x^2}. \tag{A.15}$$

The analogous expression for $\frac{\partial^2 u}{\partial y^2}$ is of the form

$$\frac{\partial^2 u}{\partial y^2} = \frac{\partial^2 \bar{u}}{\partial \xi^2}\left(\frac{\partial \xi}{\partial y}\right)^2 + \frac{\partial \bar{u}}{\partial \xi}\frac{\partial^2 \xi}{\partial y^2} + \frac{\partial^2 \bar{u}}{\partial \rho^2}\left(\frac{\partial \rho}{\partial y}\right)^2 + \frac{\partial \bar{u}}{\partial \rho}\frac{\partial^2 \rho}{\partial y^2} + \frac{\partial^2 \bar{u}}{\partial \eta^2}\left(\frac{\partial \eta}{\partial y}\right)^2 + \frac{\partial \bar{u}}{\partial \eta}\frac{\partial^2 \eta}{\partial y^2}. \tag{A.16}$$

We are at a position where we must enforce the paraxial approximation. Recall that the assumption made in the derivation of the paraxial wave equation is that

$$\left|\frac{\partial^2 u}{\partial z^2}\right| << \left|\frac{\partial^2 u}{\partial x^2}\right| \text{ and } \left|\frac{\partial^2 u}{\partial z^2}\right| << \left|\frac{\partial^2 u}{\partial y^2}\right|. \tag{A.17}$$

Therefore, in order to be consistent with the paraxial assumption, we discard $\frac{\partial^2 \bar{u}}{\partial \eta^2}$ in (A.15) and (A.16).

Evaluating the derivatives of ξ and ρ in (A.15) and (A.16) results in much simpler expressions for $\frac{\partial^2 u}{\partial x^2}$ and $\frac{\partial^2 u}{\partial y^2}$. Evaluating these derivatives, one arrives at

$$\frac{\partial^2 u}{\partial x^2} = \frac{\partial^2 \bar{u}}{\partial \xi^2} + \frac{\partial \bar{u}}{\partial \eta}\frac{\partial^2 \eta}{\partial x^2}, \text{ and} \tag{A.18}$$

$$\frac{\partial^2 u}{\partial y^2} = \frac{\partial^2 \bar{u}}{\partial \rho^2} + \frac{\partial \bar{u}}{\partial \eta}\frac{\partial^2 \eta}{\partial y^2}. \tag{A.19}$$

We have found expressions yielding derivatives in the original coordinates (x, y, z) as functions of derivatives in the new coordinates (ξ, ρ, η). These expressions are given by (A.14), (A.18), and (A.19). Substituting (A.14), (A.18), and (A.19) into the governing

equation (A.1) yields the governing equation for the transformed state. The result is a partial differential equation of the form

$$\frac{\partial \bar{u}}{\partial \eta}\left[\frac{\partial \eta}{\partial z}+\frac{s}{2k}\left(\frac{\partial^2 \eta}{\partial x^2}+\frac{\partial^2 \eta}{\partial y^2}\right)\right]=-\frac{s}{2k}\left(\frac{\partial^2 \bar{u}}{\partial \xi^2}+\frac{\partial^2 \bar{u}}{\partial \rho^2}\right). \tag{A.20}$$

Upon evaluating the derivatives of η in (A.20), we arrive at

$$\frac{\partial \eta}{\partial z}+\frac{s}{2k}\left(\frac{\partial^2 \eta}{\partial x^2}+\frac{\partial^2 \eta}{\partial y^2}\right)=\frac{2k\Pi D+s\eta\left(2\Pi_\xi^2-\Pi\Pi_{\xi\xi}+2\Pi_\rho^2-\Pi\Pi_{\rho\rho}\right)}{2k\Pi^2}. \tag{A.21}$$

By defining a function $\phi(\xi,\rho,\eta)$ as

$$\phi(\xi,\rho,\eta)=\frac{2k\Pi^2}{2k\Pi D+s\eta\left(2\Pi_\xi^2-\Pi\Pi_{\xi\xi}+2\Pi_\rho^2-\Pi\Pi_{\rho\rho}\right)}, \tag{A.22}$$

we can write the governing equation for the transformed state as

$$\frac{\partial \bar{u}}{\partial \eta}=-\frac{s\phi}{2k}\left(\frac{\partial^2 \bar{u}}{\partial \xi^2}+\frac{\partial^2 \bar{u}}{\partial \rho^2}\right). \tag{A.23}$$

As the transverse coordinates are simply renamed according to (A.10) and (A.11), the transformed initial boundary value problem describing upward propagation for the transformed state $\bar{u}(\xi,\rho,\eta)$ is of the form

$$\frac{\partial \bar{u}}{\partial \eta}=-\frac{s\phi}{2k}\left(\frac{\partial^2 \bar{u}}{\partial \xi^2}+\frac{\partial^2 \bar{u}}{\partial \rho^2}\right)\ (k>0), \tag{A.24}$$

$$\bar{u}(-a,\rho,\eta)=0=\bar{u}(a,\rho,\eta), \tag{A.25}$$

$$\bar{u}(\xi,-b,\eta)=0=\bar{u}(\xi,b,\eta),\ \text{and} \tag{A.26}$$

$$\bar{u}(M_1)=u_0(\xi,\rho). \tag{A.27}$$

Downward propagation is equivalent to reversing the sign of k. Reversing the sign of k in (A.22) results in a function $\gamma(\xi,\rho,\eta)$ of the form

$$\gamma(\xi,\rho,\eta)=\frac{2k\Pi^2}{2k\Pi D-s\eta\left(2\Pi_\xi^2-\Pi\Pi_{\xi\xi}+2\Pi_\rho^2-\Pi\Pi_{\rho\rho}\right)},\ (k<0). \tag{A.28}$$

Thus, the initial boundary value problem describing downward propagation is of the form

$$\frac{\partial \bar{g}}{\partial \eta} = \frac{s\gamma}{2k}\left(\frac{\partial^2 \bar{g}}{\partial \xi^2} + \frac{\partial^2 \bar{g}}{\partial \rho^2}\right) \ (k < 0), \tag{A.29}$$

$$\bar{g}(-a, \rho, \eta) = 0 = \bar{g}(a, \rho, \eta), \tag{A.30}$$

$$\bar{g}(\xi, -b, \eta) = 0 = \bar{g}(\xi, b, \eta), \text{ and} \tag{A.31}$$

$$\bar{g}(\xi, \rho, D) = \bar{R}(\bar{u}(\xi, \rho, D)), \tag{A.32}$$

where $\bar{R}$ is the transformed reflection operator.

An appropriate numerical scheme can then be applied to obtain approximations to the transformed states $\bar{u}$ and $\bar{g}$. In our initial investigation, we found numerical solutions via a Crank-Nicholson scheme similar to that presented in Chapter 5. In that investigation, we simply specified $R(u)$ by

$$R(u) = -u. \tag{A.33}$$

However, it became apparent that the expression for $R(u)$ given by (A.33) did not adequately predict wave reflection. As a result, we formulated the problem in terms of Gaussian beams. Correctly specifying $R(u)$ is still an open problem.

Bibliography

[1] P.W. Atkins, R.S. Friedman. *Molecular Quantum Mechanics.* Oxford University Press, 1997.

[2] Kendall E. Atkinson. *An Introduction to Numerical Analysis.* John Wiley and Sons, 1989.

[3] Partha P. Banerjea, Ting-Chung Poon. *Principles of Applied Optics.* Richard D. Irwin, Inc., and Aksen Associates, Inc., 1991.

[4] D. L. Carroll. "Modeling High-Pressure Chemical Oxygen-Iodine Lasers." AIAA Paper 94-2431. 25th AIAA Plasmadynamics and Lasers Conference. Colorado Springs, Colorado. 20-23 June, 1994.

[5] Christopher C. Davis. *Lasers and Electro-Optics: Fundamentals and Engineering.* Cambridge University Press, 1996.

[6] Lokenath Debnath, Piotr Mikusinski. *Introduction to Hilbert Spaces with Applications.* Academic Press, 1999.

[7] Lawrence C. Evans. *Partial Differential Equations.* American Mathematical Society, 1998.

[8] W. J. Firth, R. G. Harrison. *Lasers: Physics, Systems, and Techniques.* SUSSP Productions, 1983.

[9] Hiroo Fujii. "COIL Development in Japan." AIAA Paper 94-2419. 25th AIAA Plasmadynamics and Lasers Conference. Colorado Springs, Colorado. 20-23 June, 1994.

[10] Andrew G. Godfrey, William M. Eppard, Eugene M. Cliff. "Using Sensitivity Equations for Chemically Reacting Flows." AIAA Paper 98-4805. 7th AIAA/USAF/NASA/ISSMO Symposium on Multidisciplinary Analysis and Optimization. St. Louis, Missouri. 2-4 September, 1988.

[11] Gene H. Golub, Charles F. Van Loan. *Matrix Computations.* The Johns Hopkins University Press, 1996.

[12] M. Hishida, N. Azami, K. Iwamoto, W. Masuda, H. Fujii, T. Atsuta, M. Muro. "Flow and Optical Fields in a Supersonic Flow Chemical Oxygen-Iodine Laser." AIAA Paper 97-2391. AIAA 28th Plasmadynamics and Lasers Conference. Atlanta, Georgia. 23-25 June, 1997.

[13] Norman Hodgson, Horst Weber. *Optical Resonators: Fundamentals, Advanced Concepts, and Applications.* Springer-Verlag London Limited, 1997.

[14] Kenichi Iga. *Fundamentals of Laser Optics.* Plenum Press, 1994.

[15] Tosio Kato. *Perturbation Theory for Linear Operators.* Springer-Verlag, 1976.

[16] Erwin Kreyszig. *Introductory Functional Analysis with Applications.* John Wiley & Sons, 1978.

[17] Leon Lapidus, George F. Pinder. *Numerical Solution of Partial Differential Equations in Science and Engineering.* John Wiley and Sons, Inc., 1999.

[18] David C. Lay, Angus E. Taylor. *Introduction to Functional Analysis.* John Wiley & Sons, 1980.

[19] Mireille Levy. *Parabolic Equation Methods for Electromagnetic Wave Propagation.* The Institution of Electrical Engineers, 2000.

[20] D. H. Lewis, C. W. Clendening. " Modelling of COIL Lasers." AIAA Paper 82-0872. AIAA/ASME 3rd Joint Thermophysics, Fluids, Plasma, and Heat Transfer Conference. St. Louis, Missouri. 7-11 June, 1982.

[21] Timothy J. Madden. *Computational Fluid Dynamics Methodologies for Simulation of Chemical Oxygen-Iodine Laser Flowfields.* PhD Thesis, University of Illinois at Urbana-Champaign, Department of Aeronautical and Astronautical Engineering, 1997.

[22] Timothy J. Madden, Wayne C. Solomon. "A Detailed Comparison of a Computational Fluid Dynamic Simulation and a Laboratory Experiment for a COIL Laser." AIAA Paper 97-2387. AIAA 28th Plasmadynamics and Lasers Conference. Atlanta, Georgia. 23-25 June, 1997.

[23] K. W. Morton, D. F. Mayers. *Numerical Solution of Partial Differential Equations.* Cambridge University Press, 1994.

[24] Peter V. O'Neil. *Advanced Engineering Mathematics.* Wadsworth Publishing Company, 1991.

[25] A. Pazy. *Semigroups of Linear Operators and Applications to Partial Differential Equations.* Springer-Verlag, 1983.

[26] Michael Renardy, Robert C. Rogers. *An Introduction to Partial Differential Equations.* Springer-Verlag, 1993.

[27] D. B. Rensch. "Three-Dimensional Unstable Resonator Calculations with Laser Medium." *Applied Optics.* Vol. 13, No. 11. November, 1974.

[28] Walter Rudin. *Real and Complex Analysis.* McGraw-Hill, 1987.

[29] Anthony E. Siegman. *Lasers.* University Science Books, 1986.

[30] Anthony E. Siegman, Edward A. Sziklas. "Mode Calculations in Unstable Resonators with Flowing Saturable Gain. 1: Hermite-Gaussian Expansion." *Applied Optics.* Vol. 13, No. 12. December, 1974.

[31] Anthony E. Siegman, Edward A. Sziklas. "Mode Calculations in Unstable Resonators with Flowing Saturable Gain. 2: Fast Fourier Transform Method." *Applied Optics.* Vol. 14, No. 8. August, 1975.

[32] Hiroki Tanabe. *Equations of Evolution.* Pitman Publishing Limited, 1979.

[33] Hiroki Tanabe. *Functional Analytic Methods for Partial Differential Equations.* Marcel Dekker, 1997.

[34] Roger Temam. *Infinite-Dimensional Dynamical Systems in Mechanics and Physics.* Springer-Verlag, 1997.

[35] Joe F. Thompson. *Handbook of Grid Generation.* CRC Press, 1998.

[36] K. A. Truesdell, C. A. Helms, G. D. Hager. "COIL Development in the USA." AIAA Paper 94-2421. 25th AIAA Plasmadynamics and Lasers Conference. Colorado Springs, Colorado. 20-23 June, 1994.

[37] Joseph T. Verdeyen. *Laser Electronics.* Prentice Hall, 1995.

[38] J. Wloka. *Partial Differential Equations.* Cambridge University Press, 1992.

[39] Amnon Yariv. *Introduction to Optical Electronics.* Holt, Rinehart and Winston, 1976.

[40] Amnon Yariv. *An Introduction to Theory and Applications of Quantum Mechanics.* John Wiley and Sons, 1982.

[41] Amnon Yariv. *Quantum Electronics.* John Wiley and Sons, 1989.

[42] Matt Young. *Optics and Lasers Including Fibers and Optical Waveguides.* Springer-Verlag, 1992.

Vita

R. Chris Camphouse was born in Rexburg, Idaho on September 30, 1972. He graduated from Madras High School, located in Madras, Oregon, in 1990. After completing high school, Chris enrolled at Oregon State University, where he received his undergraduate degree in mathematics in 1996. Chris began graduate school at Virginia Polytechnic Institute and State University in the fall of 1996, and received his Master of Science in mathematics two years later. He was then accepted into the Ph.D. program at Virginia Tech and received his doctorate in 2001. At the present time, Chris is working as a post-doc at the Interdisciplinary Center for Applied Mathematics at Virginia Tech.